IPP-Report

Max-Planck-Institut für Plasmaphysik

Markus Reitschuster

Study of a new concept for exhaust of power and particles from a tokamak

IPP 1/340
January 2011

This diploma thesis was written at the *Max-Planck-Institut für Plasmaphysik* in cooperation with the *Culham Centre for Fusion Energy*. It concludes my studies at the physics department of the *Ludwigs-Maximilians-Universität*.

Author: Markus Xaver Joachim Reitschuster
born 16th of May 1984 in Munich, Germany

Acknowledgements

Prof. Dr. Hartmut Zohm and Dr. Erika Strumberger from the *Max-Planck-Institut für Plasmaphysik* (IPP) in Garching, Germany, guided my work on this study. Dr. Strumberger helped me with the Vacfield and Gourdon code, the usage of the local hardware, provided the AUG equilibrium and the layout of the coils. Prof. Dr. Zohm supervised my progress. I also want to thank all the people from the IPP who took the time to answer my questions and provided me with additional information.

Dr. Tom Todd from the *Culham Centre for Fusion Energy* (CCFE) in Culham, United Kingdom, provided me with valuable feedback, helped me to get the necessary data for MAST and promoted the idea of this thesis. He also gave me the opportunity to get into personal contact with the colleagues from the CCFE. Geoff Cunningham provided the MAST equilibrium to me. K. Hawkins from the CCFE's Drawing Office provided the MAST's coil geometry to me. I also want to thank Dr. Lynton Appel, Prof. Dr. Steve Cowley, A. Darke, Geoff Fishpool, Dr. Wojtek Fundamenski and Dr. Andrew Kirk who all took the time to talk to me and gave me advice.

Table of Contents

Abstract

In modern fusion experiments hydrogen isotopes are fused to helium and neutrons. Because of the high temperatures the gas is ionised, hence a plasma, which can be influenced with electromagnetic fields. The plasma is in the so-called vacuum vessel. Like any other gas it tends to expand into the whole vessel due to pressure compensation. A set of magnetic field coils keeps the plasma in its place. Due to various effects like diffusion and drifts there will always be a fraction of the particles leaving the confined plasma. These lost particles are guided away from the plasma by the magnetic field. Since the energy of these particles is still high it has to be absorbed by plates specially designed to withstand it, the divertor plates.

Today's divertors are at their maximum heat load capacity as stated in [1]. One way to increase the maximally absorbed energy is to increase the plasma-wetted area. This can be done by changing the geometry of the magnetic field. The “Super-X divertor” guides the particles to a maximal radius inside the toroidal field coils [1]. To take the Super-X divertor another step further we ask if it is possible to guide the particles to the region outside of the toroidal field coils so the size of the divertor will not be confined by the coils.

This thesis uses the fieldline geometry as a first estimate of the particles' trajectories. In the second step it analyses the trajectory of single particles using the guiding centre approach. Using these approximations, it is shown that with sufficiently small coils it is possible that no particle hits the coils. Two tokamaks were analysed, MAST (Culham, UK) and ASDEX Upgrade (Garching, Germany). MAST would need a minor alteration of the toroidal field coil's geometry, to avoid the coils being hit. This change would not affect the confined plasma itself. At ASDEX Upgrade the toroidal field coils cross-section area would have to be reduced to 8% of its real area, but such a major rebuild seems to be out of question.

I Introduction

Epitome

In modern fusion experiments hydrogen isotopes are fused to helium and neutrons. Because of the high temperatures the gas is ionised, hence a plasma, which can be influenced with electromagnetic fields. The plasma is in the so-called vacuum vessel. Like any other gas it tends to expand into the whole vessel due to pressure compensation. A set of magnetic field coils confines the plasma.

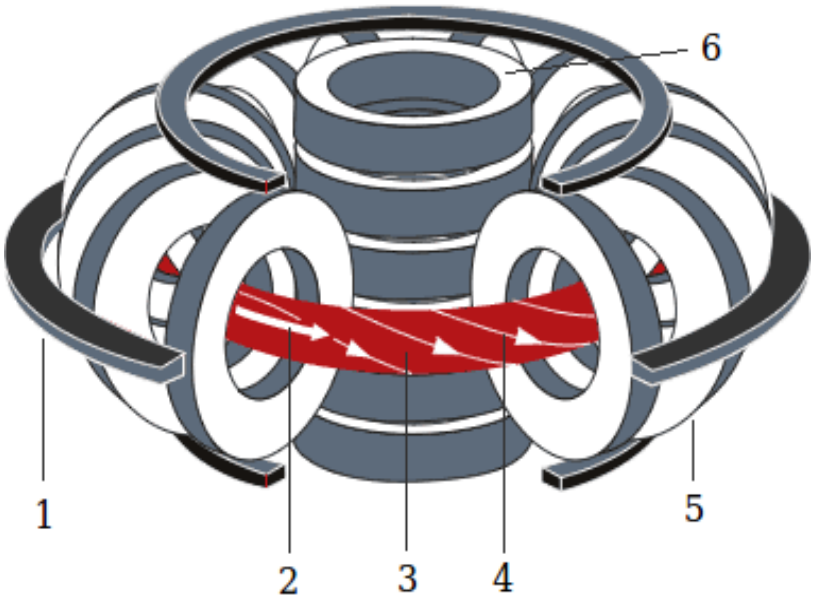

Figure 1: Schematics of a Tokamak

1 – Poloidal Field Coils
2 – Plasma Current
3 – confined Plasma
4 – Magnetic Fieldline
5 – Toroidal Field Coils
6 – Transformer Coil

Picture taken from http://www.ipp.mpg.de/ippcms/de/pr/exptypen/tokamak/index.html

Tokamaks are axisymmetric. In the R-Z plane (poloidal cut) the magnetic field has a characteristic shape. Fieldlines have a single point within the so called separatrix, do not leave it. This is the area where the plasma is confined since particles are bound to the fieldlines. In figure 2 the confined plasma is drawn yellow. Its outer boundary is called the last closed flux surface. The pressure on it is constant. Due to various effects like diffusion and drifts there will always be a fraction of the particles leaving the confined plasma. These lost particles are guided away from the plasma by the magnetic field. Since the energy of these lost particles is still high it has to be absorbed by plates specially designed to withstand it, the divertor plates (see figure 2).

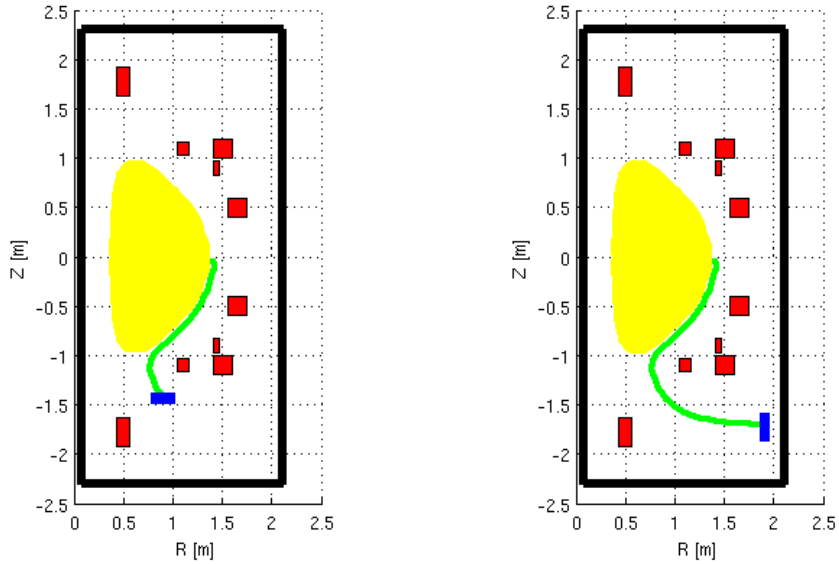

Figure 2: Sketches of a MAST poloidal cut. The read rectangles are poloidal field coil's cross-sections, the black frame is a toroidal field coil. The plasma is drawn yellow. The path of particles that have left the plasma is sketched green. The blue rectangle is a divertor plate. The left picture shows a standard divertor. The right one illustrates a Super-X divertor.

Motivation

The lost particle's kinetic energy is in the 10-100 eV range. According to [1], today's divertors absorb heat loads up to the technical limitation of 10 MW/m². The amount of energy the divertor can handle is still a bottleneck when maximising fusion gain, as stated in [6]. Another problem is backscattering of eroded particles from the divertor into the plasma since the plasma burning is very sensitive to impurities. The new MAST Upgrade will receive a Super-X divertor as presented in [1]. It guides the lost particles to the maximal radius inside the toroidal field (TF) coils (see figure 2). This allows a larger plasma-wetted divertor surface thus decreasing the heat load per surface area.

Idea

The idea of this thesis is to guide the particle flux in between the TF coils' gaps and then outside (illustrated in figure 3). Once outside, the particle flux could be enlarged arbitrarily. If it is possible to guide the particles outside, this can be used to decrease the heat load per surface area on the divertor plates and to keep the neutron flux from hitting the divertor. This may be done by moving the divertor to a position that cannot be hit by uncharged particles. And since the magnetic field decreases fast once outside the TF coils, the magnetic mirror will restrict backscattering of particles from the divertor to the plasma.

The idea was proposed by the *Culham Centre for Fusion Energy*, Culham, U.K. (CCFE).

Goal

The main objective of this thesis is to check whether it is possible to guide particles from the Scrape Off Layer (SOL) outside the TF coils without hitting them, respectively to find a setup in which it is possible.

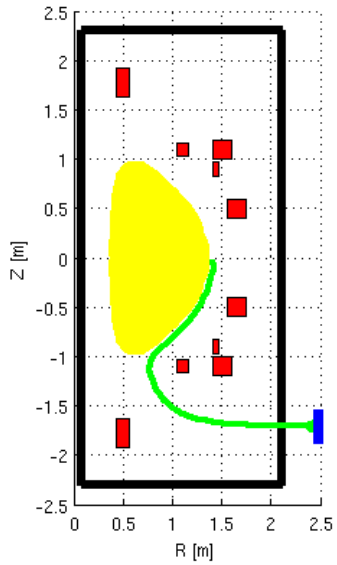

Figure 3: Divertor outside the TF coils. The particle flux could be brought to arbitrary radii thus expanded in toroidal direction.

The main figure of merit in this thesis is the Magnetic Transparency M. It is the percentage of fieldlines that are started outside the separatrix and escape without hitting the TF coils. Analogously the Particle Transparency P is defined for single particles.

In the course of my work I have collected a lot of ideas from different people. Some of them are about how to decrease the hit probability, others how to improve the quality of the calculations. Due to time restrictions it was not possible to include all of them. The ones that are not included into my work are summarized in Chapter VI .

Approach

As a first approximation for the particle flux, the fieldlines are analysed. The fieldlines are traced from the SOL to the TF coils. Therefore startpoints in the SOL are chosen and the fieldlines are computed by the Gourdon code. A post-processor checks the fieldlines' paths for hits with the TF coils.

Two tokamaks were analysed. ASDEX Upgrade (AUG) has little room for the fieldlines to pass in between the coils since AUG has a high TF current thus large coils. The second tokamak, MAST, is more appropriate for this task since its toroidal field is much lower and TF coils smaller.

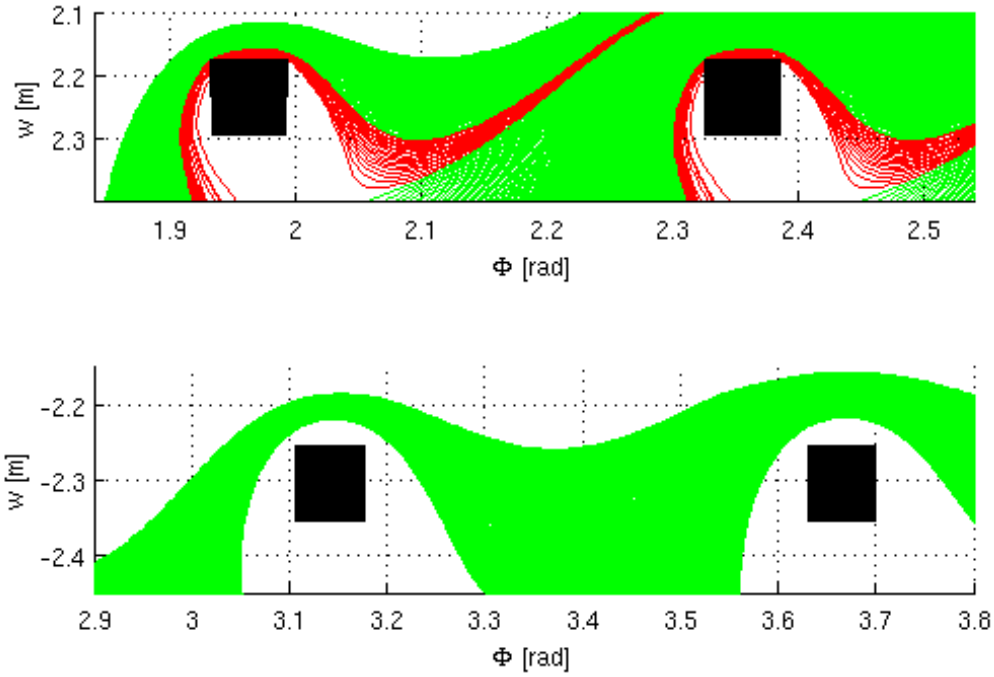

Figure 4: The TF coils' cross-sections are represented by the black squares. The fieldlines are started in SOL and move from the right to the left. Red fieldlines are the ones that hit the coils, green ones do not. The upper picture shows AUG with coils with an edge length of 12 cm (real coils have ~36cm). The lower picture shows MAST TF coils with an edge length of 10 cm (real coils have ~10 cm).

The influence of the TF coil's cross-section geometry on the fieldlines' paths is examined in order to learn how to shape the coils to minimize their chance of being hit. The size of the cross-section area is one main restriction for this proposition. The size must be small enough to evade being hit, but still large enough to be able to carry the coil's electric current. In order to minimize the hit probability but still keep a maximal cross-section area, new geometries are introduced. In figure 4 we already see that a square cross-section shape is not optimal for this task. New shapes allow better results without changing the magnetic field in the region of the plasma. If such a divertor or a corresponding experiment were to be built only the part of the TF coil that intersects the particles would need to be optimized. Changing the cross-section geometry only affects the coil's near-field and leaves the equilibrium as is.

In order to get more accurate results, the fieldlines are replaced by single particles' trajectories, using a Guiding Centre approach. The focus is on deuterium ions. Their trajectories are traced from the SOL to the TF coils and checked for hits with the coils. The influence of their pitch angle and kinetic Energy on the hit probability are also analysed.

II Summary of Prior Knowledge

1 Fusion

In fusion experiments hydrogen isotopes are confined and heated in order to fuse to helium. The most promising reaction for the realization of future reactors seems to be the fusion of deuterium and tritium.

$$D + T \rightarrow {}^{4}_{2}He + n + 17.6\,MeV \tag{1}$$

This reaction produces excess energy, which we hope, we can one day use to generate electricity providing an alternative to today's nuclear plants, which use fission of heavy particles. The advantage is that the radioactive waste's half life period is much shorter with fusion than fission. The radioactive waste of fission is product of the nuclear reaction. The radioactive waste of fusion is not from the reaction itself but from interactions of fast neutrons with the walls. So the half life period depends on the chosen material. Another advantage is that the “fuel” has to be injected continuously, which prevents an uncontrolled burning.

The conditions that are needed for sufficiently high fusion rates are extreme by ordinary standards. The temperatures have to be in the keV range (∼11 Mio.°C) for a long enough time to achieve a significant burn of particles. This can be achieved by either increasing the mass density of the hydrogen by 10^3 for a short time (∼ns) and then letting it explode (inertial confinement) or by using magnetic fields to keep the plasma from expanding (magnetic confinement). Even though a plasma is sensitive to an electric field, it does not seem possible to confine it with an electric field because the field penetrates only into a small layer (Debye Length).

2 Tokamak

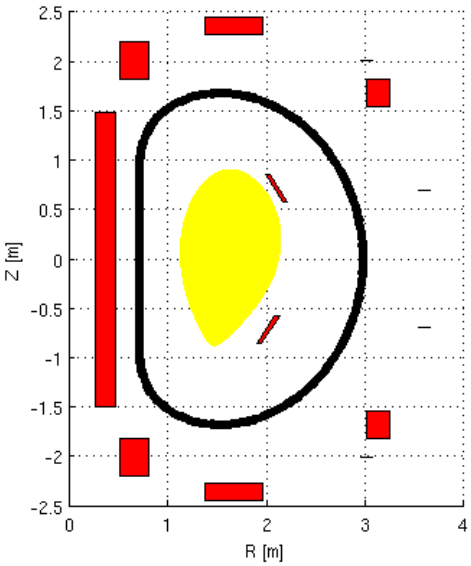

Figure 5: Toroidal plane of ASDEX Upgrade; the toroidal field coil (black), the poloidal field coils (red) and the plasma (yellow) are shown.

The tokamak is a magnetic confinement device that has (nearly) axial symmetry. The plasma is in a torus shaped vacuum chamber. The magnetic field keeps the plasma from distributing itself evenly in the vessel. The pressure on its boundary is constant. The magnetic field consist of the toroidal field from the TF coils, the field from the plasma current and the poloidal field (PF) from the PF coils.

The aspect ratio is the major radius (the diameter of the ring) divided by the minor radius of the torus (the thickness of the ring). In the case of the tokamak the minor and major radii are in reference to the plasma.

Figure 6 illustrates the meaning of the words toroidal and poloidal.

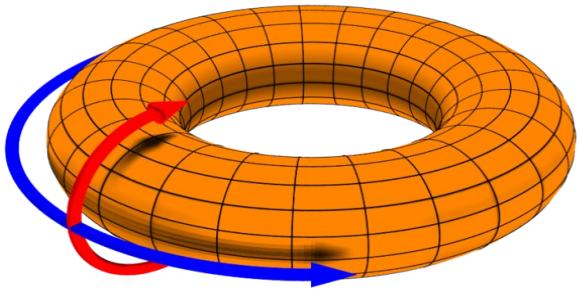

Figure 6: The red arrow shows in poloidal direction, the blue one in toroidal direction. Picture from http://en.wikipedia.org/wiki/File:Toroidal_coord.png

Toroidal Field Coils

The TF coils produce a magnetic field that is (nearly) axial symmetric, thus does not vary in toroidal direction. Near the plasma **B** points only in toroidal direction. The finite number of TF coils (AUG has 16, MAST 12) violate the axial symmetry. The toroidal magnetic field has a ripple with a periodicity equal to the number of coils. At the point of the separatrix with the highest radius this ripple shifts AUG's separatrix 0.95 mm and MAST's separatrix 1.4 mm in radial direction. The ripple is strongest close to the TF coils.

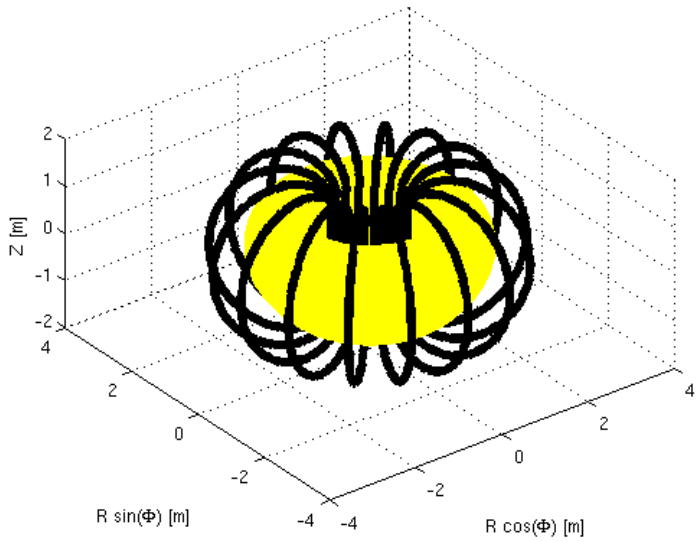

Figure 7: AUG toroidal field coils (black) and the plasma (yellow) at the plasma.

Plasma Current

With a purely toroidal field a separation of charged particles would occur due to the $\nabla|\mathbf{B}|$ drift. This produces an electric field leading to the **ExB** drift, which pushes the particles in radial direction towards the border of the vacuum vessel. To avoid this, an electric current is introduced in the plasma with a transformer coil in the middle of the torus. An auxiliary method is neutral particle injection. Both methods also heat the plasma. The plasma current creates a poloidal magnetic field which drills the magnetic fieldlines by giving them a poloidal component. The number of toroidal circulations during one poloidal circulation is called safety factor q.

$$q = \frac{toroidal\,circulation}{poloidal\,circulations} \tag{2}$$

A simple approximation is to assume the toroidal and poloidal fields are constant. This is true for an infinite aspect ratio (R/r) and cylindrical cross-section. The safety factor may then be calculated as follows.

$$q = \frac{r \cdot B_{tor}}{R \cdot B_{pol}} \qquad \frac{R}{r} \gg 1 \tag{3}$$

With r the minor radius, R the major radius of the torus. This approximation breaks down for small aspect ratios, like the one of MAST (R=0.7 m r=0.5 m). When going from the middle of the plasma to its border q increases for the equilibria that are used in this study.

Poloidal Field Coils

The PF coils generate a poloidal field, which means its toroidal component equals zero. They are used to control the position of the plasma and shape it. With them the strength of the poloidal field can be controlled thus influencing the safety factor q. At ASDEX Upgrade there are 15 PF coils including the transformer coil in the middle. In figure 8 only two are shown to keep it clear. All of the PF coils are shown in figure 5.

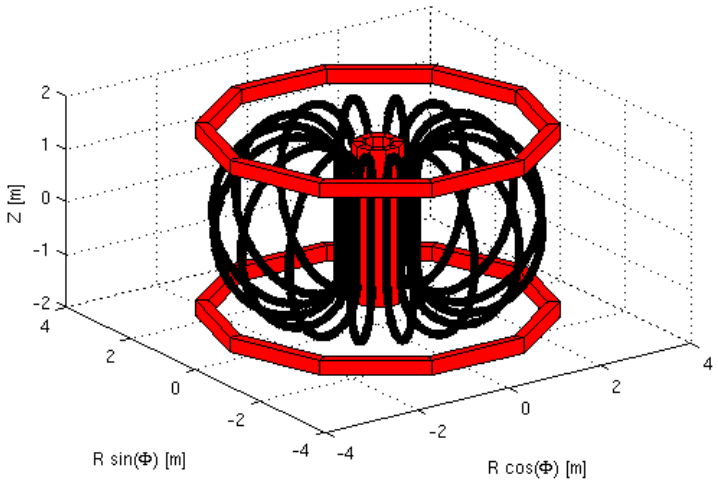

Figure 8: AUG toroidal field coils (black) and three of the 15 poloidal field coils (red) are shown. The one in the centre is the transformer coil.

Flux Surfaces

The poloidal flux Ψ is defined as the integral over B in direction of the surface vector along a surface generated by rotating the line between the magnetic axes and a point of the flux surface.

$$\Psi = \int_S \boldsymbol{B} \cdot d\boldsymbol{A} \tag{4}$$

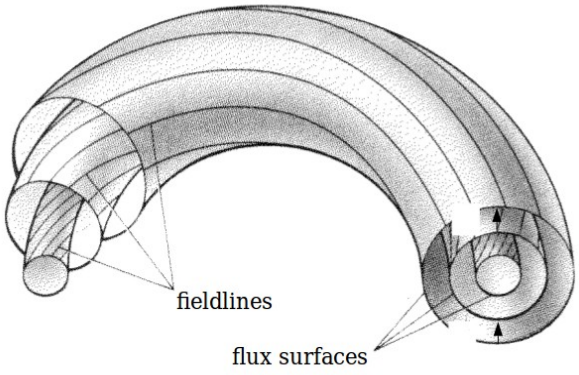

Figure 9: Fieldlines and the corresponding flux surfaces. The flux surfaces are nested with the magnetic axes in the middle.

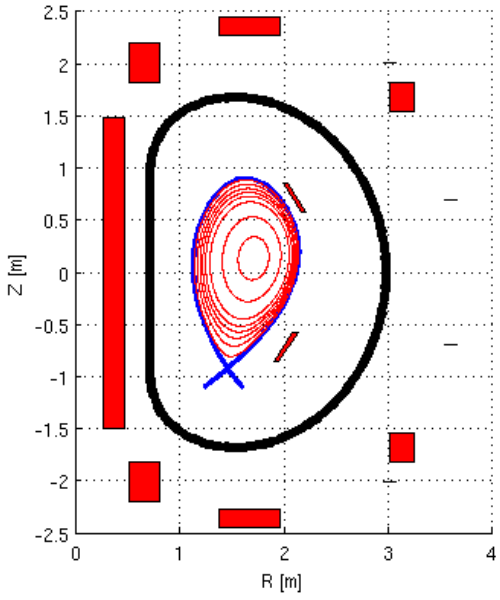

Figure 10: AUG flux surfaces (red) with q=2, 3, 4, 5 and the separatrix (blue) are plotted within a TF coil (black)

If we neglect the ripple from the TF coils, a fieldline started inside the plasma region and projected to the poloidal cut will be at the exact same R and Z coordinates after one poloidal circulation. These deformed circles expanded in toroidal direction are called closed flux surfaces (red lines in figure 10), because the magnetic flux is constant on each point of a flux surface, as is the pressure. Fieldlines cannot cross each other, so every fieldline that has a single point inside the plasma (respectively a flux surface), never leaves the plasma (or crosses the flux surface). The flux surfaces are concentric. When decreasing the distance to the plasma border the flux surface converges to the separatrix. This separatrix can be understood as a border that separates closed and open flux surfaces. Of course fieldlines are always closed; open flux surfaces are generated by fieldlines that include points outside the TF coils. In figure 10 the separatrix crosses itself below the plasma. This is called the x-point or null. The magnetic field near the x-point is mostly toroidal. Tokamaks can have more than one x-point. The magnetic field of MAST that is used in this study has two x-points, one above and one below the confined plasma. The separatrix divides the R-Z plane in several areas. Three in the case of the used AUG equilibrium. One inside the plasma (confined plasma), one below the x-point (private region) and the rest.

Scrape Off Layer

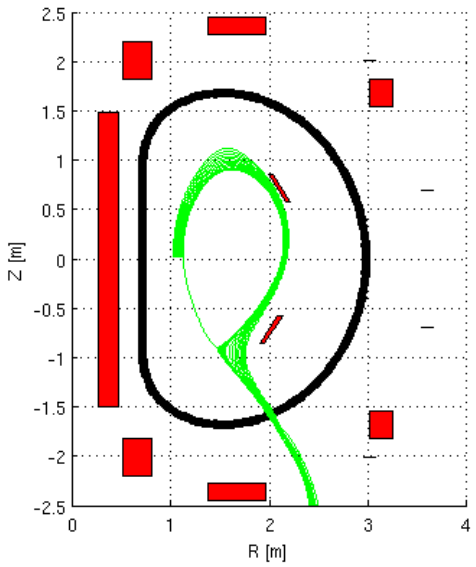

Figure 11: Poloidal cut of AUG. The particle flux starts on the left and wanders around the plasma in clockwise. When it comes close to the x-point the plasma flux expands.

The Scrape Off Layer (SOL) is the area directly outside the plasma (and separatrix) in which the particle density is low but non-zero. Particles can cross the separatrix by diffusion. Particles in the SOL are called lost particles. They have to be led away in a controlled manner, since they still have high kinetic energy and could damage the surrounding vessel wall. They are absorbed by the divertor.

In this study the tracing of fieldlines and ions always begins in the SOL. But it does not matter on which poloidal angle they start since their trajectory brings them to any other poloidal angle, when traced in both toroidal directions. Their paths are aligned to the separatrix.

Divertor

The divertor is a device that blocks the lost particles' paths and absorbs them (see figures 2 and 3). The impact of particles can erode particles from the divertor material. They must be denied to backscatter into the plasma region since impurities in the plasma affect the plasma burning. The divertor has to withstand different types of particles; thermal deuterium and tritium ions as reactants of the fusion, high energy neutrons, products of the fusion, that carry a kinetic energy of $\sim$14 eV and helium as product of the fusion.

A geometric improvement in order to increase the possible heat load, is to increase the plasma-wetted surface of the divertor. This can be done by expanding the particle flux at the divertor (putting the divertor close to the x-point where the flux has the largest expansion, see figure 11). The snowflake divertor [2] suggests using a second order x-point to expand the flux even more. Another option is to tilt the plates to decrease the angle at which the flux hits the divertor. Increasing the connection length (the path from the SOL to the divertor) will increase the plasma-wetted area through radial diffusion and reduce backscattering. This can be done for example by decreasing the poloidal component of the magnetic field near the x-point, or by relocating the divertor to a larger radius. Additionally a relocation to a higher radius will increase the circumference of the divertor, thus enlarging the plasma-wetted area.

AUG

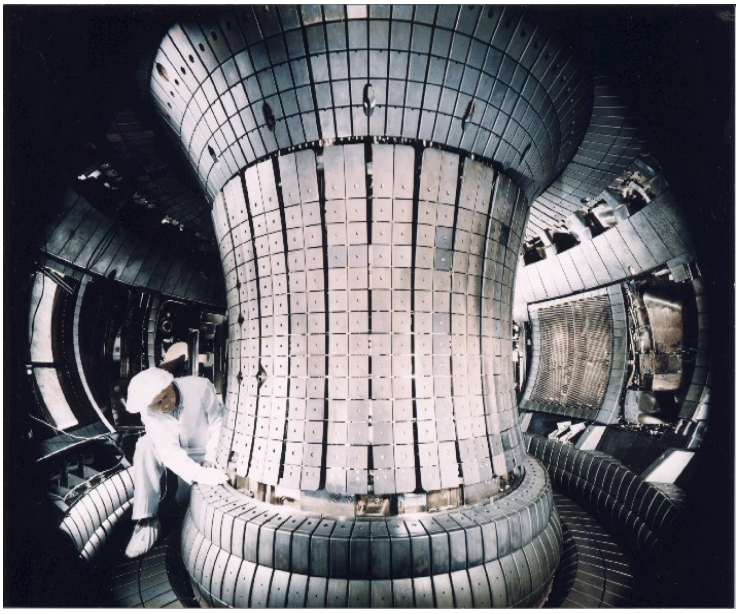

Figure 12: AUG's vacuum vessel from the inside. Picture from http://www.ipp.mpg.de

ASDEX Upgrade (Axially Symmetric Divertor Experiment) is Germany's largest fusion experiment at present. It is a tokamak located at the *Max-Planck-Institut für Plasmaphysik* in Garching, Germany. It went into operation in 1991.

minor plasma radius	0.5 m
major plasma radius	1.65 m
aspect ratio	3.3
TF coil current	1 MA
maximal magnetic field	3.1 T
Plasma current	0.4 MA – 1.6 MA
Plasma heating	27 MW
Plasma temperature	60×10^6 °K – 100×10^6 °K
Electron density	10^{20} m^{-3}

MAST

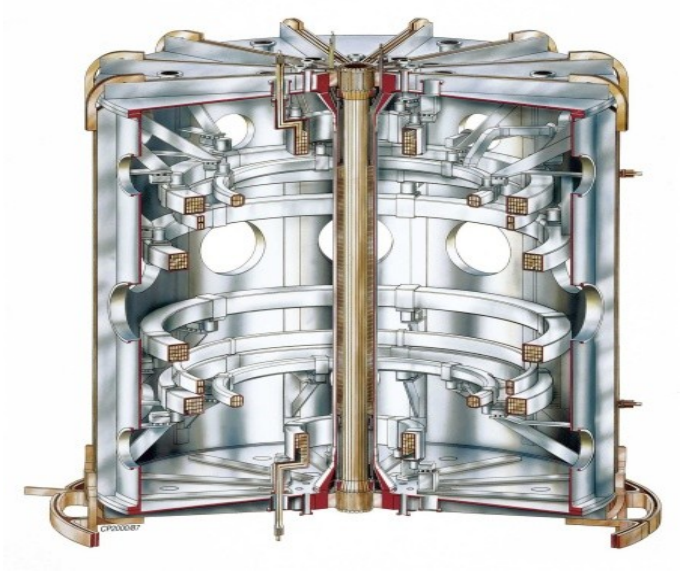

Figure 13: MAST's vacuum vessel, TF and PF coils. Picture from http://www.ccfe.ac.uk

MAST (Mega Ampere Spherical Tokamak) is a tokamak located at the *Culham Centre for Fusion Energy* in Culham, UK. MAST is a spherical tokamak (ST), that means the aspect ratio is much smaller than at conventional tokamaks (see figure 14).

minor plasma radius	0.5 m
major plasma radius	0.7 m
aspect ratio	1.4
TF coil current	170 kA
toroidal magnetic field	0.6 T
Plasma current	1.3 MA
Plasma heating	5 MW
Plasma temperature	23×10^6 °K
Electron density	$10^{20}\,m^{-3}$

One main advantage of STs is that lower magnetic fields are needed to keep the plasma stable as stated in [3]. So a ST's TF coils carries a lower electric current, giving them a smaller cross-section, so the particles have a lower hit probability.

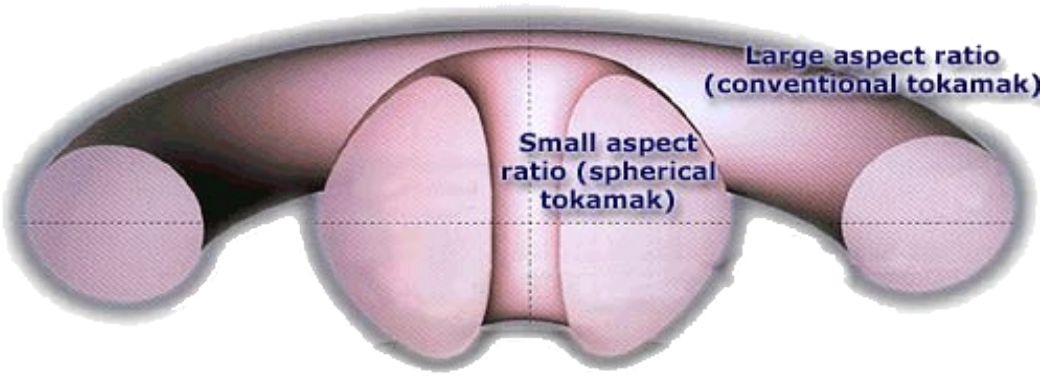

Figure 14: Comparison of spherical tokamak and conventional tokamak's aspect ratios. STs have the shape of a a cored apple, due to the smaller aspect ratio. Picture from http://www.ccfe.ac.uk

Another advantage of MAST for this study is that the TF coils have a rectangular shape (see figure 15) that leaves some room in the corners which will be used for the Super-X divertor in MAST Upgrade and could be used for for guiding the particles to a maximal radius where the gaps between the TF coils are larger.

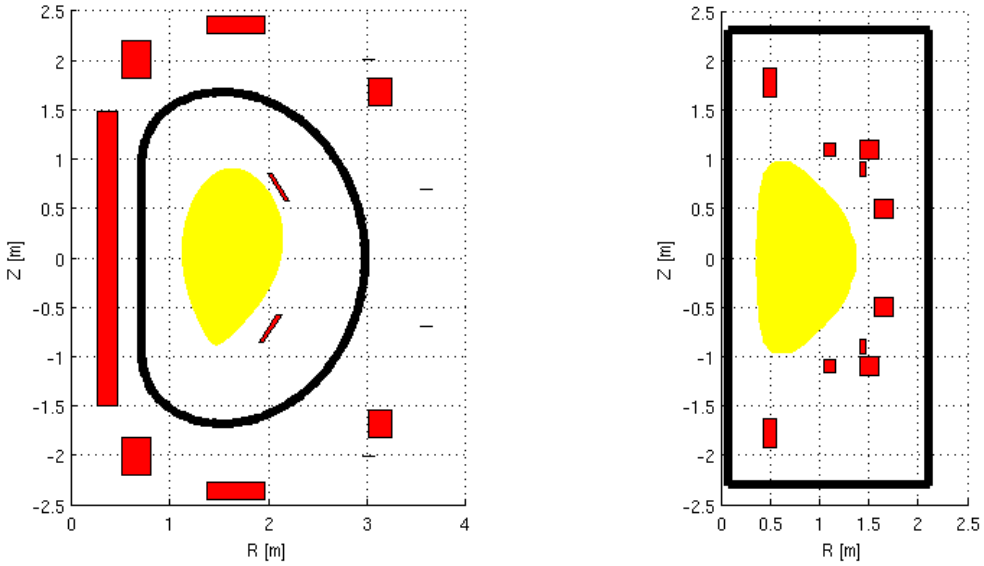

Figure 15: ASDEX Upgrade (left) and MAST (right) PF and TF coils. The PF coils are plotted with their realistic size as red rectangles. The TF coils are plotted as thick black lines but their size in the picture does not resemble their real expansion. The confined plasma is drawn yellow. Both plasmas seem to have about the same size in the poloidal cut. But since the AUG plasma is at a higher radius its volume is larger.

3 Particle Tracing

When tracing particles only single particles are considered. Particle-Particle interactions and the effect of a particle on the magnetic field are neglected (for an existing equilibrium which already includes the plasma current). The Guiding Centre approach is a method to calculate the trajectory of a charged particle without solving the full equations of motion.

$$m \cdot \dot{\boldsymbol{v}} = \boldsymbol{F} + q \cdot \boldsymbol{v} \times \boldsymbol{B} \tag{5}$$

Guiding Centre assumes the magnetic field is spatially constant (at least on the gyroradius). The particle spirals around a fieldline. In a first order approximation the gyrocentre follows the fieldlines. The trajectory of the particle is disassembled into the motion of the gyrocentre and the gyration around it, which then is neglected. If there are additional forces F besides the Lorentz force that are perpendicular to the magnetic field they lead to drifts.

$$\boldsymbol{v}_{\mathrm{GC}} = \boldsymbol{v}_{\parallel} + \frac{\boldsymbol{F} \times \boldsymbol{B}}{q \cdot B^2} \tag{6}$$

$$m \cdot \dot{\boldsymbol{v}}_{\parallel} = \boldsymbol{F}_{\parallel} \tag{7}$$

The first term of (6) means the gyrocentre follows the fieldlines. The second term is the drift of the particle. There are several types of drifts. A force parallel to the magnetic field has an effect on the particle as if there was no magnetic field.

Fieldlines

A particle's trajectory is dominated by the path of the fieldlines. Fieldlines are mathematical constructions that are used to visualise vector fields. They are parallel to the field in every point. In this case we concentrate on the fieldlines of a magnetic field. The fieldline is followed along a one dimensional parameter and projects it into three dimensional space. Since the fieldline must be parallel to the magnetic field, the curl of the fieldline's tangent with the field has to vanish. In most cases solving this equation for fieldlines is not possible without resorting to numerical methods.

$$\boldsymbol{r} : \mathbb{R} \rightarrow \mathbb{R}^3 \tag{8}$$

$$d\boldsymbol{r} \times \boldsymbol{B} = 0 \tag{9}$$

Curvature and ∇|B| Drift

If the magnetic field is not constant but its gradient is neglectable on scales of the gyroradius, the Guiding Centre approach still works but there is an additional force from the magnetic moment (induced by the gyration) and the gradient in the magnetic field. This force results in the ∇|B| drift. When following a curved fieldlines there is the centrifugal force that leads to the curvature drift. If we add the ∇|B| drift and the curvature drift we get as drift velocity:

$$\boldsymbol{v}_D = \frac{c \cdot m}{q \cdot |\boldsymbol{B}|} \cdot \left(v_{\parallel}^2 + \frac{\boldsymbol{v}_{\perp}^2}{2} \right) \cdot \frac{\boldsymbol{B} \times \nabla |\boldsymbol{B}|}{\boldsymbol{B}^2} \tag{10}$$

The indexes parallel and perpendicular are meant in respect to the direction of the fieldline. From the drift equation we see that the kinetic energy of the particle will affect its trajectory through the parallel and perpendicular velocity. A higher energy will result in a higher deviation from the fieldline.

Magnetic Mirror

The pitch angle describes the distribution of the velocity into velocity parallel to the magnetic field and velocity perpendicular to the magnetic field. The perpendicular velocity is the speed of the gyration around the fieldline. η is defined as the arctangent of the pitch angle.

$$\eta = \frac{v_{\parallel}}{v} \tag{11}$$

The magnetic moment is conserved along the trajectory as long as no collisions occur.

$$\mu = \frac{m \cdot v_{\perp}^2}{2 \cdot |\boldsymbol{B}|} = const \tag{12}$$

The kinetic energy is divided up in one part being in the velocity parallel to the guiding centre trajectory and the rest is in the gyration (perpendicular velocity). To conserve the magnetic moment the parallel velocity decreases when the magnetic field increases and vice versa. The index 0 is used for parameters at the start point of the particle.

$$v_{\perp}(\boldsymbol{r}) = v_{\perp}(\boldsymbol{r_0}) \cdot \sqrt{\frac{|\boldsymbol{B}(\boldsymbol{r})|}{|\boldsymbol{B}(\boldsymbol{r_0})|}} \tag{13}$$

The perpendicular velocity can be rewritten as η and the kinetic energy at the start point. The kinetic energy E is conserved along the way since no particle interactions are assumed. When there is no parallel energy left the particle will not go any further; it is reflected. So if η at the start point is too small the particles cannot go to areas of a too high magnetic field. Particles may move to positions r which fulfil the following condition:

$$\eta(\boldsymbol{r_0}) > \sqrt{\frac{|\boldsymbol{B}(\boldsymbol{r})|}{|\boldsymbol{B}(\boldsymbol{r_0})|} - 1} \tag{14}$$

Lamor Radius

The particles gyrate around the guiding centre trajectory. The size of the Lamor Radius (gyroradius) is

$$r_g = \frac{m \cdot v_\perp}{|q| \cdot |B|} \tag{15}$$

This can be rewritten using (13) and replacing the orthogonal velocity at the start point with the kinetic energy.

$$r_g(\boldsymbol{r}) = \sqrt{\frac{2 \cdot m \cdot E \cdot (1-\eta_0^2)}{q^2 \cdot |\boldsymbol{B}(\boldsymbol{r})| \cdot |\boldsymbol{B}(\boldsymbol{r_0})|}} \tag{16}$$

Violation of the Guiding Centre Approximation

If B is not spatially constant Guiding Centre is still a good approximation as long as the variation of B on the gyroradius is small. With higher ξ, the trajectory of that particle is less reliantly determined by the Guiding Centre approach.

$$\xi = \frac{r_g \cdot \nabla B}{B} \ll 1 \tag{17}$$

4 Numerical Approximation

4.1 Magnetic Field

Vacfield

The vacuum magnetic field from the coils is computed with the Vacfield code. It uses Biot-Savart's Law to compute it from the currents given as input.

$$\boldsymbol{B}(\boldsymbol{r}) = \frac{\mu_0}{4 \cdot \pi} \cdot \int_V \boldsymbol{J}(\boldsymbol{r}') \times \frac{\boldsymbol{r} - \boldsymbol{r}'}{|\boldsymbol{r} - \boldsymbol{r}'|^3} \, d^3\boldsymbol{r}' \tag{18}$$

The currents are approximated as infinitesimal thin current filaments. The input file consists of a list of points in cylindrical coordinates and the electric current that flows between them. For each filament a new list is started using a separator flag. The magnetic field gets computed on a cylindrical grid. The resolution and expansion are defined in Vacfield's input files. Due to the approximation as filaments it may happen that the magnetic field of a grid point is unreasonably high. This happens if a grid point is extremely close to the current filament.

Equilibrium

The Vacfield code gives us the magnetic fields of TF and PF coils. But the magnetic field from the plasma current is more complicated to get, since the plasma current itself depends on the magnetic field. So we would need to solve the equations of motion for the enormous number of particles and for the magnetic field simultaneously since the charged particle influence one another. A way out of this is shown by the theory of magnetohydrodynamics. The Grad-Shafranov equation is a two dimensional approximation for solving the equilibrium. It is a non-linear, elliptic partial differential equation for the flux function. It can be used since tokamaks are (almost) axisymmetric.

$$\Delta^* \Psi = -\mu_0 \cdot R^2 \cdot \frac{d\,p}{d\,\Psi} - 0.5 \cdot \frac{d\,(R \cdot B_{tor})^2}{d\,\Psi} \tag{19}$$

$$\Delta^* = R \cdot \frac{\partial}{\partial R}\left(\frac{1}{R}\frac{\partial}{\partial R}\right) + \frac{\partial^2}{\partial Z^2} \tag{20}$$

p is the pressure. Ψ is the poloidal flux, see equation (4). The magnetic field can be calculated from Ψ. The ripple in toroidal direction has to be added afterwards.

$$\boldsymbol{B} = \frac{\nabla \Psi \times \boldsymbol{e_\theta}}{R} + B_{tor} \cdot \boldsymbol{e_\theta} \tag{21}$$

There are codes like VMEC/NEMEC that can compute the 3D equilibrium directly, by minimizing the energy. An explanation on these codes can be found in [7]. [5] shows that the difference for the used AUG equilibrium (shot #21089) when computing the 3D field directly and when using a 2D code and later adding the ripple is neglectable.

4.2 Tracing

The fieldlines and the particles are traced with the Gourdon code. This chapters gives a brief introduction in the mechanics of the fieldline tracing. The code has to be provided with the magnetic field and a start point for the fieldline. For the tracing of single particles the mass, charge, kinetic energy and pitch angle have to be provided, too. The drifts are added at each step of the tracing. The implementation of the drifts is not described in this text.

Interpolation of the Magnetic Field

The magnetic field is computed on a cylindrical grid. For the fieldline tracing it is necessary to be able to get the magnetic field of any arbitrary point inside the grid. A trilinear interpolation is used. The magnetic field is not transformed in Cartesian coordinates first.

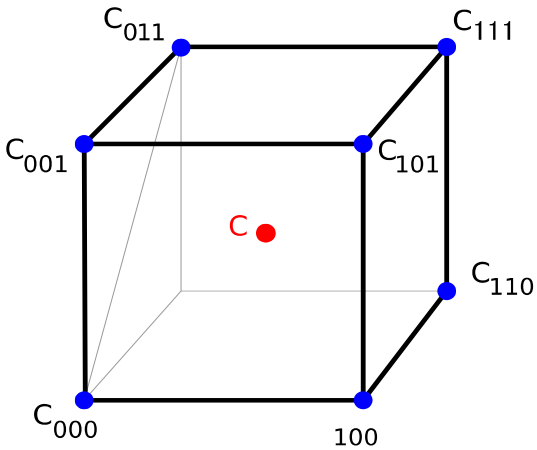

Figure 16: The point C is to be interpolated by using the 8 corners of the cube around it. The three indexes are one for each dimension, each either 0 or 1. Picture from http://en.wikipedia.org/wiki/Trilinear_interpolation

The magnetic field at the eight corners of the grid around the interpolation point are needed. This is done in this calculation by giving B three indexes i, j, k. The usage of the indexes is illustrated in figure 16. Δr is the distance in radial direction to the last grid point. r_i' is the radial distance to the corner with the index i.

$$r_i' = \begin{Bmatrix} \Delta r & i=1 \\ 1-\Delta r & i=0 \end{Bmatrix} = i\cdot\Delta r + (i-1)\cdot(\Delta r-1) \tag{22}$$

Δz and Δφ are defined analogously. Then the magnetic field on the interpolation point is:

$$\boldsymbol{B}(\Delta r,\Delta\varphi,\Delta z) = \sum_{i,j,k=0}^{1} \boldsymbol{B}_{ijk}\cdot r'\cdot\varphi'\cdot z' \tag{23}$$

Fieldline Tracing

One fieldline point is computed recursively by using the magnetic field and the fieldline's former points. Let us call the normalised magnetic field **b**. n is the index of the fieldline point.

$$\boldsymbol{b}_n = \frac{\boldsymbol{B}(\boldsymbol{r}_n)}{|\boldsymbol{B}(\boldsymbol{r}_n)|} \tag{24}$$

$$\boldsymbol{r}_{n+1} = \boldsymbol{r}_n + \boldsymbol{b}_n \cdot \Delta l \tag{25}$$

Equation (25) shows a simple technique that recursively defines the next point by adding **b** multiplied with a fixed step length Δl. One way to increase accuracy is to dynamically choose Δl. This can be done by looking at the convergence of the difference in results when decreasing Δl. This method, its drawbacks and possible improvements are discussed in [4].

The Gourdon code traces fieldlines by using the Adams-Integration-Method. That means it takes the magnetic field at the four preceding fieldline points into account.

$$\frac{d^0\boldsymbol{b}_n}{dn^0} \approx \boldsymbol{a}_{n,1} = \boldsymbol{b}_n \qquad \begin{aligned} c_1 &= 1 \\ c_2 &= 1/2 \\ c_3 &= 5/12 \\ c_4 &= 3/8 \\ c_5 &= 251/750 \end{aligned}$$

$$\frac{d^i\boldsymbol{b}_n}{dn^i} \approx \boldsymbol{a}_{n,i} = \boldsymbol{a}_{n,i-1} - \boldsymbol{a}_{n-1,i-1} \tag{26}$$

$$\boldsymbol{r}_{n+1} = \boldsymbol{r}_n + \Delta l \cdot \sum_{j=1}^{5} c_j \cdot \boldsymbol{a}_{n,j} \tag{27}$$

The derivatives are weighted with fixed factors c_j in the computation. This is no Taylor series since the derivatives of the field cannot be computed at the point $\mathbf{r}_n$.

III Approximating Solid TF Coils

In most cases equilibria are made to investigate effects in or close to the plasma. Because the distance from the points of interest to the TF coil is much larger than the extent of the coil, it is a sufficient approximation to handle the coils as single current filaments when calculating the magnetic field. But in this study the near-field effects of the TF coils matter so the magnetic field from the TF coils must represent the case of solid coils.

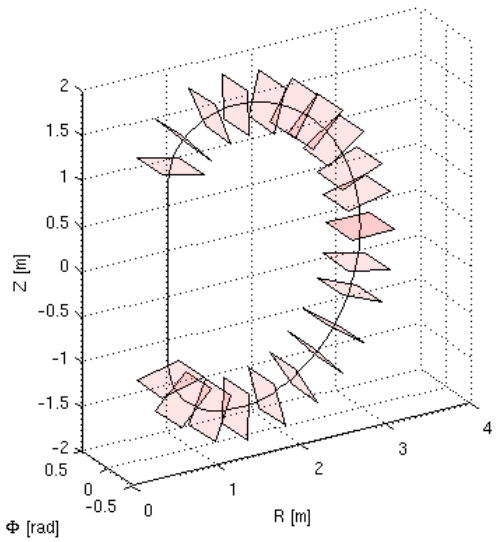

Figure 17: The D-shaped black line is the original filament. The red planes are perpendicular to the filament's path.

The Vacfield code is used to compute the vacuum magnetic field from the current filaments. To get a better representation of solid coils the number of filaments to represent a solid coil is increased.

The original filament's points (black D-shaped line in figure 17) are expanded to several points on the plane perpendicular to the coil's path (red planes in figure 17). The projection of the new filaments to the perpendicular planes can be seen in figure 18.

To keep the computations simple, the real cross-section (which varies at AUG with the poloidal angle) is approximated as a square. This still shows effects that are due to the sharp edges. Later on circle and elliptic cross-section areas are tested.

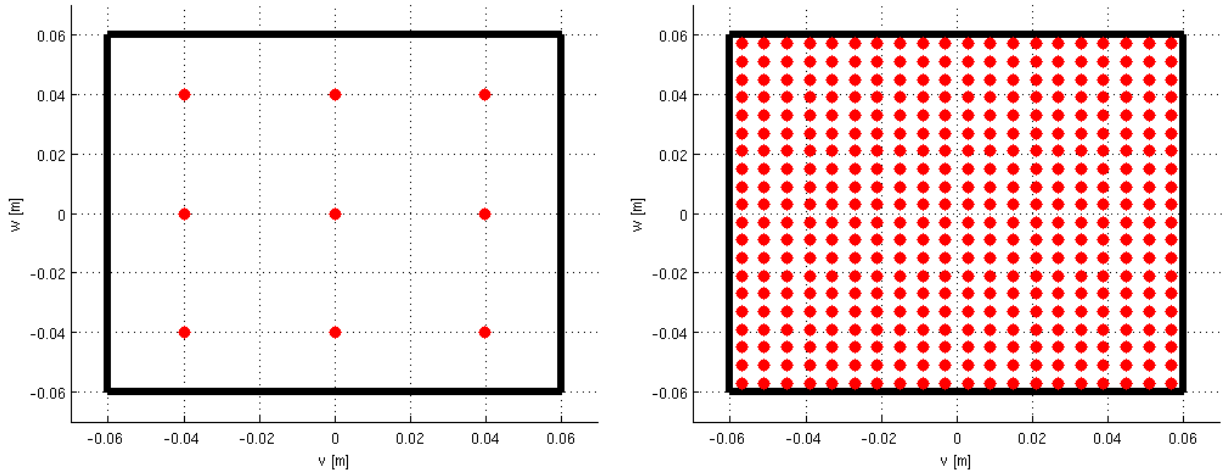

Figure 18: The left plot shows 3^2 filaments (red dots) the right plot shows 20^2 filaments. The black frame shows the edges of the coil.

1 Creating the Coil's Numerical Data

The AUG TF coils are D-shaped and have no sharp corners in the R-Z plane. The cross-section planes are spanned by the vectors **v** and **w**, n indexes the points of the one-filament coil, **r** is the position vector. **u** shows in direction of the filament's path, it is an auxiliary construction for determining **v** and **w.**

$$\boldsymbol{u}_n = \boldsymbol{r}_{n+1} - \boldsymbol{r}_{n-1}$$

$$\boldsymbol{v}_n = \boldsymbol{e}_\varphi \qquad \boldsymbol{w}_n = \frac{\boldsymbol{u}_n \times \boldsymbol{v}_n}{|\boldsymbol{u}_n \times \boldsymbol{v}_n|} \tag{28}$$

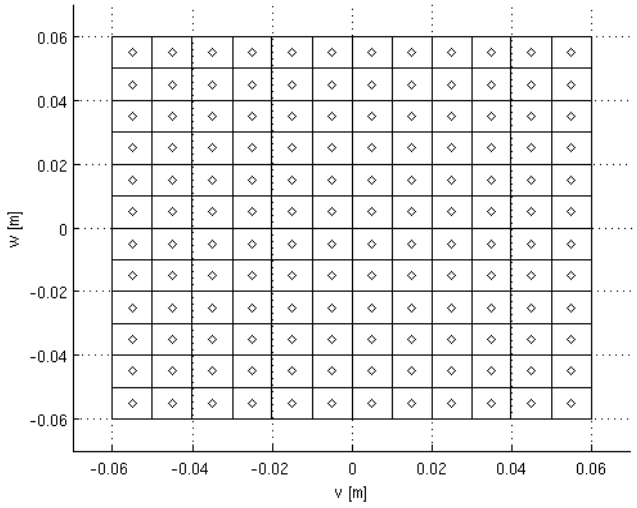

Figure 19: Filaments (rhombi) with the square area represented by them around it.

In the code a check is run after determining these vectors that makes sure a always points away from the plasma, so the filaments wont be twisted. When creating the cross-section geometry (red planes in figure 17), each filament represents a square area around it. I have chosen each filament's electric current to be the same, so the areas represented by the filaments have the same expansion. The edge length of the square is referred to as s, the number of filaments per edge is referred to as F.

With j, k being indices resembling the different filaments within a cross-section the position of the filaments in square coils can be described as:

$$x_j = \frac{s}{2} + \left(j - \frac{1}{2}\right) \cdot \frac{s}{F} \qquad y_k = \frac{s}{2} + \left(k - \frac{1}{2}\right) \cdot \frac{s}{F} \qquad j,k = 1, \ldots, F \tag{29}$$

This geometry has to be applied to the whole coil.

$$\boldsymbol{r}_{n,j,k} = \boldsymbol{r}_n + \boldsymbol{v}_n \cdot x_j + \boldsymbol{w}_n \cdot y_k \tag{30}$$

The filaments positions $r_{n,j,k}$ are used as the input for the Vacfield code which computes the vacuum magnetic field from them. This method only works if there are no sharp corners in the coil. For MAST with its rectangular coils this approach would result in a narrowing of the coils at the corners. **w** at the corner of the coil must not be normalised but stretched to the length of the square root of 2. Otherwise the cross-section defined in figure 19 would not apply to the legs of the coil but to the plane in the corner which is rotated by 45° in the poloidal cut (see figure 20).

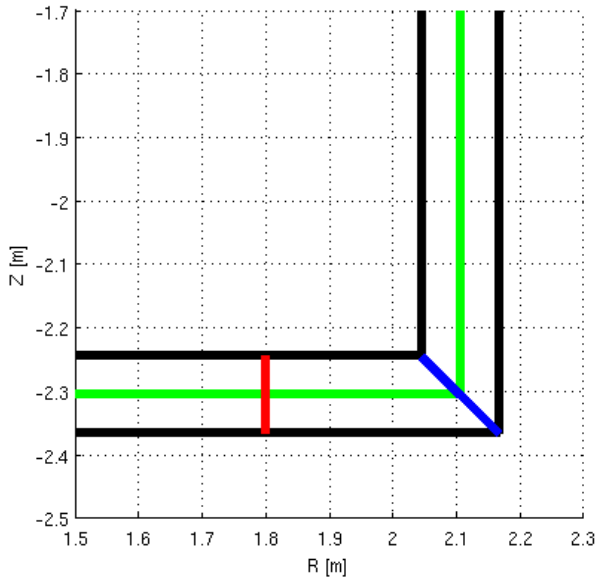

Figure 20: The green line is the original one-filament. The black lines show the expansion of the cross-section. Red is a 12 cm cross-section, blue shows that the vector a has to be stretched by the square root of two.

Since the Vacfield code interpolates between the filament points as straight lines, only four points are needed for the MAST coils. They and the corresponding **u**, **v**, **w** were adjusted by hand.

Ringwise Approximation

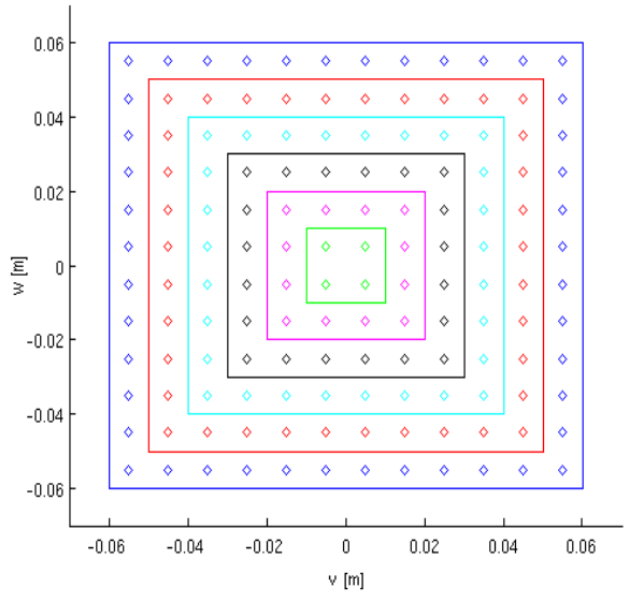

Figure 21: Ringwise approximation of the coil. The rhombi are the filaments. The colours specify the membership to a ring.

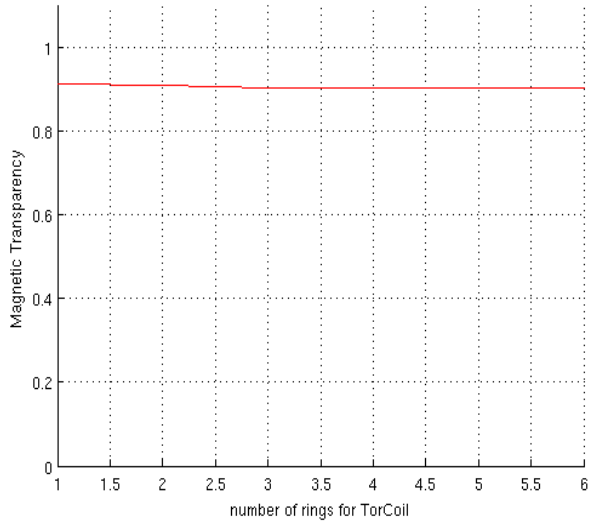

Figure 22: Hollow coils (rings=1) have a (slightly) higher chance of not being hit by fieldlines, since B is higher near the edge.

Vacfield's computation time is roughly linear in the number of used filaments. To save computation time only the outmost „ring“ is used for the AUG calculations (with adapted currents). That would be the blue ring in figure 21.

This ringwise approximation increases the magnetic field at the very edge of the coil to infinity for F → infinity. This can be avoided by choosing distance between two grid points of the magnetic field smaller than the distance of the filament to the coils border. But this could not be done in this thesis since the field files would have grown too large.

To verify that this ringwise approximation has no significant impact on the outcome of this study, the Magnetic Transparency is calculated with all filaments, with only the outmost ring of filaments and with any number of rings in between.

Figure 22 shows the development of M depending on the amount of rings considered. One ring means only the outmost one was used for the computation, Two rings mean the blue and red one from figure 21, and so on. This approximation affects the M less than 0.01 at AUG with s=12 cm, F=12 and d=1 cm. Other test cases show a similar effect and a similar size of the error.

2 Resulting Magnetic Field

When changing the number of filaments, the magnetic near-field of the TF coils changes. Figure 23 shows an AUG TF coil's cross-section; the black lines form the edges. It is not a perfect square since the plot is in cylindrical coordinates. The red dots represent the filaments used to calculate the magnetic fields. The coloured lines are lines with constant B. It is assumed that the near field shows similar behaviour at each poloidal angle (the plots are valid for each plane in figure 17). So we concentrate on Z=0 m.

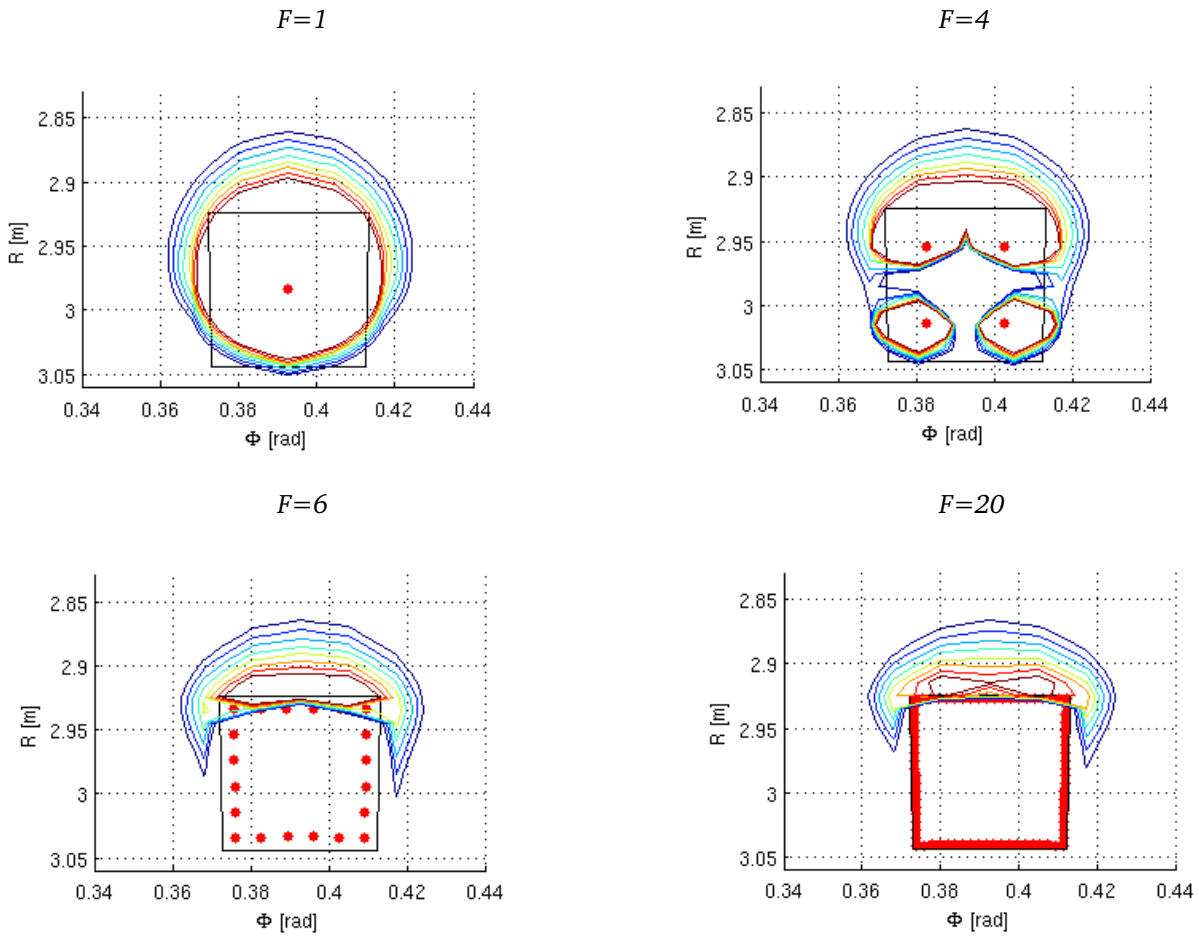

Figure 23: Contour plots at |B|=2.5, ..., 3.0 Tesla with F= 1, 2, 6, 20 from the AUG equilibrium. The shape of the near-field adapts to the shape of the coils. Note that this is not the vacuum field of the coils but B from the equilibrium, so |B| is higher on the side facing the plasma.

With one filament per coil the magnetic field close to the coils has the geometry that we would expect from circle shaped cross-sections. With increasing F the shape converges to the shape given by solid coils. We can see that the contour lines for constant |B| are drawn towards the side facing the plasma and are aligned to the coil's border (when using sufficiently high F). The coils are “shielded” by the high magnetic field which works as a magnetic mirror for the particles.

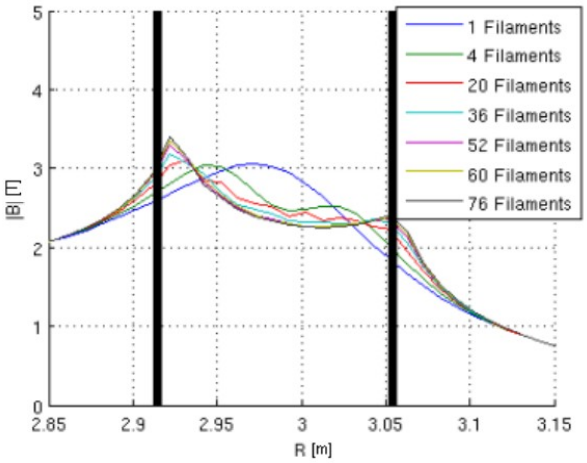

Figure 24: The black lines show the coil's borders. The coloured lines show the absolute value of B in dependence of R. The plot is made for the Z=0 m and φ=0.025 plane (which is just outside the TF coil).

The more filaments are used, the closer the filaments get to the border of the coil. This increases the gradient of |B| close to the coil's edge.

Figure 24 shows the absolute value of B for varying amount of filaments. |B| is plotted against R on the φ=0.025, Z=0 m line. This is just outside the coil.

3 Influence on the Fieldlines

The effect of the filament density on the magnetic field, therefore on the fieldlines, is localized to the region close to the coils. With increasing filament density the filaments get closer to the coil's boundary, thus the gradient of the absolute magnetic field increases (see figure 24). The higher gradient pushes the fieldline away from the TF coil's edge (figure 25). So less fieldlines hit the coils for increasing F.

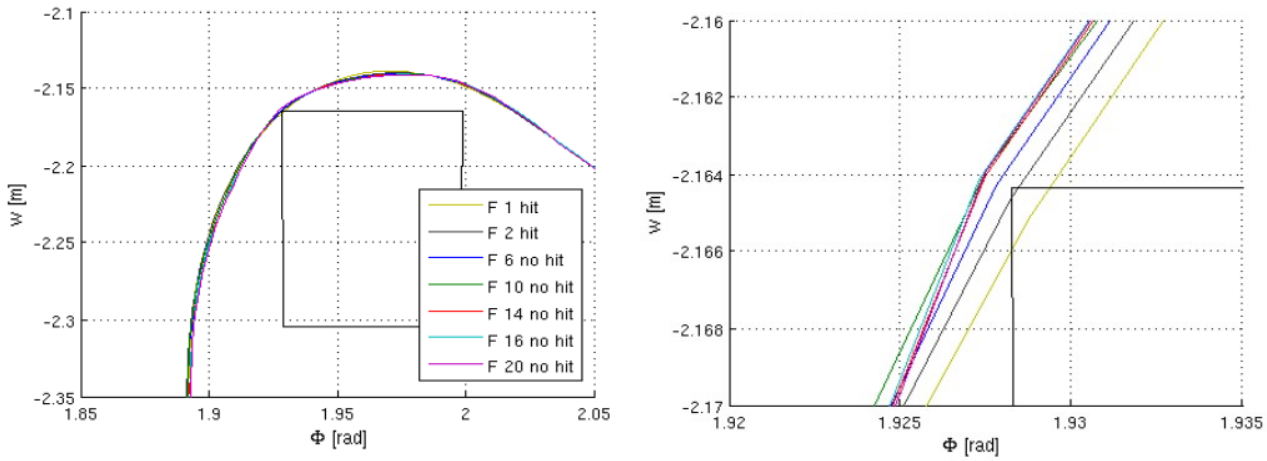

Figure 25: AUG TF coil (black square), fieldlines all started at the same point in the SOL, but for different cases of F=1, 2, 6, 10, 14, 16, 20. The right figure is a zoom of the upper left edge of the coil. The fieldline hits the coil with low F but evades it when F grows high enough.

To show this, 450 fieldlines are started in the SOL using the AUG equilibrium. All are started at the same R and Z coordinates in a toroidal interval of φ from 0° to 45°. In figure 26 we see that with two filaments 118 fieldlines hit the TF coils, when using twenty filaments only 110 fieldlines hit the coils. The same effect is witnessed for each test case examined in this thesis.

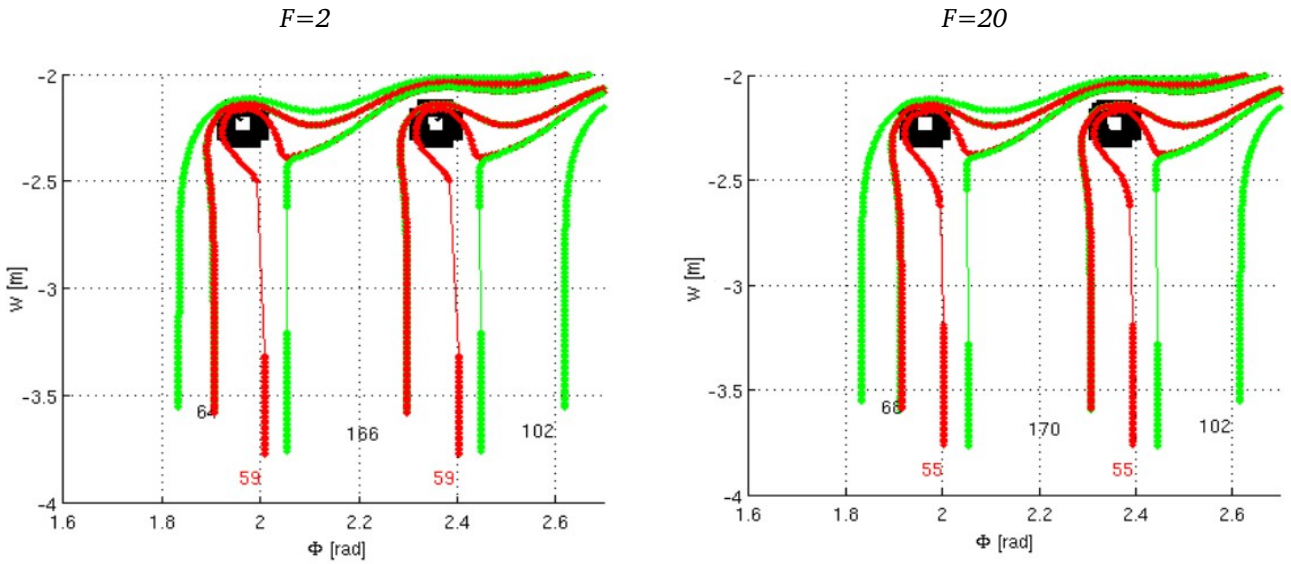

Figure 26: TF coils. Only the first and the last fieldline that hit/do not hit the coils are plotted. The black numbers are the number of fieldlines in between them that do not hit the coils. The red numbers are the fieldlines that hit the coils. The left picture is with F=2, the right one with F=20. More fieldlines leave with increasing number of filaments to represent the coils.

This leads to the conclusion that the equilibrium with one filament can be used as a worst case approximation, meaning that we will get a worse result (more fieldlines hitting the coils). This proves useful when a large number of new geometries has to be tested. The new geometries have to be implemented in the code that checks for hits, but the effort to recalculate new equilibria for each test scenario can be spared until the best candidates are found.

If the coils have a circle shaped cross-section this pushing away of the fieldline with increasing filaments is weakest compared to other shapes. This is because the magnetic field of one filament already has this circle shape (see figure 23). The effect is strongest at cross-section geometries with a sharp corners at the intersection point with the fieldlines, since they have the least resemblance with the circle shape of one filament.

IV Fieldline Tracing

As a first approximation the particles are expected to move along the fieldlines. This approximation is best for low energy particles (small drift) with most of their energy in the velocity parallel to the fieldlines (least magnetic reflections) and no diffusion. To calculate the fieldlines from a magnetic field, the Gourdon code was used with the parameters defined in VIII 3.2.

1 Magnetic Transparency M

The Magnetic Transparency resembles the percentage of fieldlines that do not hit the TF coils but leave the torus. A number of fieldlines L are started in a toroidal interval, all at a specific R and Z coordinate in the SOL. The toroidal interval is chosen to be the same as the interval between two TF coils. M is not defined for position inside the separatrix or outside the TF coils. It only makes sense if all fieldlines leave the torus, with or without hitting the coils.

$$M = \frac{L_{nohits}}{L} = 1 - \frac{L_{hits}}{L} \tag{31}$$

M depends on

- **L** number of fieldlines started
- **F** number of filaments used to represent solid TF coils
- **d** distance of fieldlines' starting points to the separatrix
- **s** size of the TF coil's cross-section area
- the resolution of the grid the magnetic field is calculated on
- shape of the TF coil's cross-section area

The parameters L, F and the grid of the magnetic field are just numerical crutches. Changing them does not change the represented real case. So M has to converge for all of them. In the following the convergence of F and L will be shown for each case separately. The convergence of M with the magnetic field's grid resolution has not been checked, since it would need a recalculation of the equilibrium for each grid resolution. The used grid resolution can be looked up in the appendix VIII 3.1.

2 Hitcoil Algorithm

The hitcoil algorithm checks which fieldlines hit the coils. It written in Matlab and works as a post-processor for the output of the Gourdon code. Besides the fieldlines it has to be provided with the TF coil's geometry. The geometry data is not linked to the fieldline data, so it is possible to feed it the fieldline data from the one-filament equilibrium and check it for hits with a variety of coil geometries. This could be used as a fast approximation to check different coil geometries, sparing the need to recalculate the fieldlines for each new coil geometry (see III 3 “Influence on the Fieldlines“).

On the downside the fieldlines have to be saved limiting their number and length by the available amount of disk space. The closer a fieldline is started to the separatrix the more toroidal circulations it will make. Due to the post-processor nature it is necessary to save the fieldline's path to the computer's hard disk. Therefore a limit to the tracing is set by the fieldline's length after which the tracing is aborted. The threshold in the Gourdon code was set to 100 m with 1 cm steps. Also the hitcoils's processing speed is slower than a pendant written in Fortran could be. The mechanics of this code are described in detail in the appendix VIII 1.

3 Distance to the Separatrix d

The fieldlines and later the particles are started in the SOL. To clarify the exact position the coordinates are not written in R and Z but as the distance to the separatrix d. This leaves one degree of freedom (along the separatrix' path). At the AUG equilibrium the choice is used to minimize the effect of the ripple from the TF coils. With MAST considerations of symmetry determine that point. **d** is the radial distance of the fieldline's starting point to the separatrix.

The R-Z projection of fieldlines that are started at different d show us that the flux expands at the x-point. As seen in figure 28 at MAST the flux expansion is greatest at the escape point of the fieldlines (their intersection with the TF coils in the poloidal cut). At AUG there is no significant flux expansion at the escape point compared to the outer midplane.

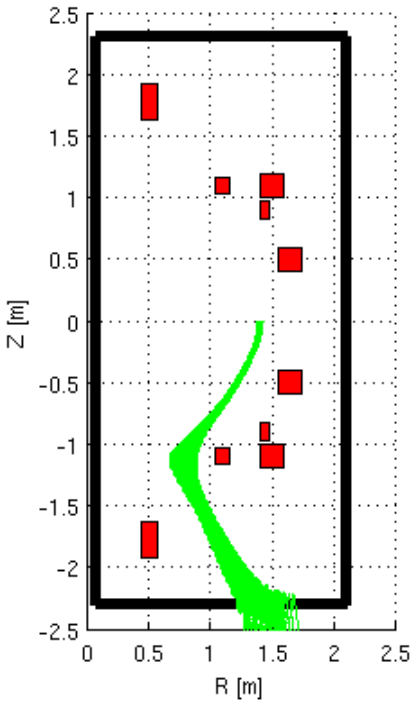

Figure 28: The fieldlines (green) are started at d=1 cm - 5 cm and at the same toroidal angle on the outer midplane (right side of the plasma in the plot).

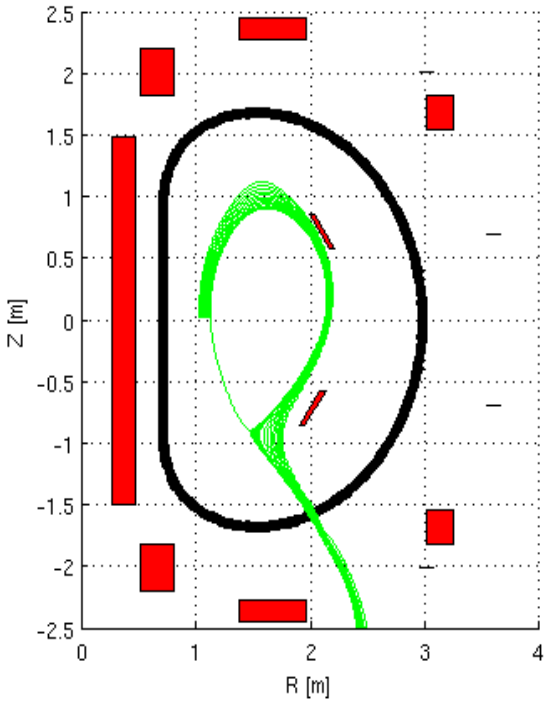

Figure 27: AUG. Projection of the fieldlines to the poloidal cut. The fieldlines start with 1mm stepping (from 0 to 1 cm) and 1 cm stepping (from 2 cm to 10 cm). The d=0 cm fieldline shows the last closed flux surface.

4 ASDEX Upgrade

The magnetic field used for the analysis of ASDEX Upgrade is from shot 21089 at t=4 s, the total plasma current is 0.8 MA and the vacuum magnetic field is 2 T. The TF coil current is 1 MA in the used equilibrium. They are capable of vacuum magnetic fields up to 3.9 T. It is the same equilibrium used in [5].

4.1 Magnetic Field

In the original equilibrium file only one filament per TF coil was used, totally neglecting the coil's cross-section expansion. For this study a lot of new magnetic fields have to be evaluated since the TF coil cross-section's geometry gets altered (new edge lengths and cross-section shapes). But since the performed changes of the cross-section geometry do not change the median point of the electric current these changes are only in the coil's near-field. The region of the plasma is far enough away from the coils for the changes to have a negligible impact on the plasma current. So a recalculation of the equilibrium, like described in II 4.1, is not performed for each new coil geometry. The new magnetic fields are just superpositions. The one filament TF coil's vacuum magnetic field gets subtracted from the original equilibrium. Then the new vacuum field from TF coils with F filaments and a coil's edge length of s is added. The exact configuration parameters used in the Vacfield code can be looked up in VIII 3.1.

4.2 Field Ripple at the Separatrix

The tokamak is often approximated as axisymmetric, meaning it does not change in the toroidal direction. But there are imperfections because of the TF coils, the ripple. This ripple periodically shifts the separatrix a little bit when moving along in toroidal direction. So the R and Z coordinates of the start points (that are chosen in a toroidal interval) have to take this effect into account in order to keep d constant for points started at different toroidal angles. Another approach is to let the fieldlines start on the plasma's High Field Side (HFS). There the ripple is neglectable as shown in [5]. B_{max} respectively B_{min} is the maximal/minimal absolute magnetic field at a constant R and Z from all toroidal points. δ is about 0.01 on the outer midplane and far less (not readable from a linear scale of this magnitude) at the chosen start points.

$$\delta = \frac{B_{max} - B_{min}}{B_{max} + B_{min}} \tag{32}$$

4.3 Scrape Off Layer

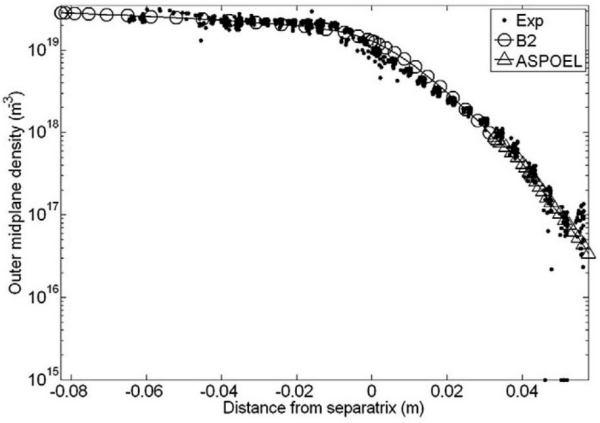

Figure 29: Particle density in dependence of d_{LFS}.

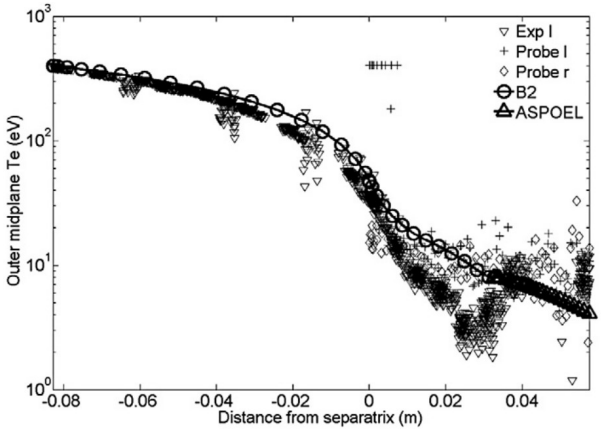

Figure 30: Electron temperature in dependence of d_{LFS}.

The particle density and the particles' temperature drops with d, as we expect from a diffusive process. The data presented in this section is taken from [8].

Figures 29 to 31 show the experimental data compared to data computed by the B2 and ASPOEL codes. The distance to the separatrix in these plots is referring to the outer midplane (d_{LFS}). As we will see in the next section this means we have to multiply with a factor of two to compare it to the d used in this thesis for the fieldlines at AUG. In figure 29 we can see the exponential decay of the particle density. It drops by a factor of 100 from the separatrix to d_{LFS}=5 cm. The same happens to the electron and ion temperature.

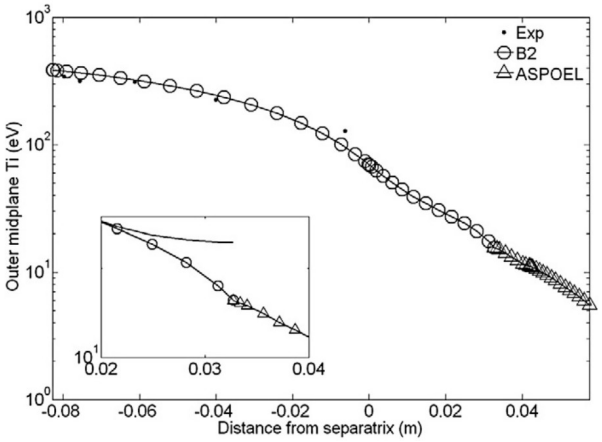

Figure 31: Ion temperature in dependence of d_{LFS}. The small plot is a zoom at the border between near and far SOL.

So it seems reasonable to do the AUG fieldline tracing from d=0 cm to d=10 cm. The data presented is from shot 11437. This is not the same equilibrium that is used in the rest of this study but this data is sufficient to give a clue of what d to consider.

4.4 Escape Area

In this study the start points of the fieldlines at AUG have been chosen to d=0 cm to 10 cm when started on the High Field Side. On the LFS the flux gets compressed; there the d=10 cm line has a distance of 5 cm to the separatrix. The largest flux expansion is near the x point. Until there the sequence of the fieldlines is preserved since fieldlines cannot cross in 3D and the tokamak is axisymmetric. But near the TF coil their paths are not parallel any more and cross each other (see figure 32 near R=2 m and Z=-1.5 m). This is due to the TF coil ripple, which is getting stronger with smaller distance to the coils. Their movement can be understood when looking at figure 36 which is a plot of the escape area perpendicular to figure 32. Near the escape point, the distance of the d=1 cm and the d=10 cm fieldline is about 8 cm. This length depends on the exact location of the x-point.

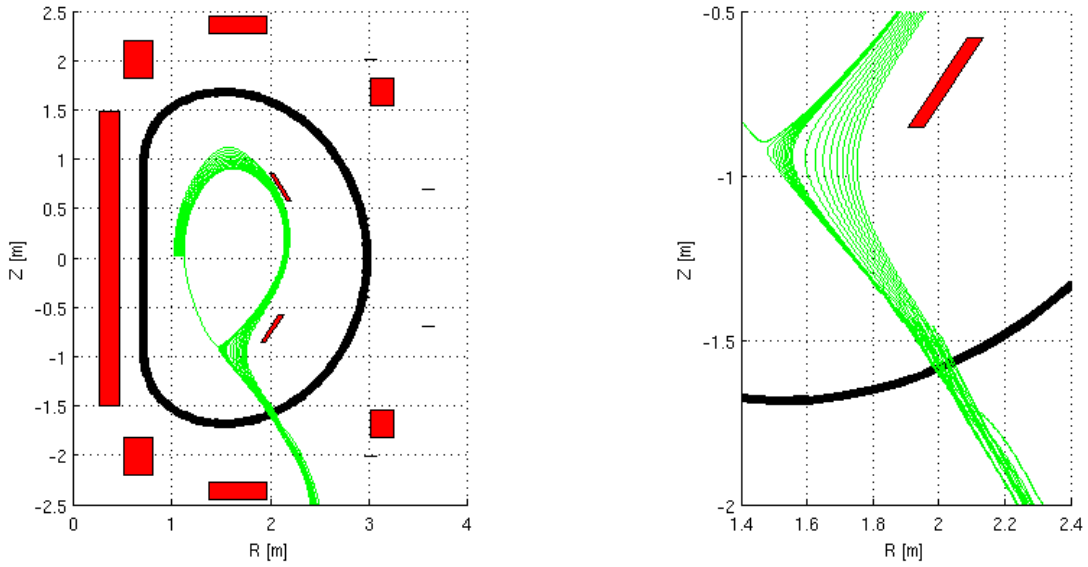

Figure 32: Poloidal cut of AUG with fieldlines started with d up to 10 cm. All fieldlines are started at the same toroidal angle. Note that the starting density of the fieldlines is not constant. Between d=0 cm and 1 cm they are started each mm and from d=2 to 10 cm they are started each cm.

The fieldlines' paths are nearly perpendicular to the coil at the escape point. This is used in the hitcoil algorithm to save computation time and it is used to visualize the fieldlines' paths close to the coils. The plane perpendicular to the coil (and parallel to the fieldline) is plotted in most of the figure showing the fieldlines close to the coils, for example in figure 36. This is the plane generated by the vectors **v** and **w** which were introduced in III 1 “Creating the Coil's Numerical Data“.

With increasing d the escape point shifts up to a higher radius, as shown in figure 33, left plot. With a higher radius the gaps between the TF coils get larger, but the TF coils themselves do not (figure 33, right plot). The relative amount of space not covered by the coils increases.

With the coils covering a smaller area the Magnetic Transparency increases.

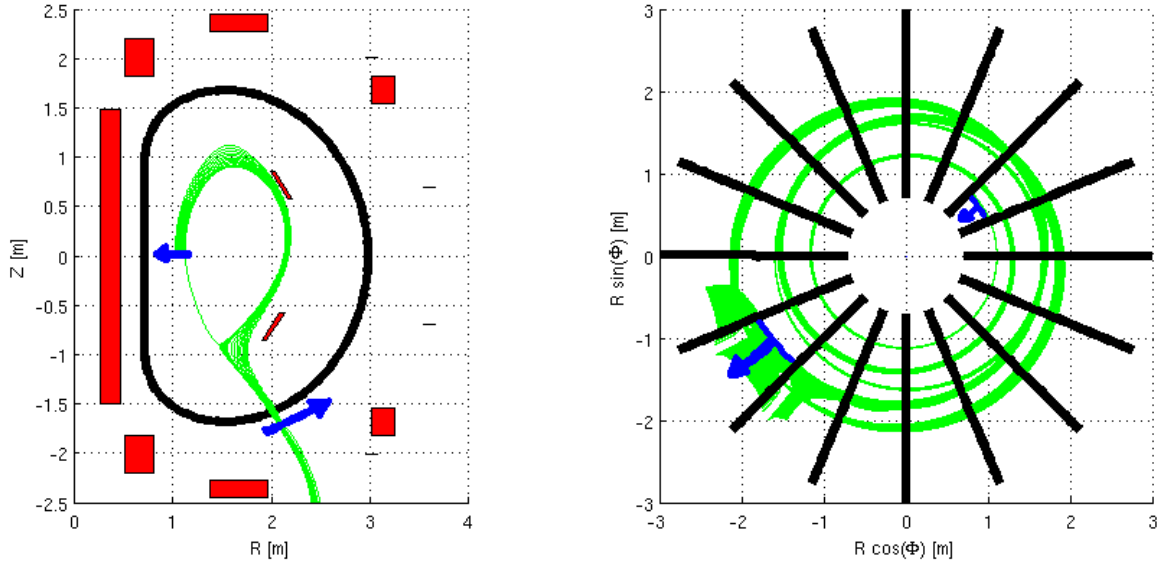

Figure 33: The left plot shows the poloidal cut with TF coil, PF coils and the fieldlines. The right plot shows the TF coils and the fieldlines from above. Increasing d shifts the escape point towards a higher radius (blue arrows).

d is correlated to the amount of particles. The particle density decreases with d. Since the goal is to get the particles from the SOL through the gaps between the TF coils we can concentrate on test cases with values for d at which the particle density is significant. As seen in the previous section values of d up to 10 cm on the HFS respectively 5 cm on the LFS will be sufficient.

9 cm (distance between the d=1 cm and the d=10 cm fieldlines) on HFS correspond to 4.5 cm on the LFS and to 8 cm at the escape point. The tilt of the TF coil at the escape point is ~20°. d is defined on the HFS for the AUG test cases. d_{LFS} is the corresponding distance to the separatrix on the LFS. Assuming a linear dependency we can approximate the escape radius as R(d).

$$R = d \cdot \frac{\Delta s_{escape}}{\Delta s_{start}} \cdot \cos\alpha_{tilt}$$
$$R \approx 0.8 \cdot d \qquad (33)$$
$$R \approx 1.7 \cdot d_{LFS}$$

But this increase of M with d is too small to see at AUG since M(d) also oscillates because of a variation in fieldline density which will be subject of chapter IV 4.8.

There is also a smearing of the escape points' radii for fieldlines that have been started with the same d but at different toroidal angles. Figure 34 shows that the d=1 cm fieldlines distribute over a length of 11 cm. The d=10 cm fieldlines (figure 35) do expand over an length of 6 cm. Strangely the maximal radius for d=10 cm and for d=1 cm is the same. Just the low radius border is shifted upwards compared to d=1 cm.

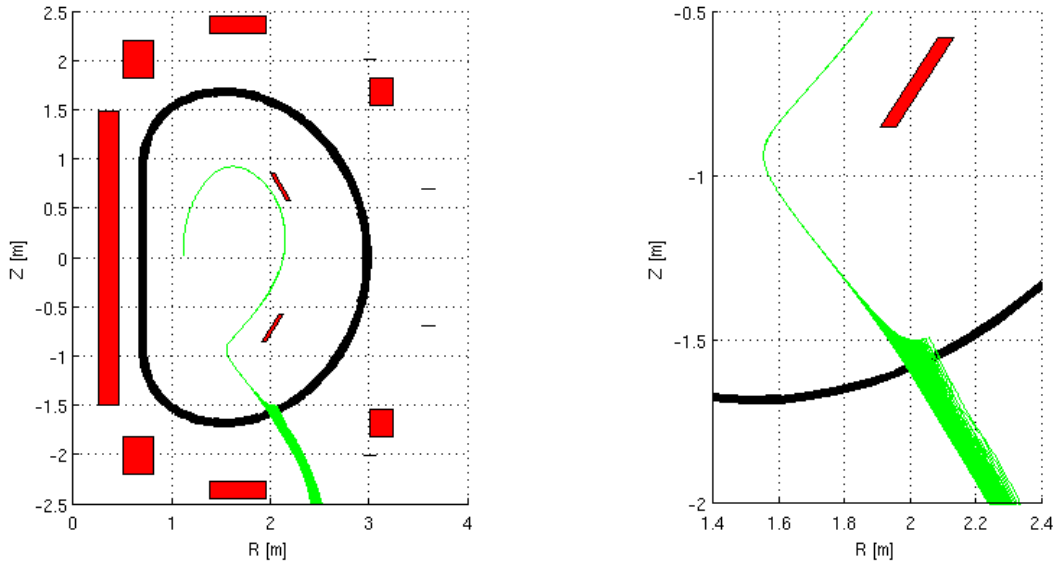

Figure 34: AUG Fieldlines (green) projected to the poloidal cut. All 450 fieldlines are started at the same R and Z coordinate (d=1 cm) but in equidistant toroidal angles between 0° and 45°. They are smeared over a length of 11 cm at the escape point.

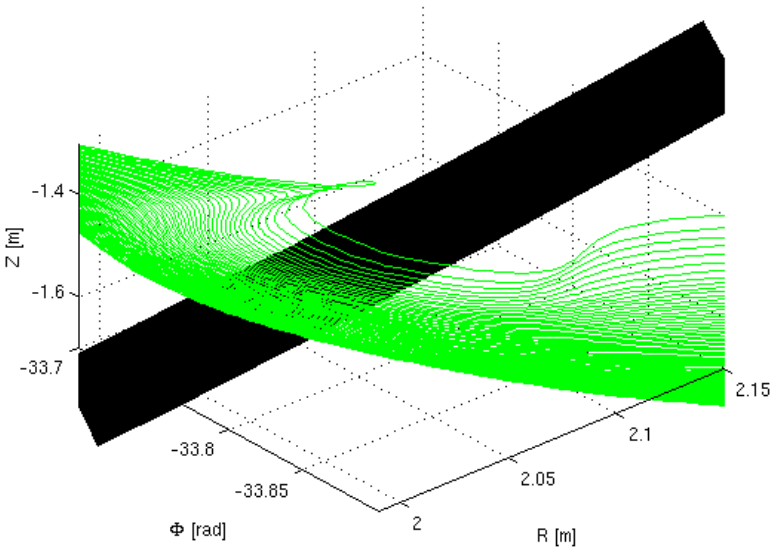

Figure 35: The fieldlines are started at d=10 cm and visualized as a 3D plot. The fieldlines that get closest to the coil are pulled down to lower Z the most by the TF ripple. They are the ones with the strongest shift to a higher escape radius.

4.5 Square Cross-Section

AUG's real TF coils have a cross-section that changes with the poloidal angle. The part of the coil at low R has a trapeze cross-section, while the outer part has a more rectangular shape. This thesis went without a detailed reconstruction of the coils. They were approximated with square cross-sections. Figure 36 shows the escape area. Since all fieldlines are perpendicular to the coil they are projected to the plane parallel to the TF coil's cross-section. Every 40th fieldline is plotted thick so that the compression of the fieldlines can be seen. The fieldlines have a distinctive point at which it is decided which fieldline go back inside the torus (and travel through the next TF coil) and which leave.

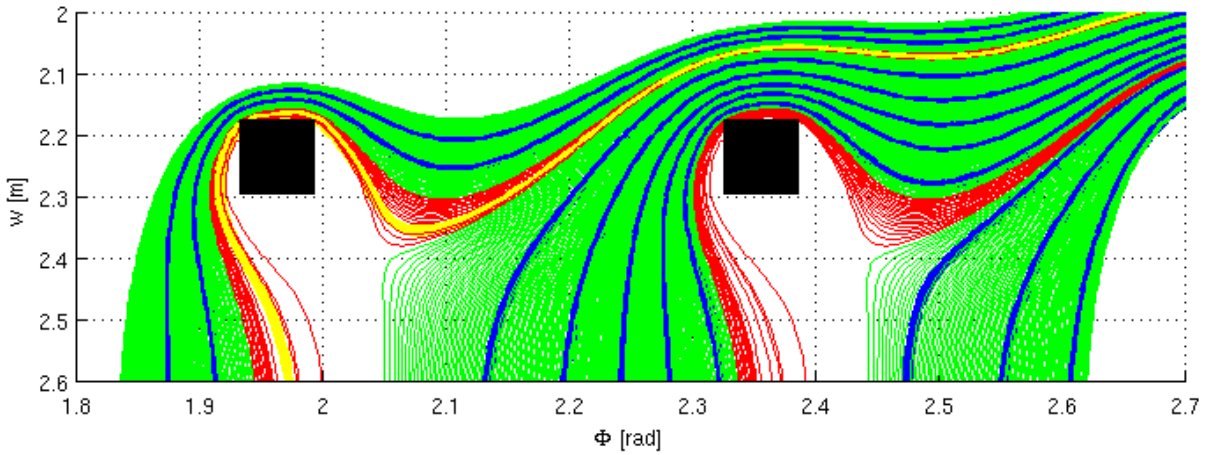

Figure 36: AUG s=10 cm d=1 cm. The plane perpendicular to the coil at the escape point is plotted. Every 40th fieldline is drawn thick, to visualize the compression of the fieldlines, the others are thin green (no-hit) respectively red (hit) lines. The thick lines' colours are blue and yellow depending on whether they hit a coil. The point where the fieldlines "decide" whether they go back inside the torus is where the green and red fieldlines split when approaching a coil.

M(L) Convergence

The Magnetic Transparency M must converge for the number of fieldlines L started in a toroidal interval. L could be chosen arbitrarily high if not for computational restrictions. I found that for the AUG test case 450 fieldlines started in 45° (toroidal interval between two TF coils) is both sufficient to give useful results and does need a reasonable amount of resources.

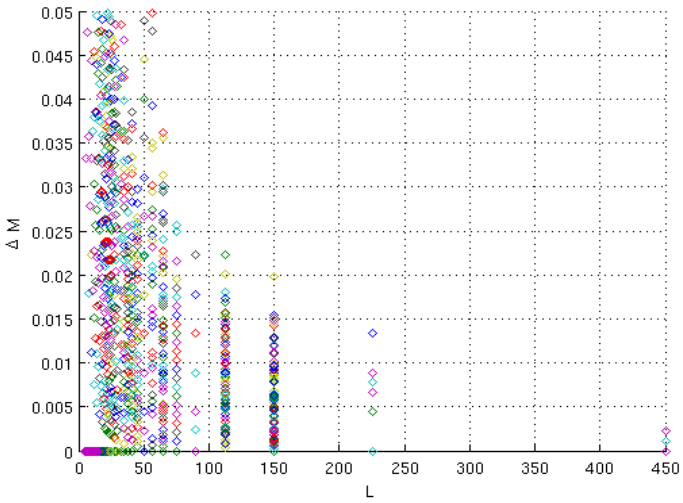

Figure 37: The points display the test cases (varying F, s, d). Due to the high number of cases they are not shown individually. The colours are used to allow to better distinct between the points.

To illustrate this ΔM is plotted against the number of fieldlines in figure 37. In the first run 450 fieldlines are checked, in the second run only every second fieldline is taken into account, in the third run every third fieldline is checked, and so on. ΔM is the absolute difference in M when increasing F.

$$L_1 = 450$$

$$L_i = \left\lfloor \frac{L_1}{i} \right\rfloor \tag{34}$$

$$\Delta M(L_i) = |M(L_i) - M(L_{i+1})|$$

M(F) Convergence

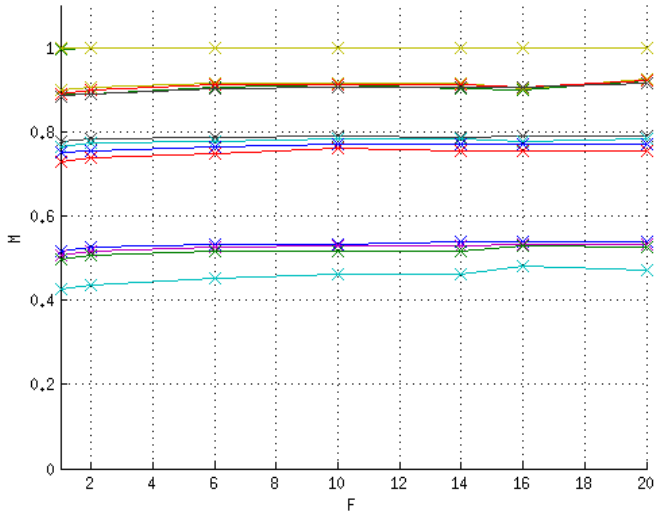

Figure 38: Magnetic Transparency M plotted against the number of filaments per edge F. Each line represents one of the 16 different test cases (s=10, 12, 14, 18 cm d=1, 2, 3, 5 cm). It does not matter which test case is which line since all show the same behaviour and the influence of these parameters on M will be discussed in the following sections.

When increasing the number of filaments per edge F, the Magnetic Transparency rises and converges to the value for infinite F (solid coils). In Chapter III 3. “Influence on the Fieldlines“ the reasons were discussed. With increasing filament density the filaments get closer to the coil's border thus increasing |B| at points close to the border, pushing away the fieldlines.

This effect is strongest with square cross-sections. As we can see in figure 38 this increases M by 0.05. This suggest using only one equilibrium (with one filament) and just implementing the coil's geometry in the hitcoil algorithm should be sufficient to get a first estimate.

M(s)

The coils cannot have an arbitrary small cross-section area due to material restrictions (mechanical stability and the electric current they have to carry). Additionally the coils would need some kind of shielding around them.

There is an maximal (optimal) TF coil's edge length below which no fieldline hits the coils. Fieldlines that get closer to the coils do not come from the SOL. The optimal edge length for AUG is about 10 cm as seen in figure 39. At higher edge lengths **s** more and more fieldlines begin hitting the coils.

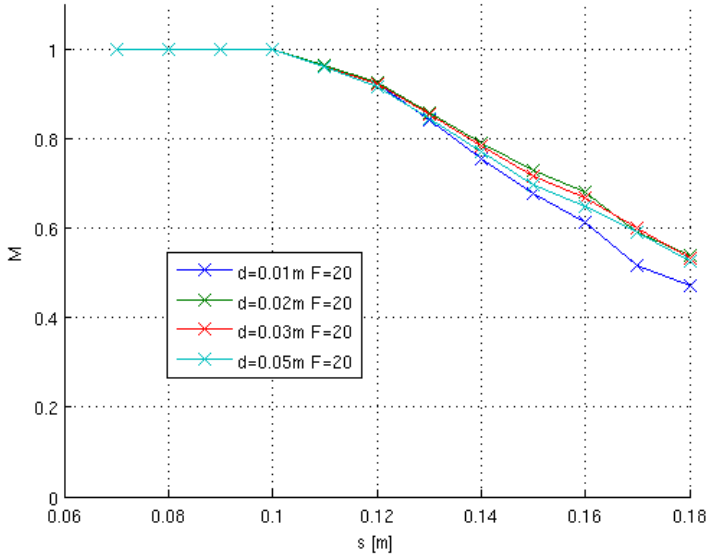

Figure 39: AUG, square TF coil cross-section. The Magnetic Transparency is plotted in dependence of the TF coil's edge length.

But the real s for AUG is about 36 cm. In order to build an AUG like tokamak with this kind of divertor the lower limit of the coil size can be estimated by choosing to increase the current density up to a level of 5 kA/cm², which is about the technical limitation. But even then s would still be 14 cm and fieldlines would hit the coils. So besides minimizing the TF coils cross-section area, some optimization of the TF coil's cross-section geometry is needed.

4.6 Cross-Section Optimization

One way to optimize the TF coils without changing the equilibrium itself is to change the shape of their cross-section (see figure 40). This alteration has to be done only locally at the escape point. The following results are from test cases with conserved s=18 cm and d=1 cm. For other s and d the qualitative results are the same. s in the case of non-square shapes is

defined as the square root of the cross-section area. From the tested cases square cross-section are closest to the real case. M is 0.55 with the square shape. By using a circle cross-section M can be increased to 0.6 and less computation for the magnetic field is needed since M(F) is almost constant for circle shaped coils; the one filament approximation is best for circle shaped cross-sections. When switching to elliptic shaped cross-section M can be increased up to 0.75, but this demands much more tweaking since it's rotation in respect to the fieldlines and its eccentricity need to be adjusted.

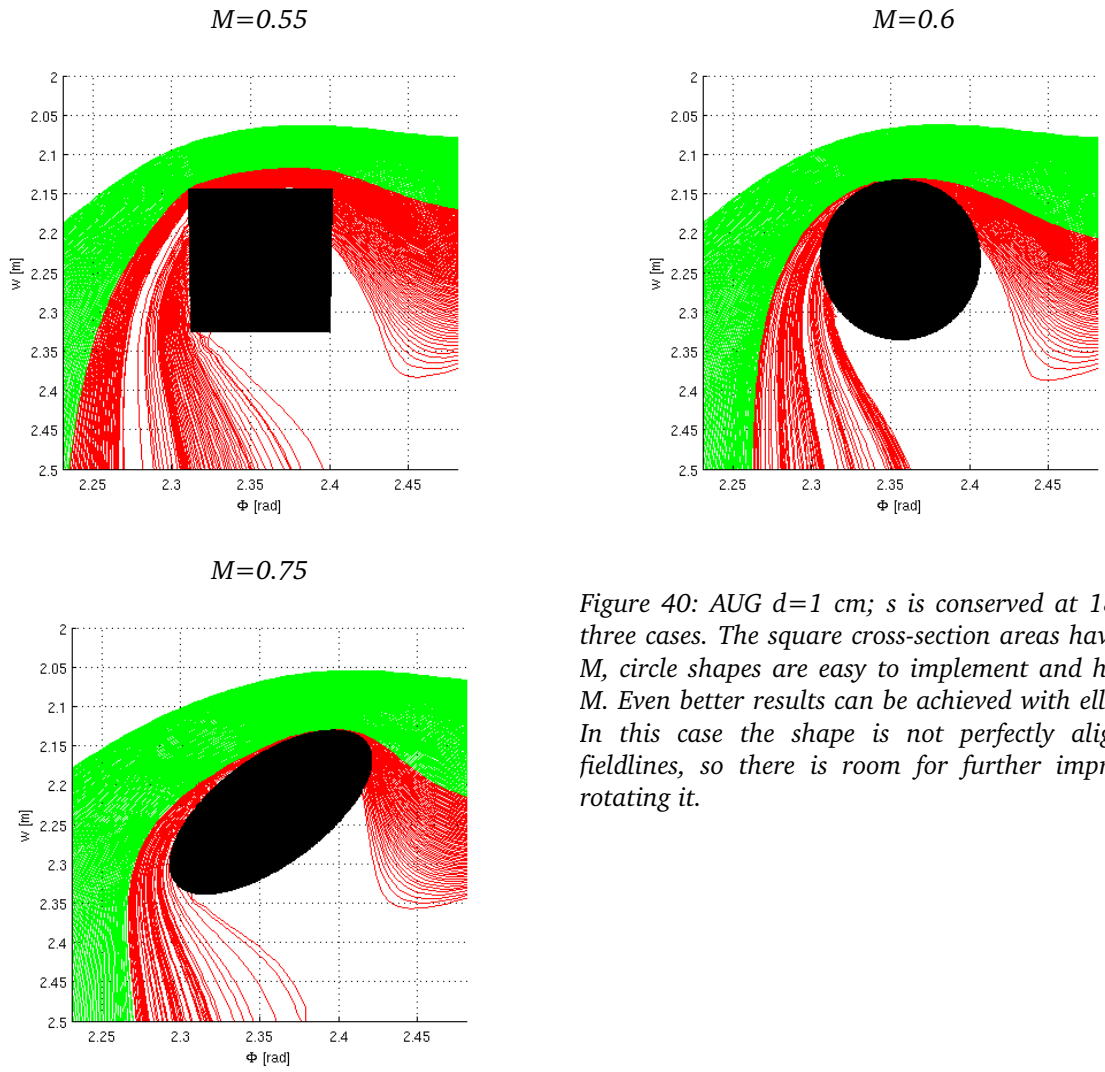

Figure 40: AUG d=1 cm; s is conserved at 18 cm for all three cases. The square cross-section areas have the lowest M, circle shapes are easy to implement and have a better M. Even better results can be achieved with elliptic shapes. In this case the shape is not perfectly aligned to the fieldlines, so there is room for further improvement by rotating it.

As we will see in IV 4.7 the fieldline's angle towards the TF coils changes when shifting the escape point to higher radii. So when optimizing them, the coil's optimal rotation is not constant but changes when moving to higher radii.

Even elliptic shapes are not optimal. The largest cross-section area with M=1 could be determined by a iterative algorithm. It starts with the F=1 case and uses the closest fieldline to define the shape on the side facing the plasma. On the other side of the cross-section the

shape is less relevant since no fieldlines from the SOL get there. Then this shape is used to calculate a magnetic field with a high F. The fieldlines will move away from the new shape. Again the shape is determined by the closest fieldline. From here calculating a new field with the shape and creating a better shape by using the field alternate until the changes in one iteration step are neglectable. The median point of the electric current has to be conserved, of course. Since this is a feasibility analysis and does not claim to present a final concept this optimization is left to following studies.

4.7 Elliptic Cross-Section

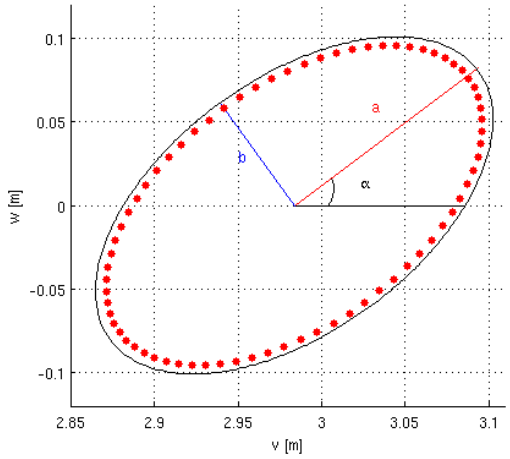

Figure 41: Schematics of the construction of the elliptic cross-sections. The basis vectors v and w are used in the same manner as in Chapter III 1. "Creating the Coil's Numerical Data", so v points in toroidal direction, w points towards the plasma.

The elliptic cross-sections were tested with a cross-section area of (18 cm)². The coils were approximated by calculating a ring of 80 filaments. The computed magnetic fields vary in the rotation applied to the coil and the eccentricity (see figure 41). The major axis will be called a, the minor b. The angle of rotation α is measured between the toroidal direction and a.

M(L) Convergence

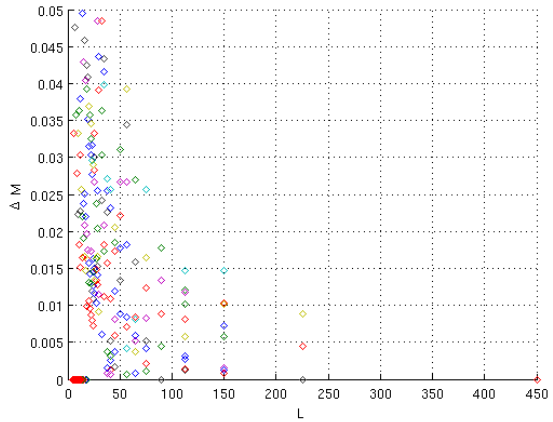

Figure 42: The points display the different test cases (varying F, s, d).

As for square shapes, the Magnetic Transparency converges with the number of fieldlines L (even faster than with square shapes). Again L is chosen to be 450.

For the definition of ΔM, please refer to Chapter IV 4.5.

M(α, a/b)

In order to optimize the elliptic cross-section, the Magnetic Transparency is computed in dependency of α and a/b. The figures 43 and 44 show this for fieldlines started with different distances to the separatrix d. The d=1 cm case obviously looks quite different than the other plots due to the bump at α=2.5. A description of the cause is presented in the next section.

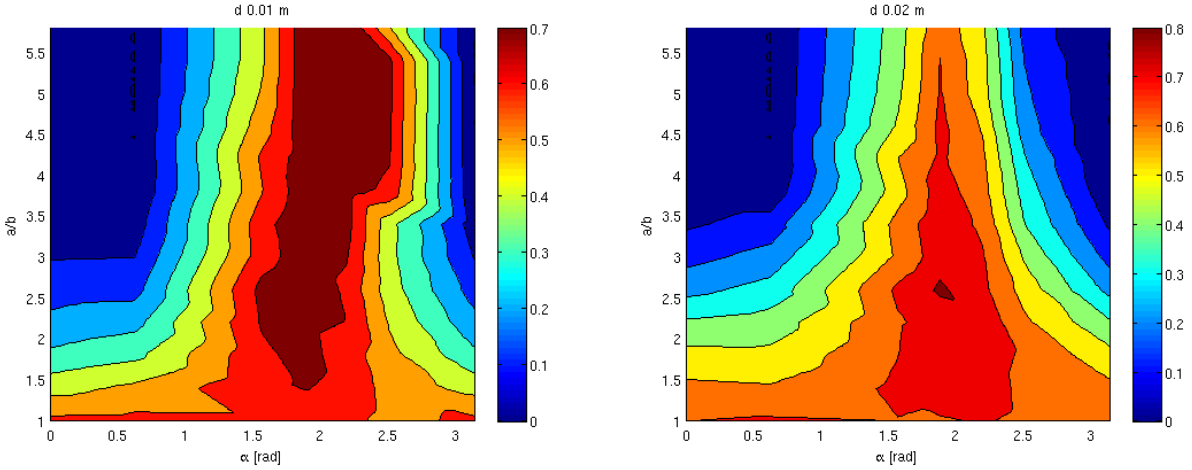

Figure 43: M is plotted as a colour in dependency of the rotation α and a/b. The fieldlines are started at d=1 cm (left plot) respectively d=2 cm (right plot). M has been calculated on a grid with α=0π, 0.2π, 0.5π, 0.6π, 0.7π, 0.8π, π and equidistant a/b=1, 1.4, … 5.8. Note that the colourmap in the d=1 cm is not the same as the colourmaps from the other plots.

M is maximal for α at which the major axis is parallel to the fieldlines (α=2). The minimal M occurs if the major axis is perpendicular to the fieldlines, thus blocks their way (α=0.5). We can see that good values are a/b=2.5 and α=2. The Magnetic Transparency rises up to 0.7 for d= 1 cm, and up to M=0.8 for d>1 cm.

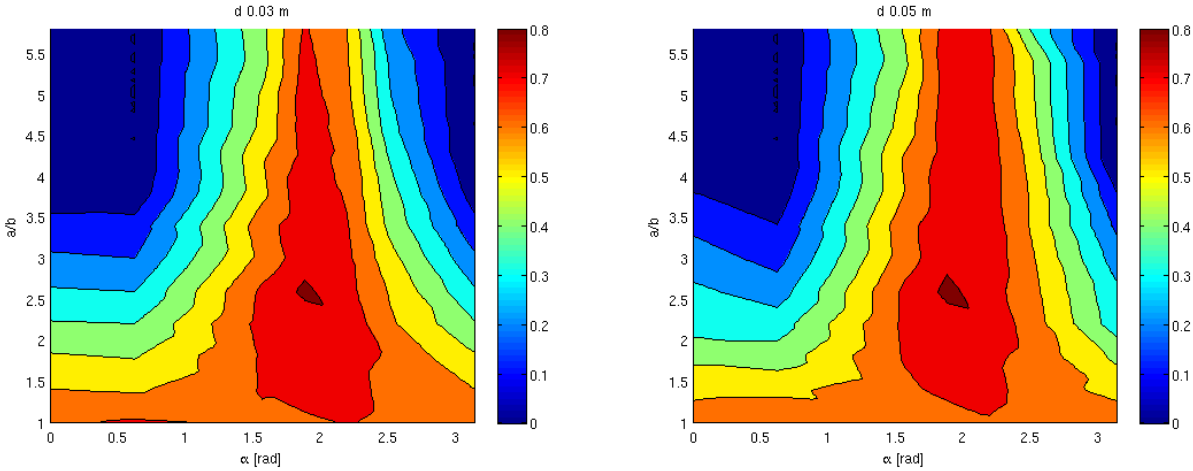

Figure 44: Same as Figure 43 for d=3 cm (left plot) respectively d=5 cm (right plot).

We see that for high enough a/b, M decreases. If the ellipse is elongated enough it will block the fieldline's paths regardless of α.

The a/b=1 case is a circle shape. It should be independent of the rotation. But since the coils are approximated with filaments a rotation of the circle results in a rotation of the exact position of the filaments. Figure 45 shows that an error in M of about 0.02 has to be taken into account, that is due to the exact position of the filaments (refer to the appendix VIII 2 for a detailed description of the construction of elliptic cross-sections). This error has to vanish with increasing F.

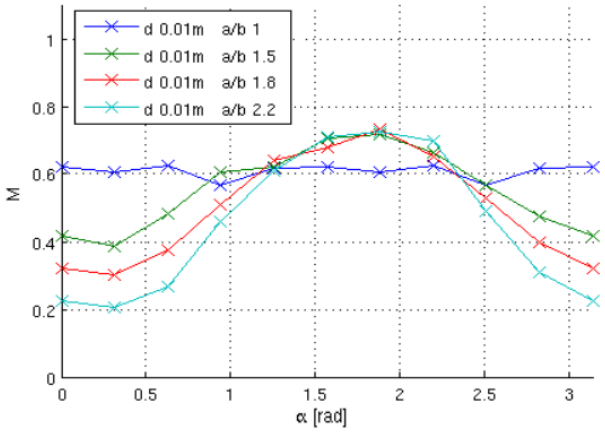

Figure 45: The optimal α does not change when varying a/b. Even though a/b=1 is a circle, M is not constant due to numerical errors.

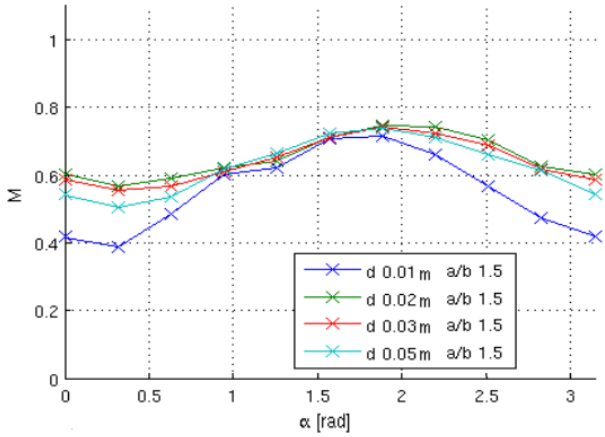

Figure 46: The optimal α to avoid fieldlines hitting the TF coils is about two. But it is dependent on where the fieldlines intersect with the coil.

Figure 46 shows how M changes when rotating the cross-section for constant a/b. Four lines are plotted, each one with different d. The optimal α changes for different start points. As d increases, the optimal rotation increases. Changing d means shifting the escape point of the fieldlines (see IV 4.4 “Escape Area“). So an optimal TF coil would have an elliptic cross-section with its rotation along the poloidal angle. On the other hand it looks like a/b can be chosen constant in poloidal direction. Perhaps more accurate computations (higher P and F) could reveal that the optimal a/b has a small dependence on d.

Whether this idea of “twisted coils” proves useful is questionable since the possible improvement of M is marginal (~0.03) and it would rob the experiment some of its flexibility, because the TF coils would be optimized for one x-point position. The x-point position influences the position of the escape point. And such twisted coils could be problematic with respect to the mechanical stability and fabrication.

4.8 Fieldline Density

Expansion of Fieldlines started at different toroidal Angles

When tracing the fieldlines from the SOL, the expansion in poloidal direction varies not only when looking at different d (see IV 4.4 “Escape Area“) but also for fieldlines started at different toroidal angles. In figure 47 we can see that the expansion has a maximum at the outer midplane. There the first fieldlines are “accelerated” towards the x-point (movement meant as distance in R-Z per Φ) while the last fieldlines are still slowly moving towards the midplane. This happens for axisymmetric fields with no TF coil ripple, too. So there are already density fluctuations without the ripple.

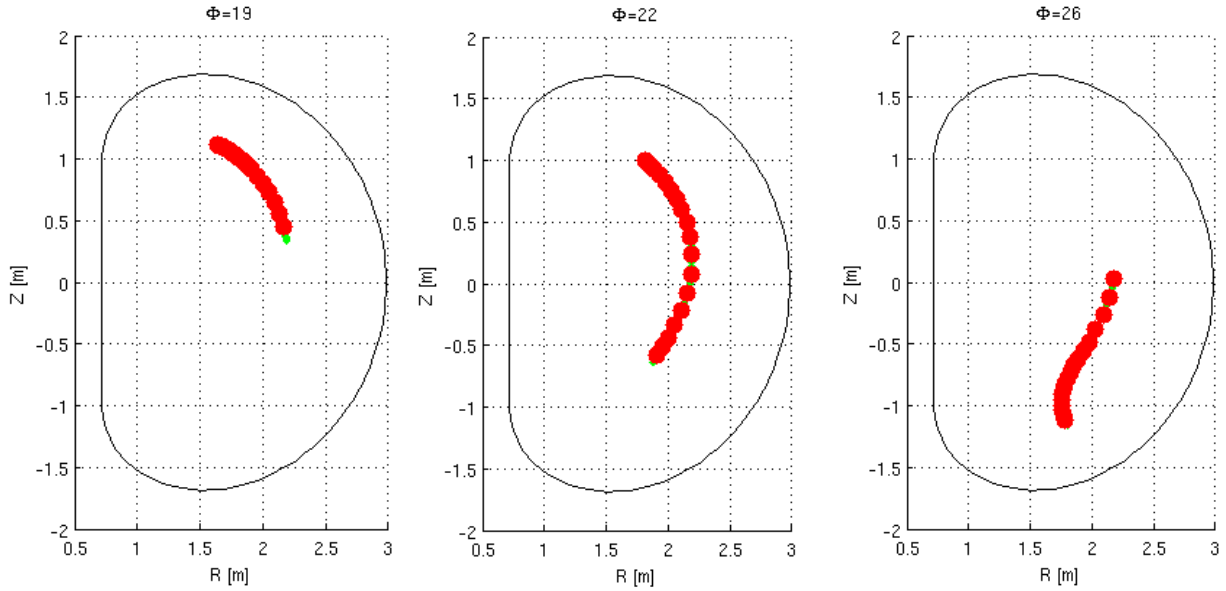

Figure 47: AUG s=10 cm F=20 d=10 cm The toroidal angle [rad] of each plot is written above the respective plot. 360 fieldlines are traced, started equidistantly in the interval from 0 to 2π. Every 20th fieldline is drawn thick red, the others are thin green points. The overall distance between the first and the last fieldline along the points in between varies with the toroidal angle.

When we add the field ripple from the TF coils the fieldline's path will not only by shifted by the different toroidal start angle. If the toroidal offset of the fieldline to a TF coil's toroidal angle is close to zero the toroidal field is higher compared to an offset of π/16 (in between two coils). So fieldlines are concentrated towards the toroidal angles between the TF coils. Those variations in fieldline density can also be seen when looking at the poloidal cut (at a specific toroidal angle) as in figure 48. So these fluctuations from the ripple have to be added on top of the fluctuations from the axisymmetric field. The consequence for the Magnetic Transparency is described in the next section. After that a more detailed tracing of the fieldline density is done.

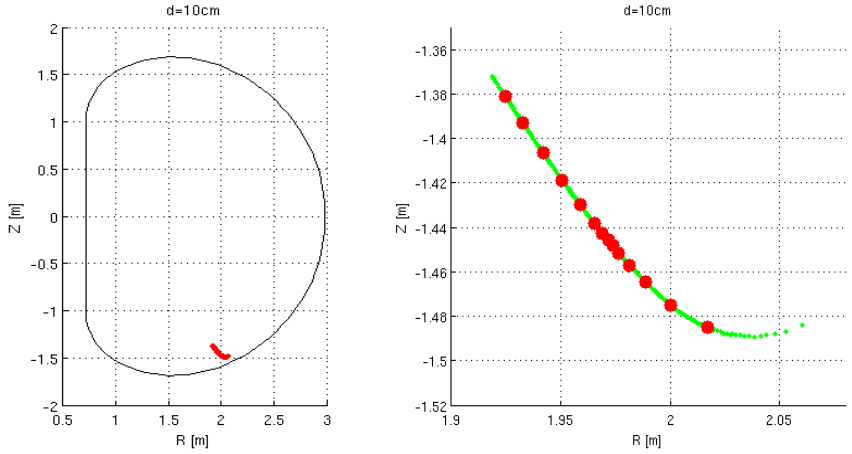

Figure 48: AUG s=10 cm F=20 d=1 cm. 450 fieldlines are traced from the toroidal interval corresponding to two TF coils. From each fieldline one point is plotted: the last point of the fieldline that is at the same toroidal angle as the second last TF coil all fieldlines go through. The right plot is a zoom of the left one. On it every 20th fieldline's point is plotted thick and red, the other are plotted thin green.

Fluctuation of Fieldline Density close to TF coils

When comparing the plots in figures 43 and 44, we see an odd behaviour in M for d=1 cm which suggests that M can increase with increasing a/b for constant α=2.5. In figure 49 we see that the filament density at the border of fieldlines that hit the TF coil and the ones that do not is increased. In the a/b=3 case this shift in the density is small compared to the a/b=5 case. At a/b=5 the density is increased mostly below the border, so much more fieldlines do not hit the coil and M is increased (like at the bump in the left plot of figure 43).

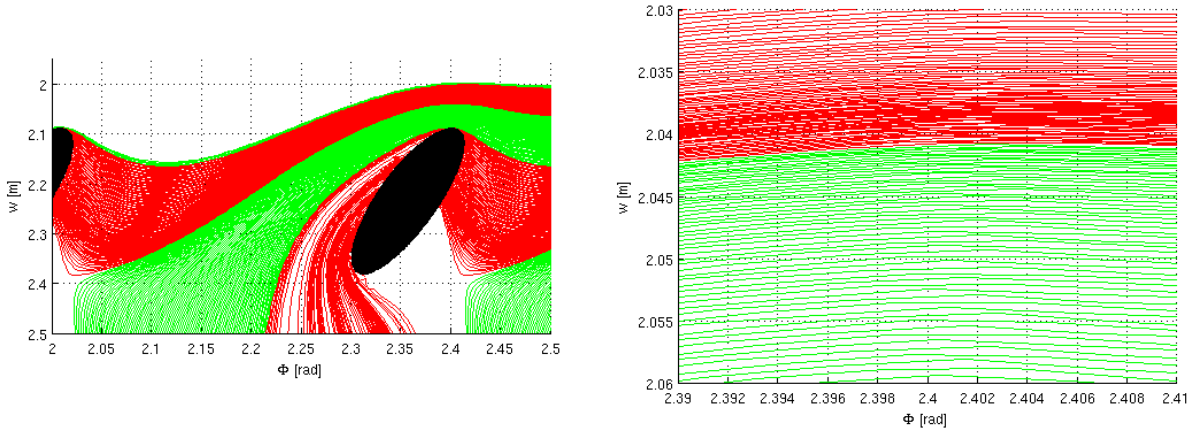

Figure 49: Escape plane in the test case with a/b=3 $\alpha=0.8\pi$ d=1 cm. The right plot is a zoom on the area above the coil. One can see that the density of the fieldlines increases slightly on the border of fieldlines that hit (red) and fieldlines that do not hit the coils (green).

This variation in fieldline density occurs with all shapes and both MAST and AUG. Figure 48 shows the fieldline density in the poloidal cut. It does not increase monotonously towards the coil as would be expected for an axysymmetric field but it has a maximum at R=1.97 m, Z=-1.45 m.

TF coil Ripple generates a Variation in Fieldline Density

Now we concentrate on the fieldline density along the curves generated by fieldlines started at equidistant toroidal angles. ε is the coordinate along the flux in a poloidal cut at a given Φ. So ε is a curvilinear coordinate along the lines from figure 47. ε=0 m is the coordinate of the last fieldline (the one started at highest Φ or more graphic: the last one to approach the x-point). The ε coordinate of the first fieldline will be the overall flux expansion. All other fieldline's ε will be in between depending on their distance to them.

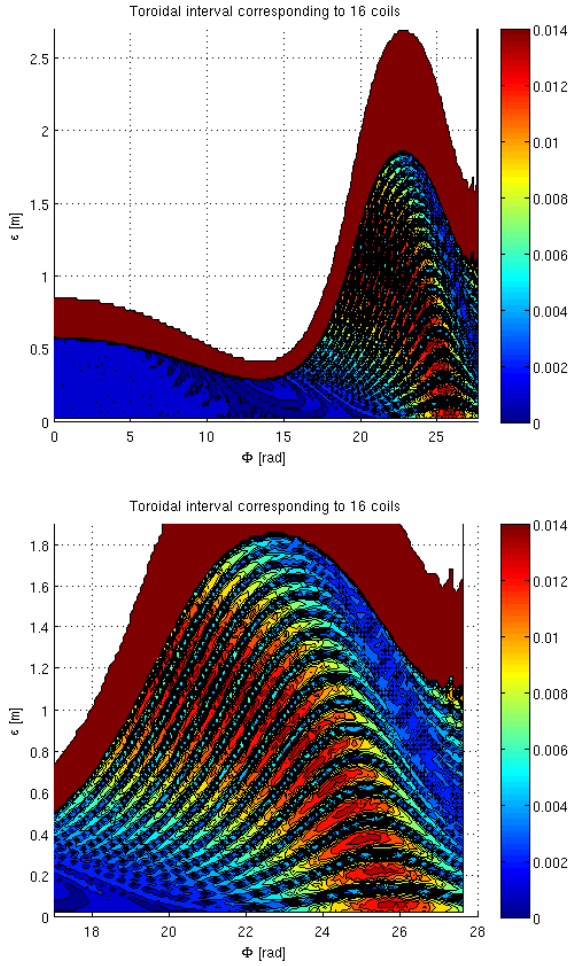

Figure 50: The lower plot is a zoom of the upper one. 360 fieldlines were started with equidistant toroidal angles from 0 to 2π at d=10 cm. The distance between two fieldlines, both at a specific toroidal angle, is shown as the colour. The red area on top is because one additional fieldline was started with 2π distance to the rest of the fieldlines. The colour red shows low fieldline density (high distance between two neighbouring fieldlines) and blue stands for a high density. The colourbar shows the distance in [m]. The expansion near Φ=22 is when the fieldlines median is at the outer midplane. At Φ=27 the fieldlines approach the TF coils.

Figure 50 shows that the fieldlines from different toroidal angles are pushed together when they reach a maximal Z (Φ=12-17). They are pulled apart at the outer midplane (Φ=20-25, figure 47 plot in the middle). The plot in figure 50 stops at Φ=27.5 because at that angle the first fieldline leaves the torus. We can see that the density has a ripple from the TF coils; there are 16 low density spots in figure 50 in an interval of 2π (from Φ≈20-26). These spots are at different ordinates since ε corresponds to a different start point (it increases monotonously with the number of the start point) and the different fieldlines reach the midplane at different toroidal angles.

For an axisymmetric field we would expect the density ρ(ε) to be a convex function at the outer midplane with its minimum at about ε/2. But the ripple of the TF coils at the outer midplane is strong enough to have a significant effect on the fieldline density. The same effect can be witnessed close to the TF coils but it is stronger since at ripple is stronger at the escape point than at the outer midplane. We can see the expansion from the first few coils at Φ=27.

Varying d

When decreasing d the fieldlines get closer to the x-point. The ratio of toroidal field by poloidal field increases with proximity to the x-point, as does the length of the fieldline (the path is mostly in toroidal direction). So decreasing d increases the (toroidal) length of the fieldline between the outer midplane and the escape point. The first bump in figure 51 at Φ=12 is at the outer midplane, the second one that begins at Φ=20 is at the escape point. The distance between those two decreases with increasing d (compare figures 50, 51 and 52).

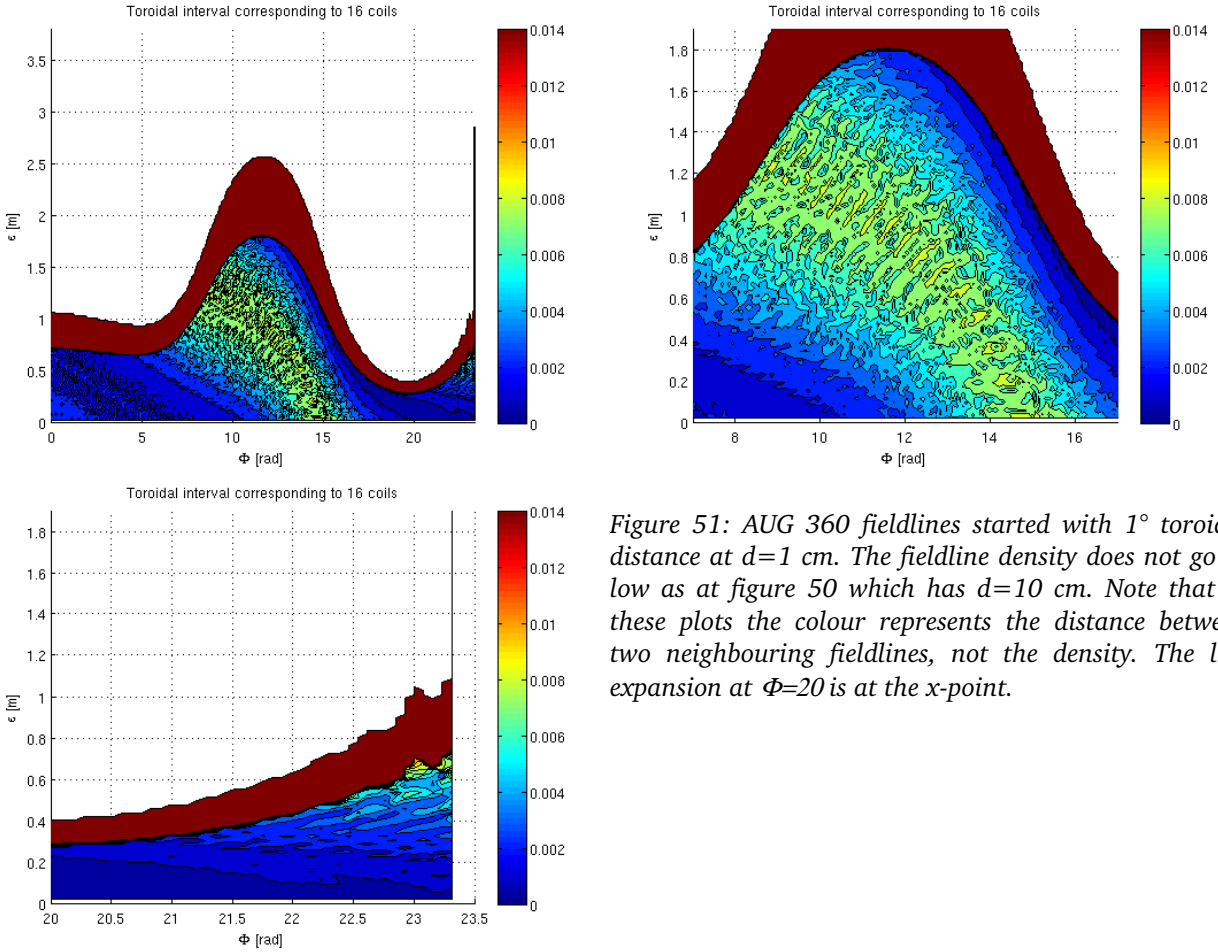

Figure 51: AUG 360 fieldlines started with 1° toroidal distance at d=1 cm. The fieldline density does not go as low as at figure 50 which has d=10 cm. Note that in these plots the colour represents the distance between two neighbouring fieldlines, not the density. The low expansion at Φ=20 is at the x-point.

The density of the fieldlines shows the ripple from the TF coils in the low density spots which can be seen in figures 50, 51 and 52 which are 16 in number just as the TF coils. For higher d the density drops to lower values at the spots and stays at higher densities in between them. So the variation of density at the outer midplane rises with d. This is most likely since the ripple increases with d on the outer midplane (the ripple is highest close to the coils and smallest in the area of the confined plasma).

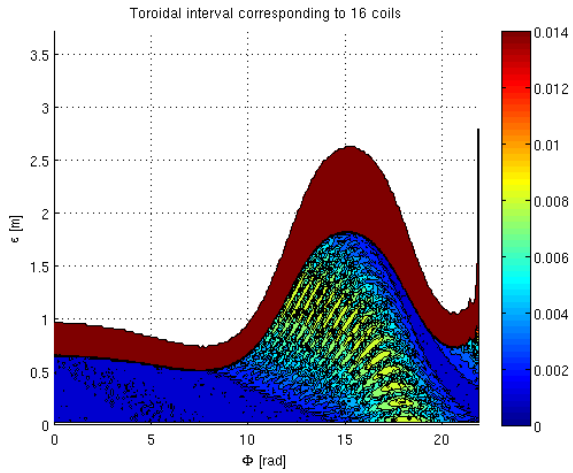

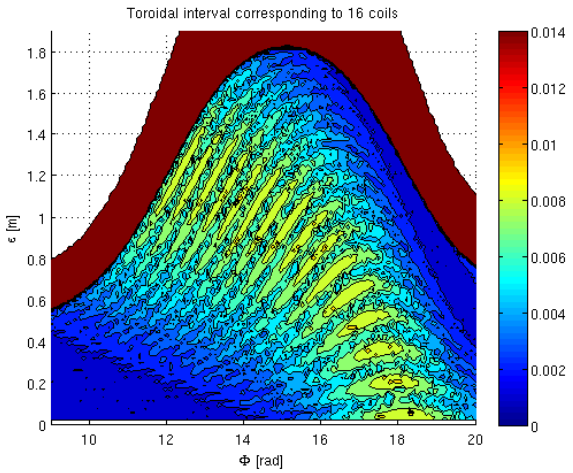

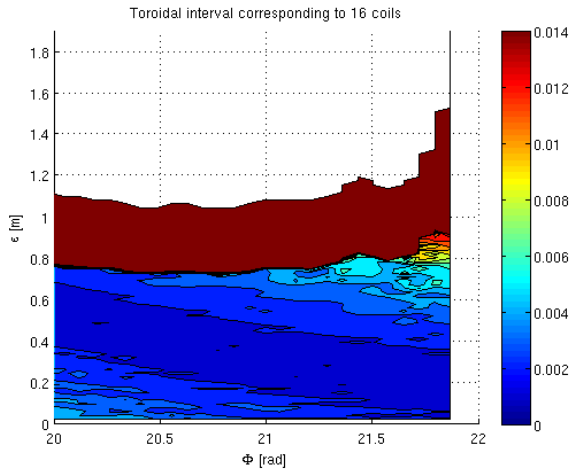

Figure 52: Same as figures 50 and 51 but with d=5 cm.

The observations made for the expansion at the outer midplane can be transferred to the expansion close to the TF coils. So it is to expect that we see a sudden drop in M(s) when s gets large enough so that the coils begin intersecting the high fieldline density areas. Another, in my eyes more significant, effect comes from this varying density. M(d) shows an oscillation. This can be seen in figure 53.

M(d) oscillates since the distance between the coil and the high fieldline density area varies with d as can be seen in figure 54. The high fieldline density areas wander between areas where they hit the coils (low M) and areas where they do not (see figure 54).

The frequency of the oscillation increases for decreasing d for d<3 cm and increases for increasing d for d>4 cm. The slope of the connection length of the fieldlines (in the calculations measured as length between start point on the HFS and the point of the fieldline that comes closest to the TF coils) has much resemblance with the frequency of M(d). A varying connection length from the outer midplane to the TF coils could result in another location of the density spots if the spots are not created from the TF coil's near field but from the midplane. This question is left to further studies since this does not affect the outcome of this one. For this study the s=10 cm line in figure 53 is important and this effect does not influence M=1 cases.

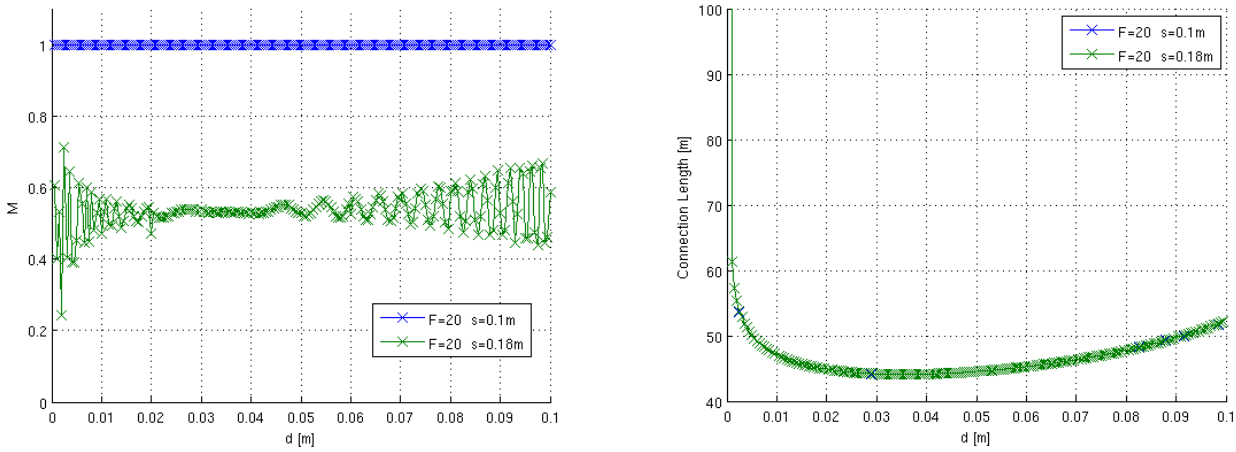

Figure 53: The left plot shows M(d) with a resolution of 0.5 mm. M oscillates with d. The oscillation frequency's course is quite similar to the connection length (right plot).

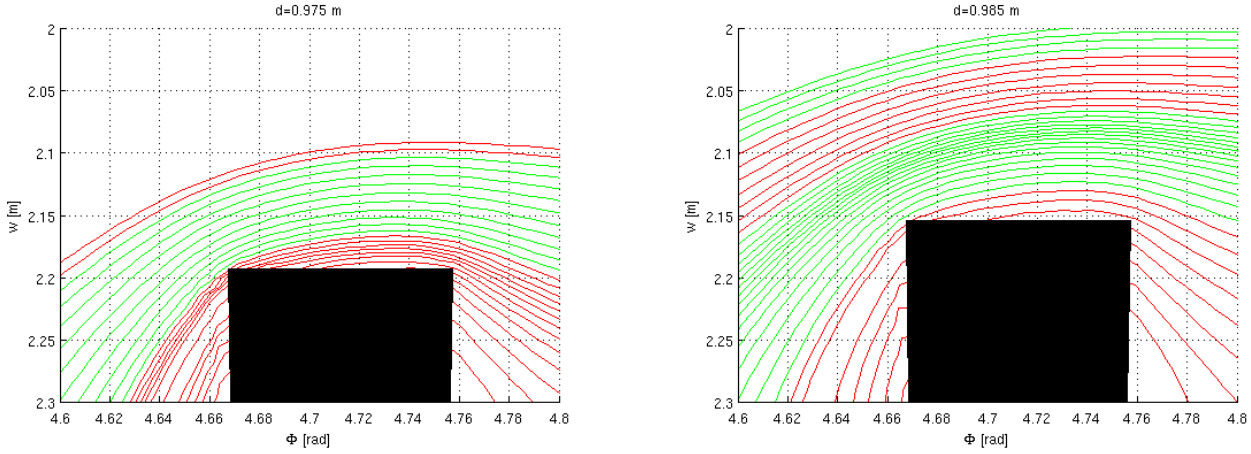

*Figure 54: In these plots 450 fieldlines were started in the toroidal interval between 0 and π/4. The high density area's distance to the coils varies with d. This distance influences M since the high density areas wander from hit areas (left plot) to no-hit areas (right plot). Since hit and no-hit areas alternate in direction of **w** (for example in the right plot the lower area of red fieldlines hits the coil at Φ=4.7, the next set of red fieldlines will hit the next coil) a continuous shift of the densities results in an oscillation in M.*

Physical relevance

For this study the variation of the fieldline density plays a minor role since the study concentrates on parameters for the coils which allow a Magnetic Transparency of one. Only the boundaries of the flux are important to determine which coil parameters allow no fieldline to hit any of the TF coils.

But for a more detailed study of the possibility of guiding the particles through the gaps between the coils, it should be important to look at ways to concentrate areas of high particle density to the middle of the gaps. But it is questionable if this effect still occurs once diffusion is also considered.

4.9 Summary

- There is a maximal cross-section area of the TF coil greater than zero at which no fieldline from the SOL hits the coil. At AUG this area is about a factor ten smaller than the real cross-section area of the TF coils.

- The maximal cross-section area of the TF coils at which no fieldline from the SOL can hit them can be increased by a smart choice of cross-section shape at the escape point. This redesign does not affect the plasma region.

- M(F) is lowest for F=1 and increases with higher F. So the computationally easy F=1 case can be used as a worst case approximation.

- Due to the ripple from the TF coils the fieldlines' density does not increase monotonously towards the coils but has fluctuations. The position of high densities of fieldlines relative to the coils varies with d. It is shifted through the alternating hit and no-hit areas, so M(d) oscillates.

If such a divertor would be considered, an ASDEX Upgrade like device does not seem to be the perfect candidate. Of course there are more options to reduce the hits on the coils than the cross-section changes that have been covered in this study. For example saddle-coils outside the TF coils that create a radial field could be introduced. But such additions might have an impact on the equilibrium.

5 MAST

Since MAST is a ST, its TF coil's current is low. MAST's TF coils carry a current of about 170 kA each, while AUG's coils have (in the used equilibrium) 1 MA. The cross-section of MAST's coils is about 100 cm², while at AUG it is about 1300 cm². Since the fieldlines avoid an area around the coils this lets us expect that MAST is a more suitable candidate for this kind of outside divertor.

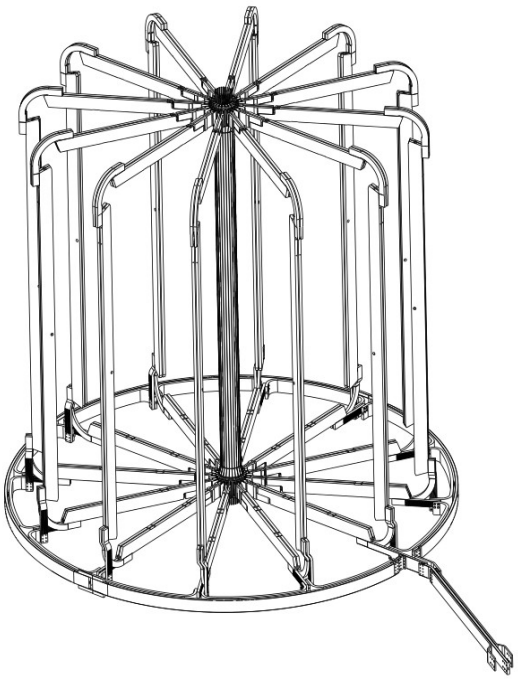

Figure 55: MAST's toroidal field coil layout, which was provided to me by the CCFE's drawing office

5.1 Equilibrium

I was provided with the layout of MAST's coils and a 2D equilibrium by the CCFE. The 3D magnetic field was approximated by simply creating the 3D vacuum magnetic field from the TF coils (Vacfield code) and adding the 2D magnetic field.

$$\begin{pmatrix} B_{eq,r} \\ B_{eq,\varphi} \\ B_{eq,z} \end{pmatrix}(r,\varphi,z) = \begin{pmatrix} B_{vac,r} \\ B_{vac,\varphi} \\ B_{vac,z} \end{pmatrix}(r,\varphi,z) + \begin{pmatrix} B_{2D,r} \\ 0 \\ B_{2D,z} \end{pmatrix}(r,z) \tag{35}$$

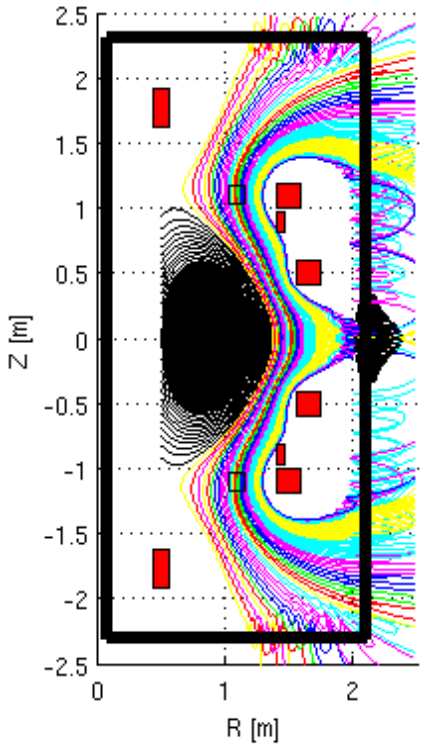

Figure 56: Projection of fieldlines to the poloidal cut. The fieldlines were started at Z=0 m, φ=0. Their colour shows after which coil they leave the torus.

This approach lacks the poloidal plasma currents, so the strength of the toroidal field inside the plasma region might be wrong. But this does not affect the tracing of fieldlines outside the confined plasma.

Unfortunately the grid is small; R spans from 0.5 m to 2.5 m, Z from -2.5 m to 2.5 m. It is not possible to trace fieldlines outside of these borders, since the Gourdon code does not support extrapolation of the field. So the fieldlines are cut of at these borders. This hampers finding the separatrix, calculating the q-profile and determining hits. Figure 58 shows the q-profile of the used MAST equilibrium. The safety factor q is calculated using the number of poloidal and toroidal circulations. Therefore q can only be computed correctly for fieldline that make at least one full poloidal circulation. But as seen in figure 56 there are fieldlines inside the separatrix that do not make a full poloidal circulation (black fieldlines ending at R=0.5 m).

To verify the quality of the new equilibrium it is checked whether there are closed flux surfaces. When starting a fieldline inside the separatrix, tracing it 50 toroidal circulations and projecting it to the R-Z plane the fieldline is closed and shows about 1 mm thickness (see figure 57). This is most likely due to the ripple from the TF coils, which is subject of the next section.

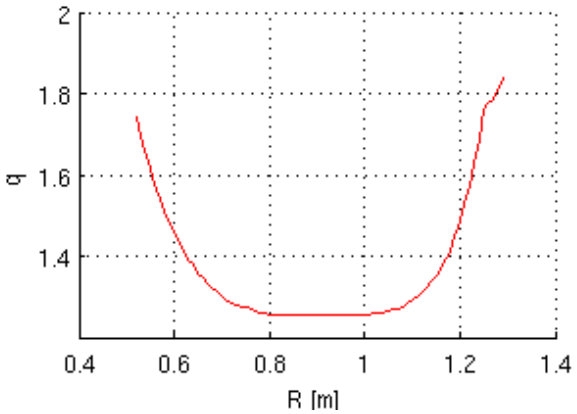

Figure 58: q-profile of the used MAST equilibrium. The glitch at R=1.25 m is due to the too small grid size.

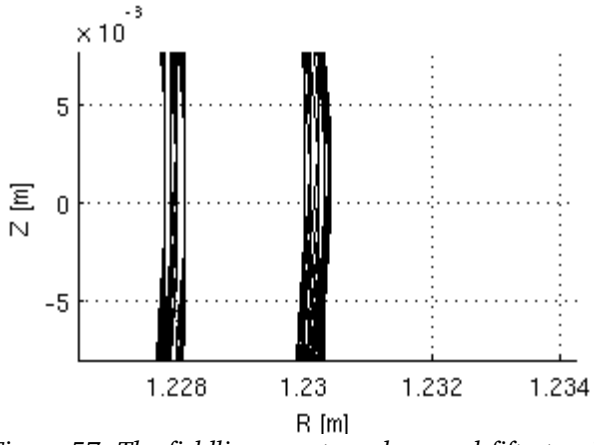

Figure 57: The fieldlines are traced around fifty toroidal circulations. The flux surfaces have a thickness of about 1 mm.

5.2 Spatial Ripple of the Separatrix

At AUG the fieldlines were started on the HFS to minimize the effect of the toroidal ripple on d. But the double-null configuration (two x-points) of the used MAST equilibrium (see figure 56) prevents starting the fieldlines on the HFS. One point of the separatrix was found by starting fieldlines at Z=0 m, φ=0 and varying R. Those fieldlines were traced and it was checked whether they leave the torus after no more than fifty toroidal circulations. Because of the magnetic field's grid size some fieldlines within the separatrix will leave the grid, so the tracing is aborted before they make a full poloidal circulation (see figure 56). So if a fieldline leaves the grid at R=0.5 m it is counted as inside the separatrix. The last fieldline (while increasing their start point's R) that is inside the separatrix was found at R=1.3756 m. This is considered one point of the last closed flux surface.

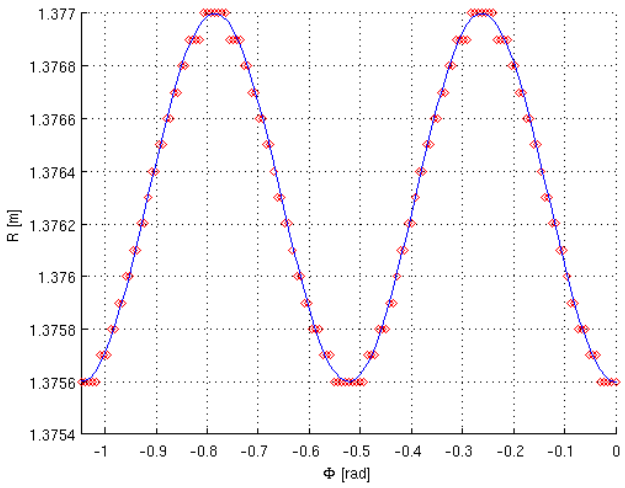

Figure 59: Ripple of the separatrix at Z=0 m on the outer midplane. The red dots are computed by starting a fieldline in the vacuum magnetic field of the TF coils. The blue line is an interpolation as a cosinus.

The ripple of this fieldline is shown in figure 59. It is computed by starting a fieldline at the found separatrix point in the pure TF coil vacuum field. Since the overlaying 2D equilibrium has no toroidal magnetic field this approach gives a fieldline that returns to its start position (in R and Z) whenever it is at the same toroidal angle as a TF coil. In all following MAST test cases this ripple is taken into into account when determining the start points. They are defined by starting at Z=0 m and by d. The ripple is added to the start point's R coordinate.

The computed ripple R(Φ) is:

$$R_0 = 1.3756\,m$$
$$A = 7\,mm \tag{36}$$
$$N_{coils} = 12$$

$$R(\Phi) = R_0 + A\cdot(1-\cos(N_{coils}\cdot\Phi)) \tag{37}$$

5.3 Escape Area

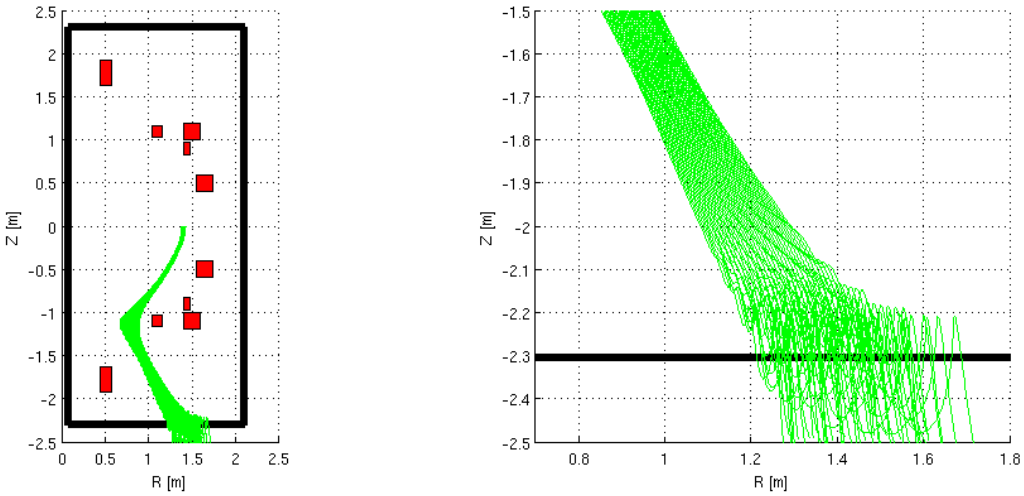

Figure 60: MAST poloidal cut with PF and TF coils. The fieldlines are started with d=1 cm to 5 cm from the outer midplane at the same toroidal angle and traced to the TF coils. The right plot is a zoom of the left one at the escape area. A higher d moves the fieldline's escape point to a higher radius.

In figure 61 the fieldlines were started with d=1 to 5 cm. The flux expands to 45 cm. So a small change in d will result in a larger change at the escape radius compared to AUG. Note that d_{MAST} should be compared to $d_{AUG,LFS}$ and not d_{AUG} since both should be measured at a corresponding point, the outer midplane in this case. The fieldline's path is almost perpendicular to the TF coil (and perpendicular to the R axes) at the escape point. Fieldlines started in a toroidal interval, all with the same d have different escape radii (see figure 62), too. The d=1 cm fieldlines are smeared over 12 cm.

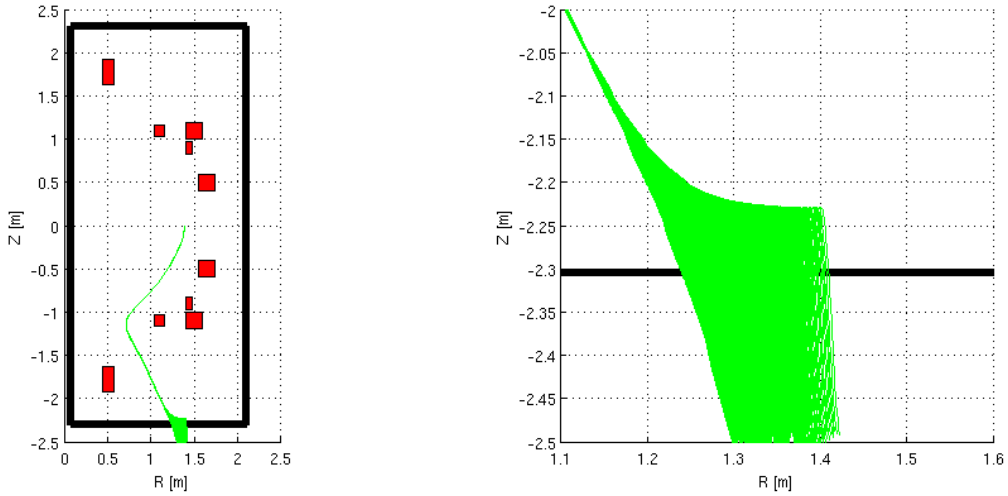

Figure 61: Fieldlines started in a toroidal interval, all with d=1 cm. The fieldlines are smeared over 12 cm.

5.4 Restriction of the Magnetic Field's Grid Size

As described before, the magnetic field is defined on a grid, which ends at |Z|=2.5.

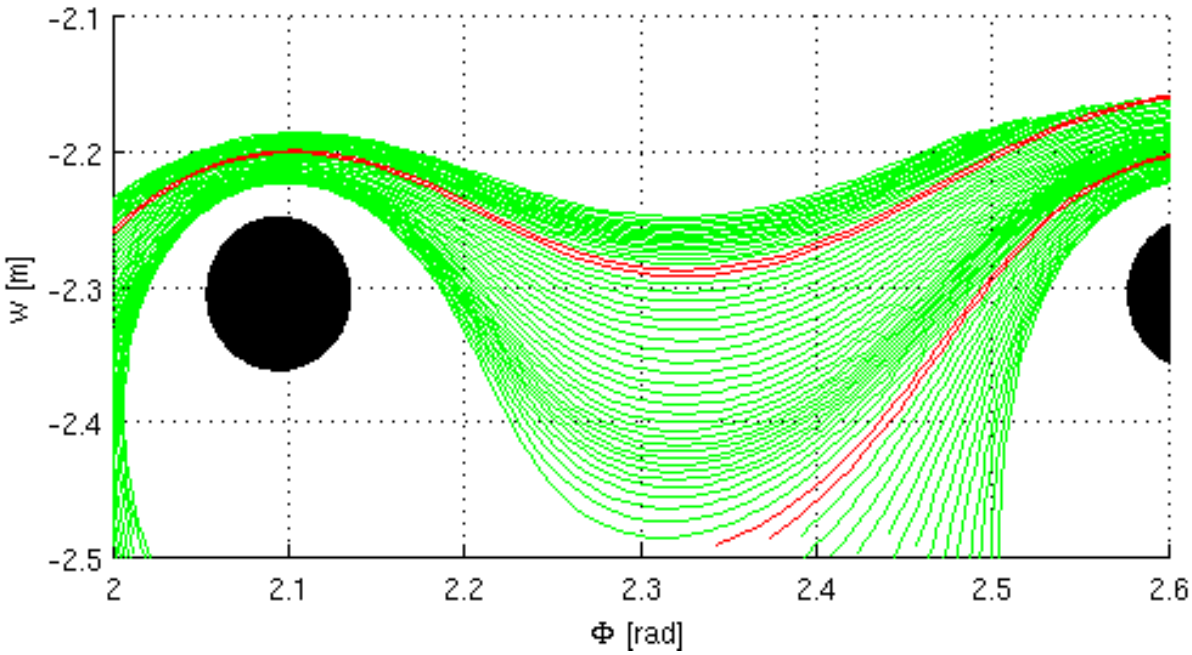

Figure 62: MAST escape area close to the TF coils. The black squares are the TF coils' cross-sections. The lower red fieldlines are the first (from top to bottom) whose tracing is interrupted, since it leaves the grid on which the magnetic field is calculated. The upper red fieldlines will show the same behaviour but at the next coil.

Figure 62 shows fieldlines close to the TF coils. The ripple from the TF coils is obvious. The fieldlines that are plotted red are not traced further since they leave the grid. But I suspect them not to leave the torus for good but to return inside the torus again, if being traced further. They are counted as no hits, even though they could hit the next coil. This numerical issue distorts M to higher values. And the extent is hard to estimate. There is no reason why only the fieldlines plotted red in figure 62 could return. The one below could also be not lost yet. And so on. I could not find a reasonable clear-cut distinction without tracing the fieldlines further (compare with figure 36, AUG fieldlines at escape area, there it is obvious to the eye which fieldline depart and which go back to the coil).

So the following results are valid with the restriction that the particles are intercepted at Z=-2.5 m. This could be true for an experiment that tests the escape points of the lost particles or a divertor that is placed at that radius. But such a divertor would not have a great advantage over the Super-X except that the plates could be more accessible for maintenance.

An attempt to increase the definition area of the magnetic field is shown in the figures 63 and 64. The 2D magnetic field (from equation 35) was extrapolated in Z direction using an exponential decrease. The exponential decrease was chosen because it gave the smallest deviation when comparing interpolated data on the edge of the original magnetic field with the corresponding interpolated one. The extrapolation was done for each different radius separately.

$$\boldsymbol{B}(r,z) = \boldsymbol{B_0}(r) \cdot e^{-a(r) \cdot (z-z_0)} \tag{38}$$

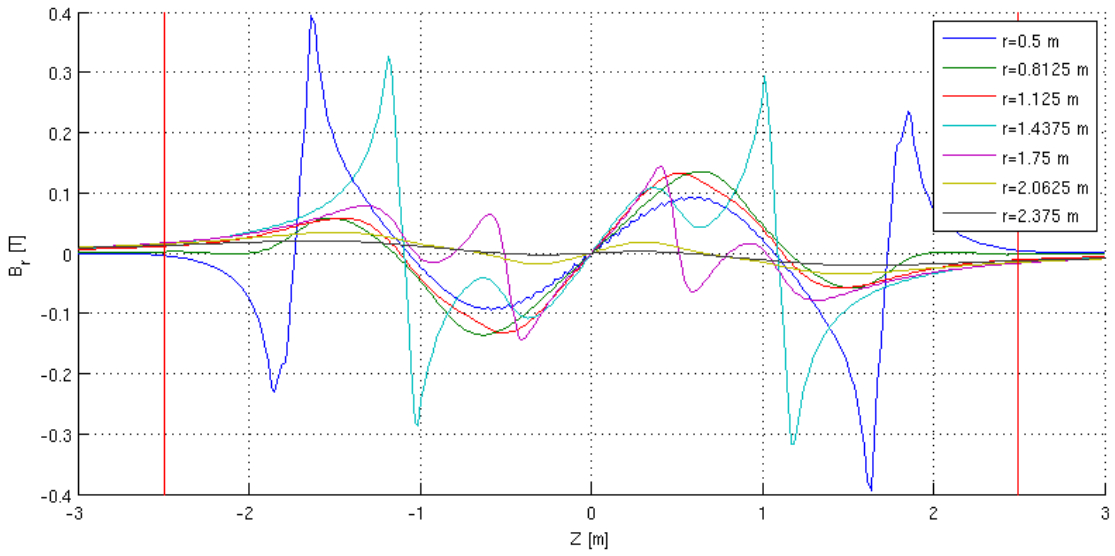

Figure 63: The ordinate shows the component of B in direction of the radius. It is plotted against the Z coordinate. Different lines show it at different radii. The red boundaries show the extend of the original grid. The values 3>|Z|>2.5 are extrapolated.

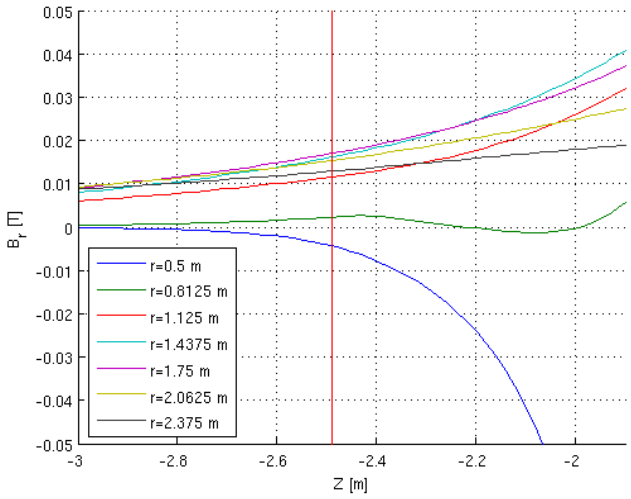

Figure 64: Zoom of figure 63 to show the lower extrapolated area. At the r=0.8125 m line a salient point can be seen at Z=-2.57 m. This is because the extrapolation was kept as a simple exponential decline. In that case an overlaying oscillation would have given a more realistic result.

Of course this is just an approximation since the divergence of the magnetic field is not zero with this extrapolation. I have chosen this method since it was easy to implement and it showed good results at the edge of the original grid. The outer three grid points of the original grid were extrapolated as well to compare them to their original values.

The expanded 3D magnetic field was calculated in the same way as the original one (see equation 35). In this new magnetic field the fieldlines spiral around the TF coils (see figure 65). Their distance to the coil decreases while spiralling. From figure 56 it can be estimated that this behaviour is no product of the approximation (38) but a generic effect from the MAST TF coils, since it also happens for fieldlines inside the original grid at the outer leg of the TF coil ($|Z|<2.5$ m and $R\approx2.1$ m). By looking at the fieldlines that come close to the outer leg it can also be estimated that fieldlines spooling around the coils will escape at $Z\approx0$ m. Even the ones whose first intersection point with the coil is at the lower leg tend to escape there if the fieldline does not separate from the coil at the TF coil's corner at $R\approx2.1$ m and $Z=-2.3$ m.

The fieldlines come closer to the coil while spiralling, so they will hit the coil more likely than at the original field. This suggests that measures need to be taken to intercept them early or they need to be lead away from the coil by changing the magnetic field. The interception at $|Z|=2.5$ m is already realized with the original grid so the further calculations on MAST use the original magnetic field.

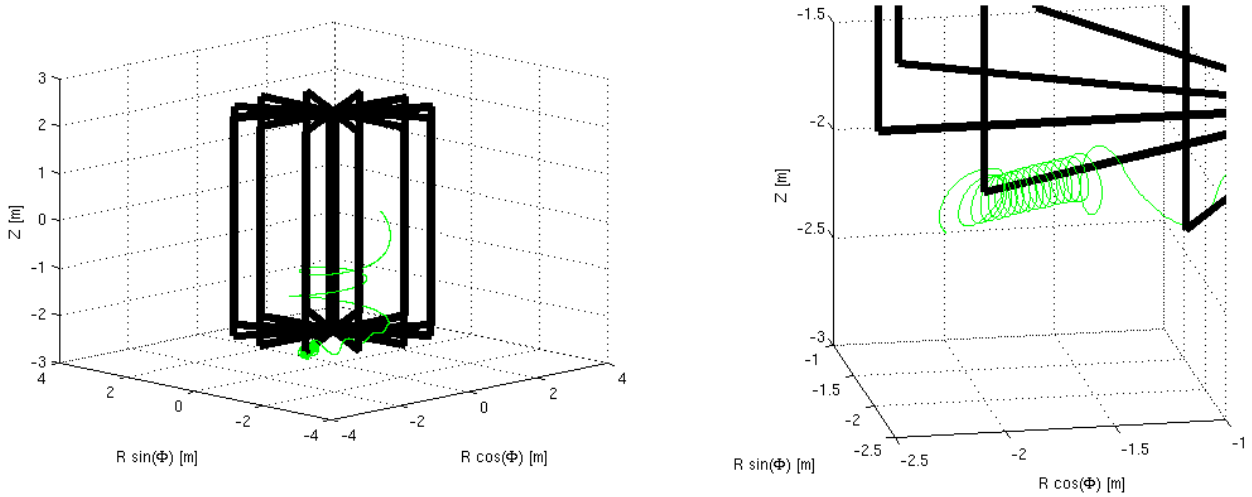

Figure 65: MAST's TF coils (black) with one fieldline which is started at d=2 cm. When coming close to the TF coils it starts spiralling around one.

5.5 Square Cross-Section

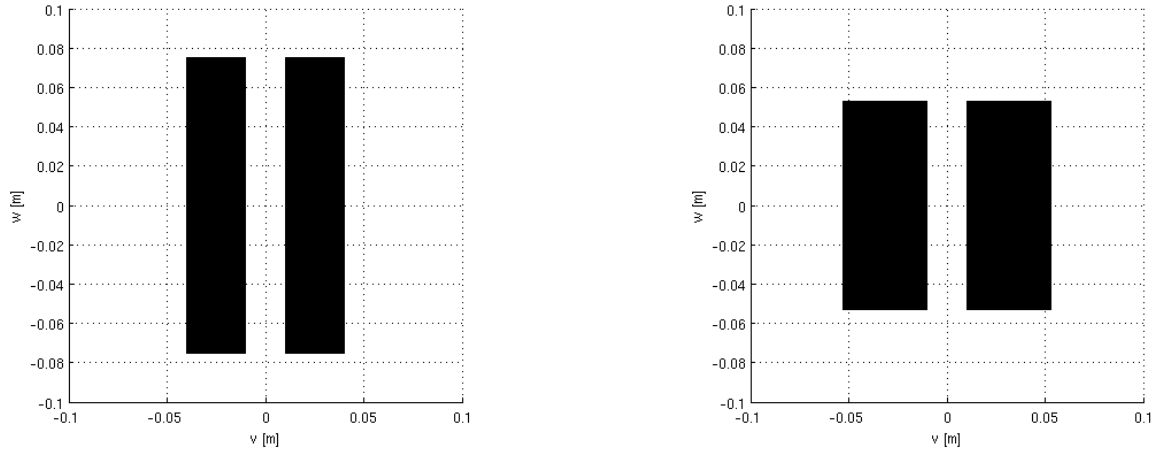

Figure 66: MAST TF coils. The left figure shows the real coil's cross-section. The right one is a square alternative with the same cross-section area (90 cm²). The edge length is (because of the gap) 10.95 cm. The distance between the legs is left at 2 cm.

MAST's real TF coil consist of two legs. Each of them has a cross-section area of 3 cm times 15 cm. Each of them carries 85 kA. If the TF coil's electric current density would be increased up to 5 kA/cm² the cross-section area of each leg could be reduced to 17 cm² instead of the original 45 cm². Then the minimal s would be 5.25 cm, leaving the gap between the legs at 2 cm. It should be possible to reduce the gap between the coils by not leaving air between them but an insulator. The following calculations are made for square and circle shaped cross-sections without a gap between them.

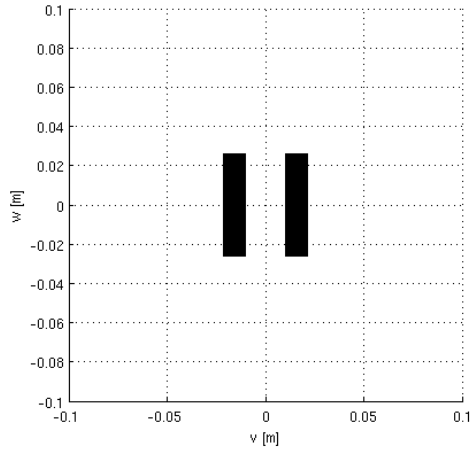

Figure 67: Minimal cross-section of a TF coil for MAST with 5 kA/cm². There is still optimization possible by reducing the gap between the legs.

M(L) Convergence

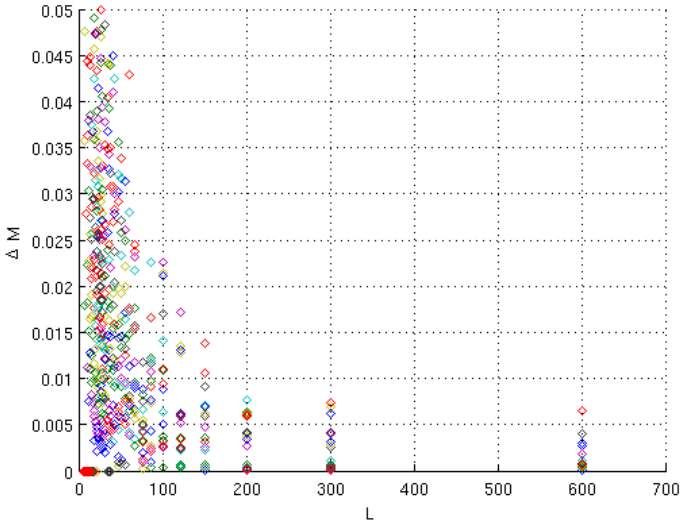

Figure 68: ΔM in dependence of L, like already shown for AUG in IV 4.5 and IV 4.7. Each colour represents a different test case (varying s, d, F fixed at 40).

M converges with increasing L, but slower than it did at AUG. Again the chosen value of L is a compromise between computer resources and numerical accuracy.

M(F) Convergence

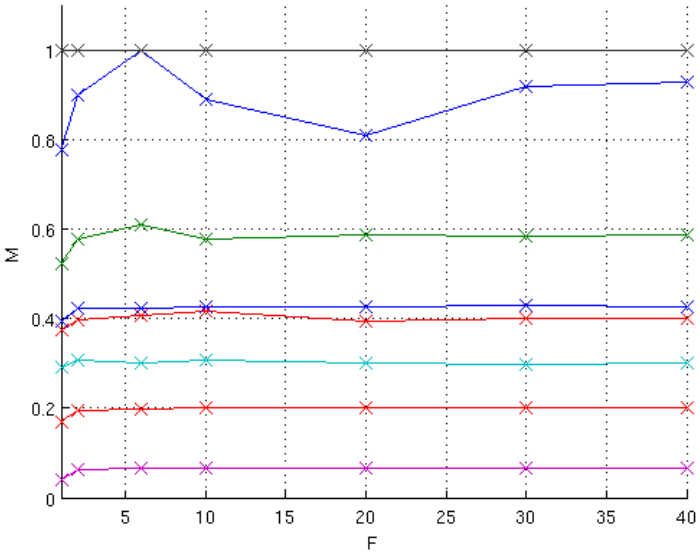

Figure 69: Magnetic Transparency rises with F. Some numerical issues lead to a drop in M with rising F. The differently coloured lines resemble different s and d. Again the exact association is unimportant.

Again we have to make sure the Magnetic Transparency converges with the amount of filaments used to represent the coils. Figure 69 shows M with increasing F at MAST. In all cases the one-filament approximation is the worst case. But in three cases (top blue, top green, top red) there is at least one F at which M drops with increasing F. This seems to be due to the numerical issue discussed in IV 5.4 “Restriction of the Magnetic Field's Grid Size“.

M(d)

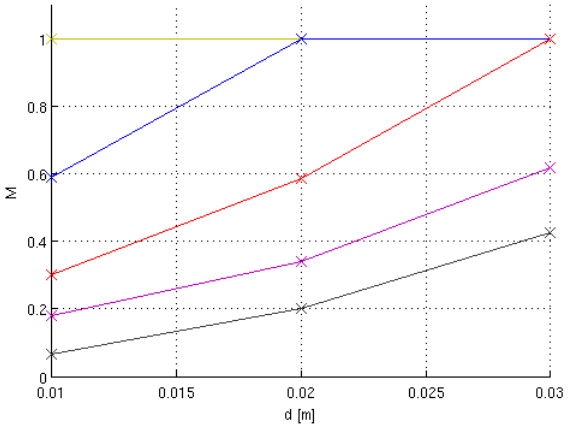

Figure 70: MAST M(d) with F=40. Coloured lines resemble different s.

As expected M rises with d. But its slope is higher than the slope of M(d) from the AUG test cases. When we apply the MAST parameters from section IV 5.3 “Escape Area“ to (33) we get:

$$R_{AUG} \approx 1.7 \cdot d_{AUG,LFS}$$
$$R_{MAST} \approx 11 \cdot d_{MAST} \qquad (39)$$

This means MAST's escape points shifts faster to higher R with increasing d than they do at AUG. Of course this linear approximation does not exactly resemble the real connection between R and d. The coefficient in (39) increases with d as long as the escape radius is smaller than 2.1 m. Above that value the fieldline's escape point is always at R=2.1 m since the coils only go so far. A more detailed analysis of M(d) will be shown for circle shaped cross-sections, especially a higher resolution in d reveals the M(d) oscillation.

M(s)

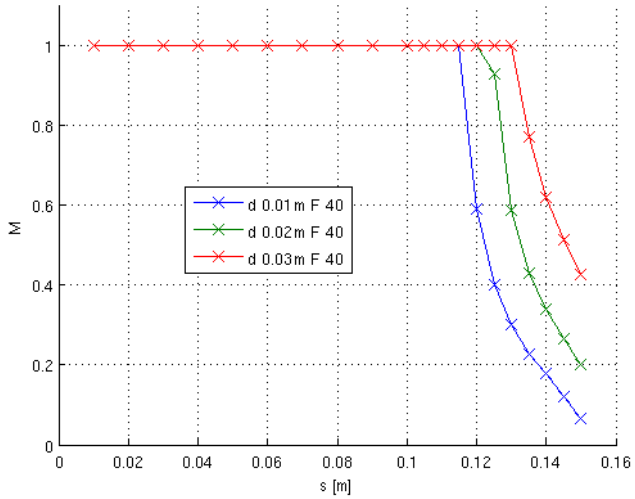

Figure 71: MAST M(s) for three different d. Again we see that there is a maximal s at which no fieldline hits the coils. This s is even higher than at AUG.

In figure 71 we see that, in contrast to AUG, MAST shows an optimal s depending on d. At AUG the lines for different d overlap from M=1 to 0.8. When the escape radius increases, the area covered by the TF coils decreases, M is increasing, so the optimal s increases with increasing d. This is too small to notice at AUG but at MAST it makes a significant difference (see equation 39). For s=11.5 cm no fieldline started with d>1 cm hits the TF coils. This s is high enough that the real coil's cross-section can fit into it (see IV 5.5 page 58).

5.6 Circle Cross-Section

M(L)

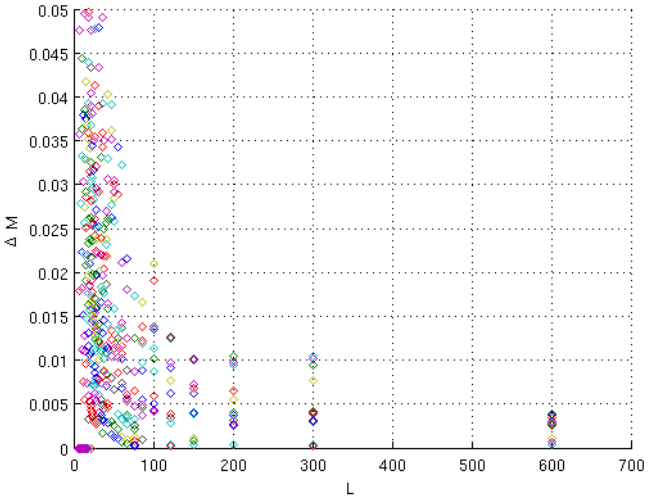

Figure 72: ΔM(L) on the left shows that M converges much faster for this F=1 circle shape than for the F>1 square shapes.

The circle shapes have been calculated with F=1 because it evades problems from filaments that get too close to a grid point in the escape area which would lead to unreasonably high B at that grid point due to the mechanics of the Vacfield code. With F>1 and varying s it is bound to happen and in the process creating glitches in M. So with F=1 the curve of the Magnetic Transparency is more smooth. This F=1 approximation may be done since M will be lower than in the F>1 cases, so it is a worst case approximation.

M(s)

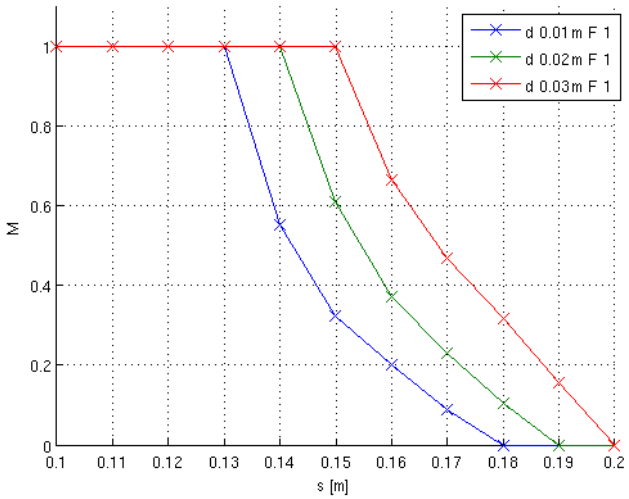

Figure 73: M(s) circle shaped cross-section

The optimal s is higher with a circle shape than with a square cross-section shape, as expected. The cross-section can be chosen up to (13 cm)² and no fieldline with d>1 cm hits any coil as seen in figure 73.

As we will see in the next section the values of d for which the lines are plotted have all in common that the oscillation of M(d) is at a low M, so the high fieldline densities all lie in hit areas. But for smaller s it is not possible to pick d values at which this is true for varying s.

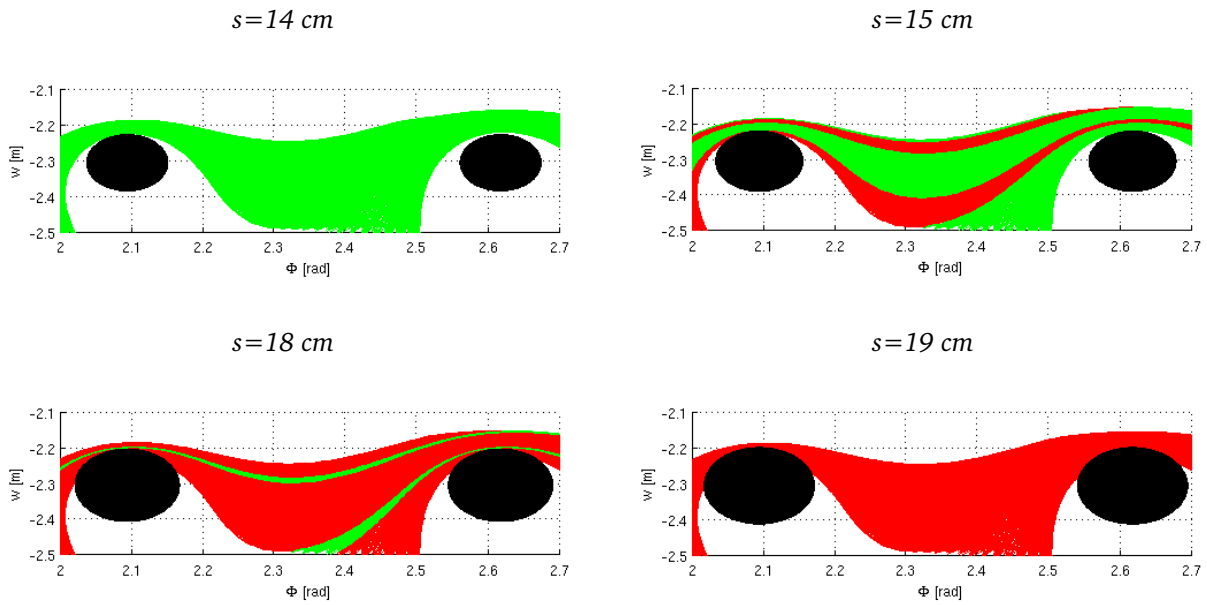

Figure 74: MAST circle shapes d=2 cm F=1. Even though there are gaps between the coils at s=19 cm all fieldlines hit the coils. By looking at the s=18 cm case one can see that the expansion of the coils' cross-section in toroidal direction is not problematic. But when the shape grows in radial direction (towards the plasma, to higher values of w) the fieldlines get cut off.

M(d)

In this test case M(d) has been calculated with a resolution of 0.1 mm in d starting at d=0.1 mm. In figure 75 we see that M(d) oscillates. This is due to the shift of the fieldline density relative to the border between fieldline that hit the TF coils and those that do not (see figure 76). The varying fieldline density has already been introduced in IV 4.8 “Fieldline Density“.

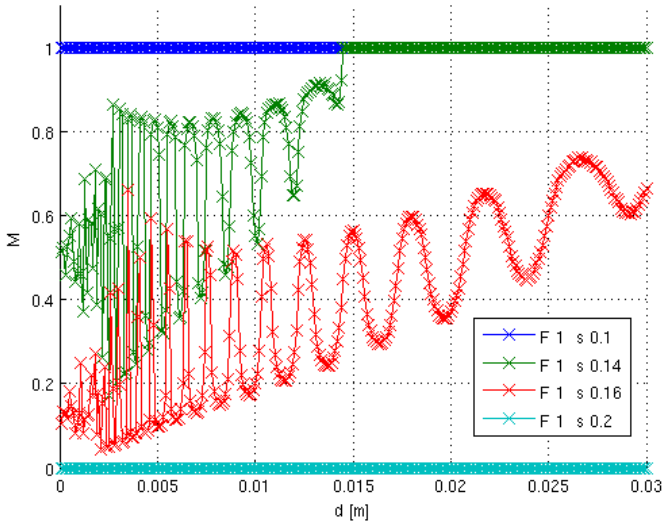

Figure 75: MAST circle cross-section F=1. M(d) oscillates with a frequency that increases with decreasing d.

Since the frequency of the oscillation increases with decreasing d, below a certain d the resolution of d cannot keep up with it and M(d) looks like an arbitrary quiver. A very reassuring conclusion from figure 75 is the path of M(d) for s=10 cm. M does not drop below one even for d=0.1 mm. That would have been problematic since the particle density (and particle energy) is highest close to the separatrix and decreases with d.

Contrary to AUG we can now see that M increases with d since at MAST the escape point shifts to higher radii more quickly (estimation in equation 39). This prevents us from seeing the oscillation frequency increasing again. The connection length at this MAST equilibrium drops up to d=6 cm. For higher d it increases again. So the possibility of a correlation of the oscillation and the slope of the connection length still exists.

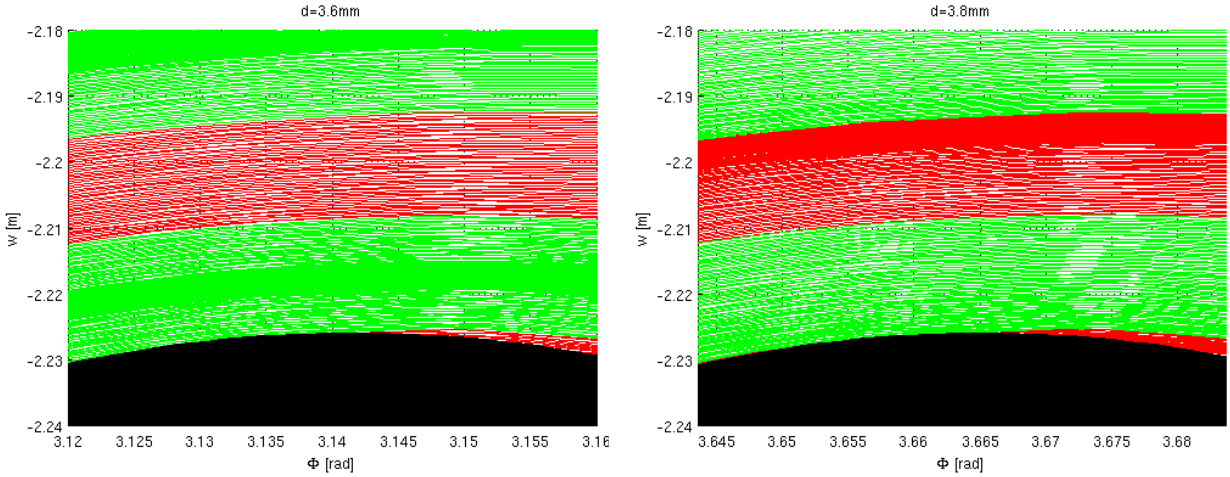

Figure 76: MAST s=14 cm The plots show the escape plane for different d. The black section in the lower part of the plots is the TF coil's cross-section. Again red fieldlines hit and green do not hit the coils. The first red section from the top are the fieldlines that hit the next coil. In both pictures areas can be seen where the colour is continuous (no white spaces between them), these are areas of high fieldline density. At d=3.6 mm (left plot) this high density area is in the no hit area, at d=3.8 mm it is in the hit area. So M(d=3.6 mm)>M(d=3.8 mm). When d is increased more the high density area wanders back in a no-hit area.

5.7 Summary

- The magnetic field is saved on a grid. The size of the grid implies that the fieldlines are intercepted at $|Z|>2.5$ m. If they are not intercepted, the fieldlines from the SOL spiral around the TF coils.

- The maximal s with M=1 is dependent on d. With s=10 cm, M equals one down to d=0.1 mm in the worst case approximation F=1. This is a possible cross-section area which is larger than the real one.

- The coils get hit less often if the fieldlines leave at a larger radius. The radius of the escape point grows with the distance of the fieldline's start point to the separatrix. So the particle flux should be guided past the TF coils at a maximal radius in order to minimize the impact on the coil. This supports the idea of using a Super-X divertor like guidance of the particle flux.

MAST is a much better candidate for such a divertor than ASDEX Upgrade. But the TF coil's cross-section would still need to be altered, then the results do not forbid such a divertor at MAST. Running the computations for MAST Upgrade could improve the results since it will have a Super-X divertor hence the escape point is at a higher radius.

V Guiding Centre Tracing

The fieldlines were a first approximation of the particle's trajectories. Now the particle flux is approximated as single particles by using the Guiding Centre approach. This incorporates the $\nabla|B|$ drift and the curvature drift. Again the Gourdon code is used for the particle tracing. Deuterium particles were traced. η is used as a short form for $\eta(r_0)$.

1 Particle Transparency P

The Particle Transparency P is defined analogously to the Magnetic Transparency. It is the percentage of particles that are lost and do not hit the coils.

$$P = \frac{T_{\text{nohits}}}{T_{\text{lost}}} \tag{40}$$

T_{nohits} is the number of particles that hit the coils.
T_{total} is the number of started particles.
T_{lost} is the number of particles leaving the torus (independent on whether they hit coils)

When tracing particles we find that particles with a low pitch angle are trapped by magnetic mirrors. It will also be seen that high energy particles do not leave the torus due to the drifts. So there is a significant number of particles that are started outside the separatrix but do not leave the torus (or hit the coils). The Particle Transparency does not take these particles into account (T_{lost} is the numerator not T_{total}).

A particle is not counted as lost if it circulates around the torus more than fifty times or the length of its trajectory exceeds a predefined threshold of 20 m. These computational restrictions prevent the test from flooding the available disk space, since the current implementation of the hitcoil algorithm is a postprocessor that needs to read the trajectories from the disk. A particle is only counted as a lost particle if it leaves the grid on which the magnetic field is defined.

2 ASDEX Upgrade

The fieldline approximation has already shown that AUG is not a good candidate for this kind of divertor. But the single particle tracing is done for AUG, too, to analyse the effects of the kinetic energy and the pitch angle on the trajectories and on the Particle Transparency. AUG was tested with square cross-sections of the TF coils.

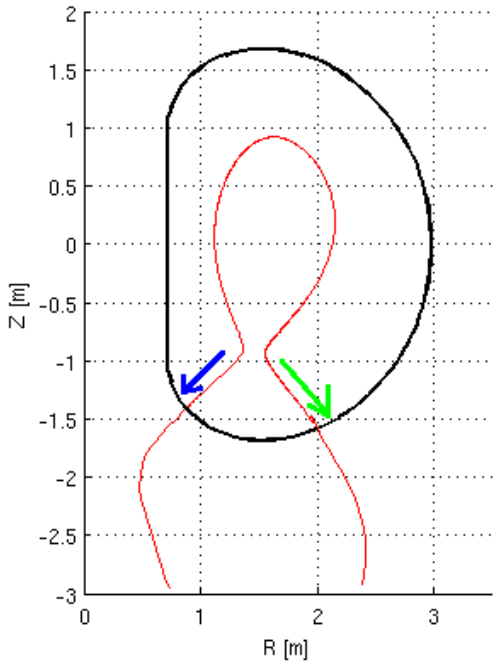

Figure 77: Counter-Particles (green arrow) intersect the TF coil on a higher radius than the Co-Particles (blue).

The parameter s is chosen so that M does not equal one but gets close since we want to see effects but are not interested in cases where M is too low since they are without meaning for a realisation of such a device. Twenty filaments are used to be able to compare the results with the equivalent fieldline cases, which are done for AUG with square cross-section shapes with F=20.

Since the particles are aligned to the fieldlines they can basically move in two directions. Particles that move towards the escape point with the high radius are called Counter-Particles, the ones moving towards the inner escape point are called Co-Particles (see figure 77). This definition is made according to their toroidal direction in respect to the plasma current.

In the following the word path is used to describe the trajectory ignoring the movement of the particle, so just the points that are in the gyration centre's trajectory with no reflections and no time dependence.

2.1 Varying Particle Density

η is chosen to be 0.9 to minimize distortions of the results by reflections at magnetic mirrors. The distance to the separatrix in this is chosen to be on the outer midplane (LFS). The ripple from the separatrix is taken into account. The reasons for starting them on the LFS and not the HFS are described in the next chapter. The Particle Transparency does not take the gyroradius into account for hit-determination yet. An oscillation in P can be found as seen in figure 78. It is analogue to the M(d) oscillation from IV 4.8 “Fieldline Density“. The reason is the variation in trajectory density as seen in figure 79.

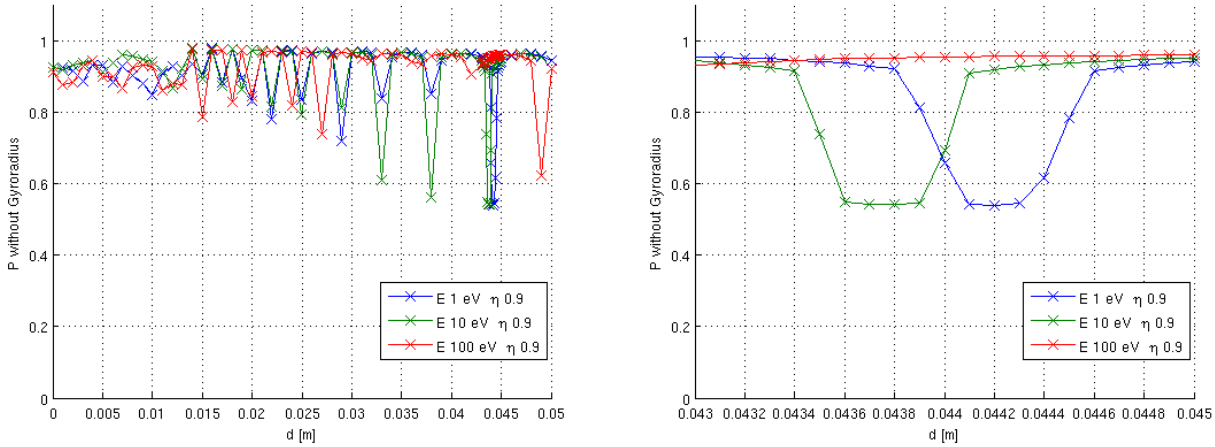

Figure 78: AUG $P(d_{LFS})$ s=12 cm F=20 Like at the fieldline tracing we can see the oscillation of M with d. The right plot is a zoom of the left one. The resolution in d is 1 mm. Except between 0.043 mm and 0.045 mm, there the resolution is 0.1 mm.

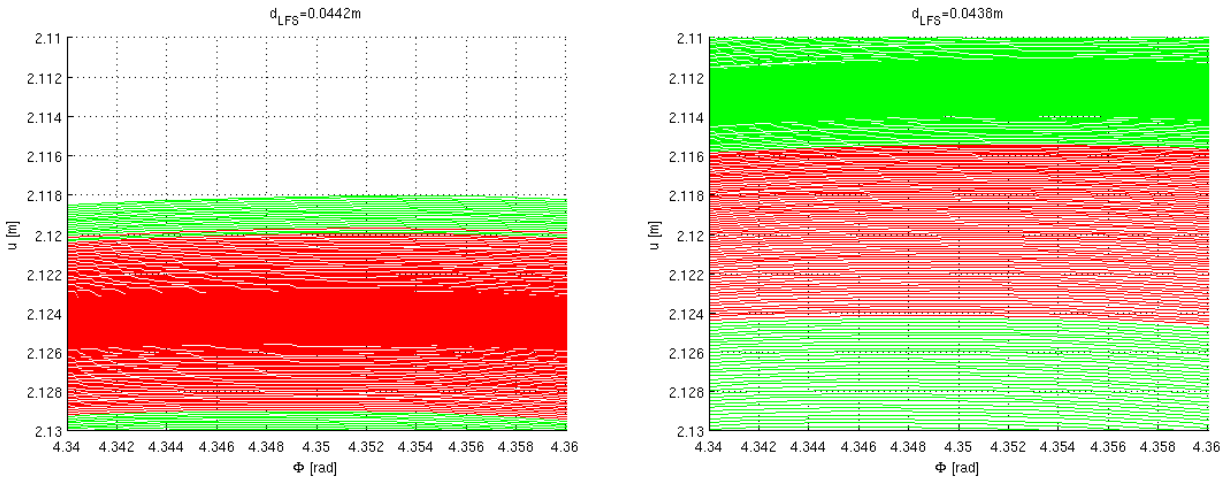

Figure 79: The plots show the escape plane for two different values of d. We can see that the high density area as well as the hit-area move with the escape radius. The reason for the oscillation of M(d) is again the shift of high trajectory density areas relative to the no-hit areas.

2.2 Kinetic Energy

Path

The kinetic energy E influences the particle's path because of the ∇|B| drift and the curvature drift. Using formula (10) and substituting perpendicular and parallel velocity with kinetic energy and pitch angle we get:

$$\boldsymbol{v}_D = \frac{c \cdot m}{q} \cdot E \cdot \left(2 - \frac{|\boldsymbol{B}(\boldsymbol{r})| \cdot [1-\eta^2(\boldsymbol{r_0})]}{|\boldsymbol{B}(\boldsymbol{r_0})|}\right) \cdot \frac{\boldsymbol{B}(\boldsymbol{r}) \times \nabla|\boldsymbol{B}(\boldsymbol{r})|}{|\boldsymbol{B}(\boldsymbol{r})|^3} \tag{41}$$

The drift velocity depends linearly on the kinetic energy. The drift brings the particles closer to the x-point until they finally switch from being lost particles into confined particles (see figure 80). So high-energy particles, even though started outside the confined plasma, do not leave the torus. This is also influenced by η as can be seen in equation 41 but for a given η, E can be always chosen so that the particle does not leave. But for a low enough E it is not possible to choose η in a way that the particle is confined (η is restricted to values between minus one and one).

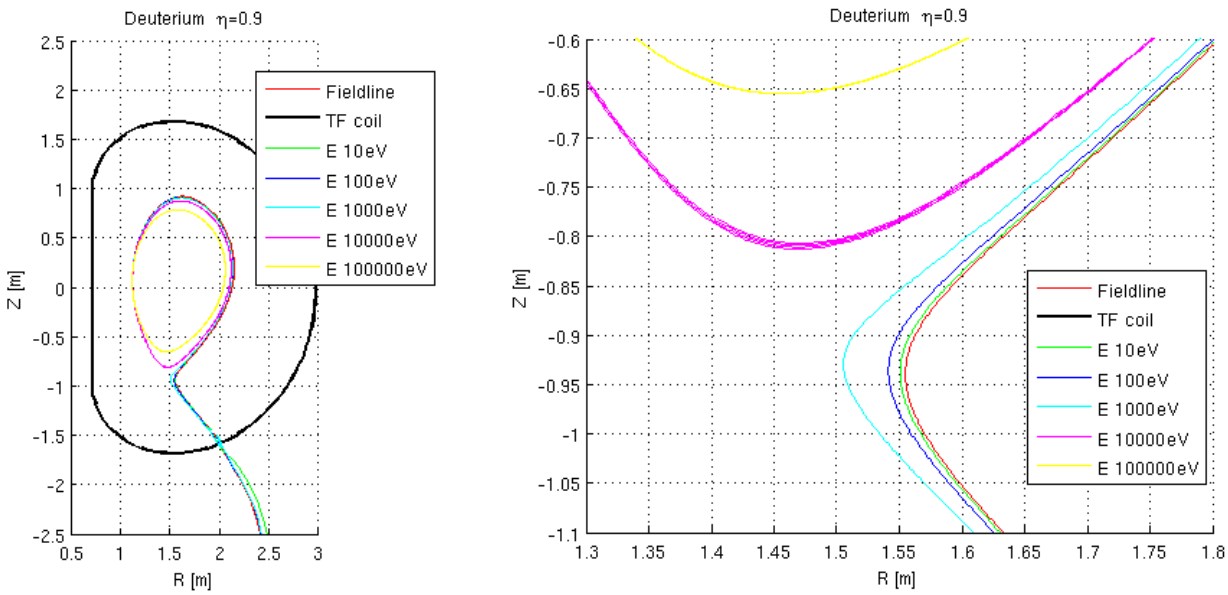

Figure 80: Increasing kinetic energy E leads to approach of the x-point. A too high E (the exact value depends on d) will confine the particle.

Due to this effect the mapping of d to d_{LFS} will be more complex than with the fieldlines. So the the particles will be started on the outer midplane. This will also make the results comparable to the particle density and temperature profiles from IV 4.3 “Scrape Off Layer”.

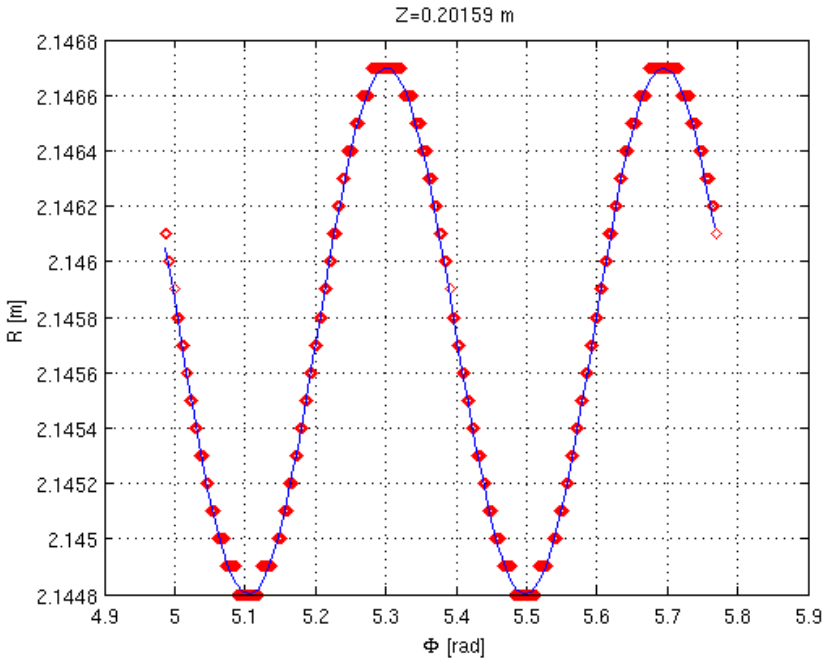

Figure 81: Spatial ripple of the separatrix at Z=0.2016 m on the LFS. This is the position where the separatrix has the highest radius. The red dots are the points calculated by the Gourdon code. The blue line is an interpolation as a cosinus.

In order to find the spatial ripple of the separatrix, fieldlines were started in a toroidal interval on the HFS all at d=0 cm. So the ripple from the HFS is considered to be zero. The point of a fieldline with the maximal radius gives the ripple on the LFS. Only one poloidal circulation was permitted to make sure that the maximal radius is taken after the same length for each fieldline. If the points from different numbers of poloidal circulations were taken q must be an integer. Even if this is the case the numerical error of the toroidal angle would accumulate with the circulations. The computed ripple R(Φ) is

$$\begin{aligned} R_0 &= 2.1448\,m \\ A &= 0.95\,mm \\ N_{coils} &= 16 \end{aligned} \tag{42}$$

$$R(\Phi) = R_0 + A\cdot(1-\cos(N_{coils}\cdot\Phi)) \tag{43}$$

From now on the particles will be started at Z=0.2016 m and the radius of the separatrix including the ripple plus d_{LFS}.

P(E)

When the particle comes close to the TF coils, the drift is directed in radial direction, so the escape point is shifted towards a higher radius by the drift. But this effect is small compared to the shift from increasing d (see figure 83). The amplitude of P(d) reaches values of up to 0.4 while the change in P(E) is about 0.15. The variation due to E is not additionally to the variation of d but can be translated into an additional offset of d. So an analysis of P(d) also gives the range in which P(E) will vary. We can see a that P(E) shows fluctuations at the same energies as the escape radius does. This implies that the fluctuations have the same reason as the P(d) oscillation.

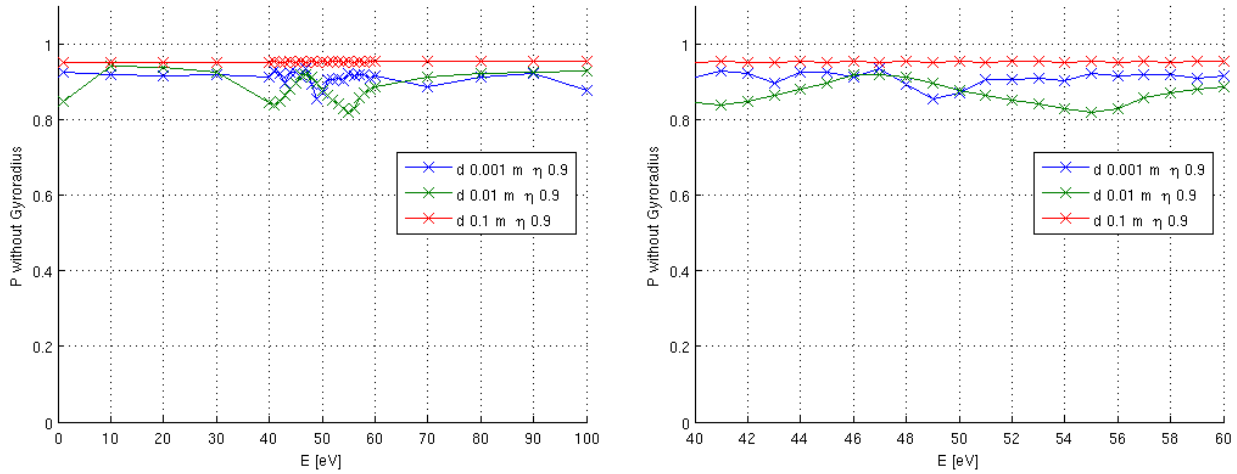

Figure 82: AUG s=12 cm F=20 The variation of P(E) is correlated to the shift of the escape radius as a comparison with figure 83 shows.

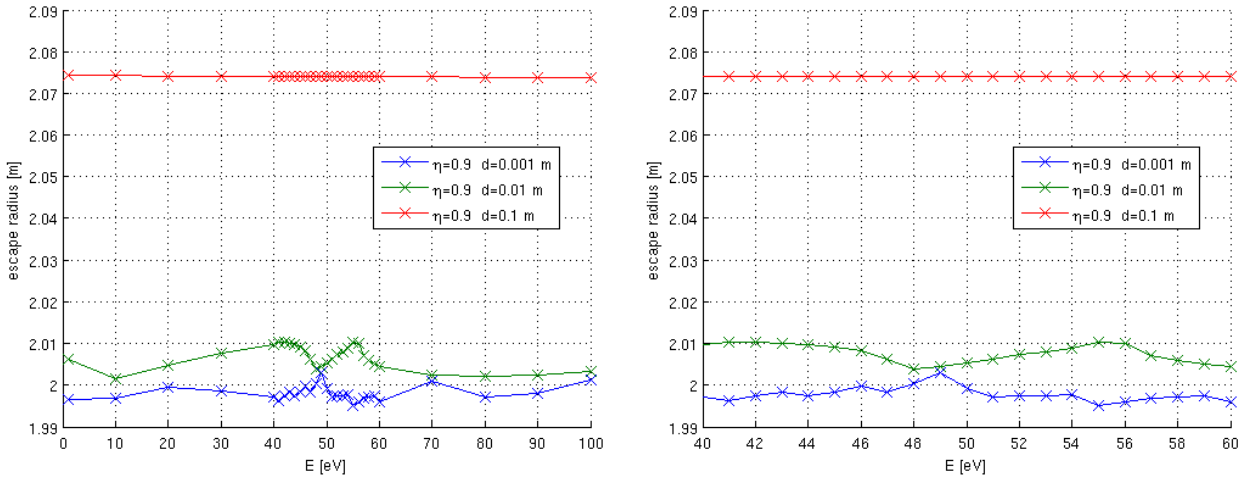

Figure 83: AUG s=12 cm F=20 The escape radius is plotted against the kinetic energy for different d. The escape radius is determined as the point at which a trajectory comes closest to the centre of the TF coil's cross-section. We would expect a monotonous increase in escape radius for increasing E. But other distortions (like from the determination of the escape point) outweigh this effect. The determination of the escape point as the radius of the trajectory at the same toroidal angle as the last TF coil it passes through should give more smooth results. But for this study it is enough to know that the shift from E is much smaller than the shift from d (in the chosen boundaries of d=0.1 cm to 1 cm and E=1 eV to 100 eV).

2.3 Pitch Angle

The pitch angle's effect on the particle's trajectory can be divided in two parts.

- A change of the direction along the path may occur because of the reflection of particles at points of high $|B|$. Particles with higher η get reflected less likely.

- The path itself does change due to the drifts. In equation (41) we see that the pitch angle has an effect on the trajectory but it is multiplied with the kinetic energy. So for low energy particles we expect no change in the path itself with changing η.

Path

Expanding the brackets from equation (41) shows that the drift increases with η_0^2. This has the same effect on P as E; the escape radius is shifted so P variates because of the trajectory densities.

$$\boldsymbol{v}_d \sim 2\cdot E - E\cdot\frac{B}{B_0} + E\cdot\frac{B}{B_0}\cdot\eta_0^2 \tag{44}$$

The drift's term including η_0 (η at the start point of the trajectory) is multiplied with E. So we get an effect on P from the changed path. The reflection condition shows that B/B_0 has a maximal value of η_0^2+1 on points the particle is able to reach, if it would be higher the particle would have been reflected before. Since the maximal value for η_0 is one, the second term cannot outweigh the first one. The third term cannot be negative but is always smaller than the second term. Hence the drift cannot invert its direction and the maximal value is two times the kinetic energy (when $\eta_0=1$).

All three terms from (44) can be of the same magnitude.

$$\begin{aligned} \frac{B}{B_0} \in [0;2] \quad &\rightarrow \quad E\cdot\frac{B}{B_0} \in [0;2\cdot E] \\ \eta_0^2 \in [0;1] \quad &\rightarrow \quad E\cdot\frac{B}{B_0}\cdot\eta_0^2 \in [0;2\cdot E] \end{aligned} \tag{45}$$

Reflected particles

Now we do not concentrate on the path but on the movement of the particle along the path. The velocity has already been substituted by kinetic energy and pitch angle so the reflections on magnetic mirrors are left to discuss. The reflection condition is based on the pitch angle alone, not the energy (see equation 14). The absolute value of the magnetic field close to the TF coils is higher than at the chosen start points of the particles for both the MAST and the AUG magnetic field. So a low enough η will prevent the particles from leaving the torus. |B| is highest where the trajectory intersects the TF coil in the poloidal cut. Due to the TF coils' ripple the magnetic field is not constant for those R and Z values but has a toroidal dependency. In between the coils |B| is lowest, in proximity to the coils |B| is high. So the coils are shielded from the particle flux by the magnetic mirror (see also III 2). At higher radii |B| drops to lower values in between the coils. We expect Co-particles to be reflected more likely, since the TF coils have a smaller toroidal distance at their escape points. The Counter-Particles intersect the coils a a higher radius, so they have a higher chance of escaping.

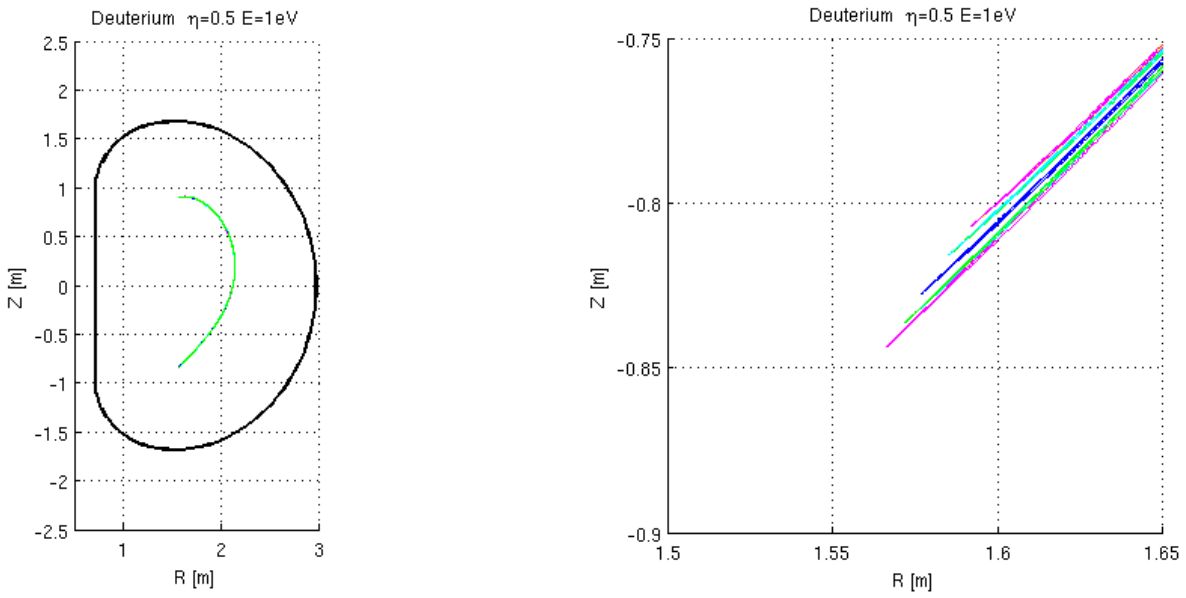

Figure 84: AUG s=12 cm F=20 Several particles (different colours) are started on the LFS with d=1 cm at different toroidal angles. Particles with η≤0.5 cannot get close to the coils since they are reflected at the x-point.

If the particle's path hits the TF coil it does not necessarily mean that the particle hits the coil. If its pitch angle is small enough the particle will be reflected back towards the confined plasma. Since the drift does not depend on the particles direction of movement it still shows in the same direction as before and it changes the particle's path on its way back and brings the particle into the private region (beneath the x-point). It comes close to the TF coil at a lower radius again and will therefore be reflected again towards the original escape point. The new escape point will have different R and Z coordinates, this poloidal offset depends on the particle's path, thus its kinetic energy. With 1-100 eV the offset is insignificant compared to the

TF coil's size. The offset is of the same magnitude as the fieldline smearing introduced in IV 4.4 “Escape Area“. But there is also a toroidal offset; the toroidal angle of the first and the second escape attempt differ more than the distances between the TF coils in toroidal direction. So there is a fair chance that the particle catches the gap between the coils at one of the next escape attempts. So P (single particles) is higher than M (fieldlines).

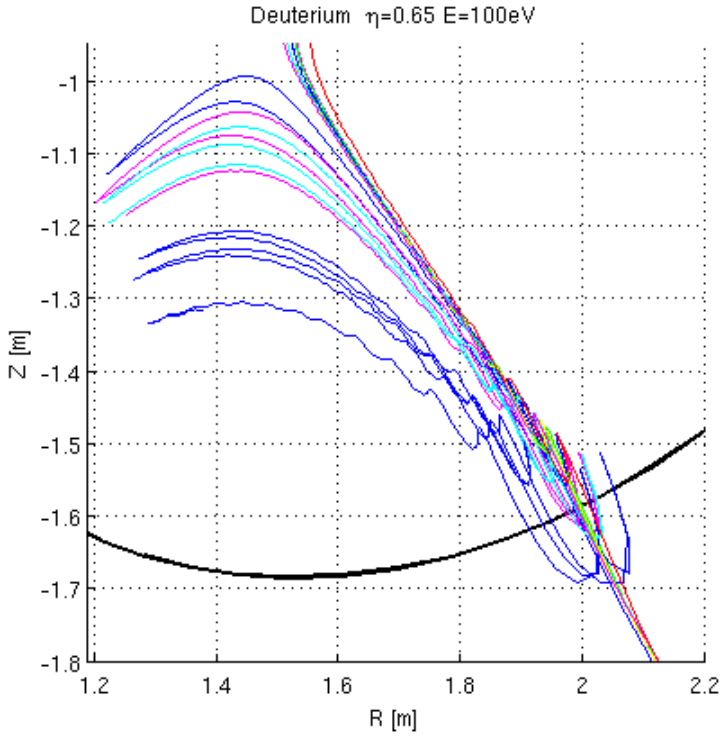

Figure 85: AUG s=12 cm F=20 Several particles (different colours) are started on the LFS with d=1 cm at different toroidal angles. The red line is the corresponding fieldline (started at Φ=0). Particles whose η is high enough to get across the x-point (η>0.5) might still be reflected at the TF coils. This depends on which toroidal angle they approach them. If they do not hit the gap between the coils they get reflected back. Due to the drift they get into the private region. From there the next escape attempt is started, which could be successful since it is at another toroidal angle (and with any luck between the coils).

With the current implementation most of the particles trapped in the private region are counted as not lost, since the movement in the private region soon exceeds the threshold for the trajectory's length. Since the hit on square coils always takes place at the same part of the cross-section (the corner) and the equipotential lines of |B| around the TF coils in its near-field do not change significantly with the escape point, a particle that got reflected once before at a TF coil is not capable of ever hitting a coil. So the P determined in this way is a worst case approximation. But this explanation only works if η_0 and E are assumed to be constant on the trajectories. As soon as particle-particle interactions are introduced it will be necessary to estimate the interaction rate in the private region. If the particles stay in the private region long enough to develop a thermal equilibrium, the “new” high η particles will be able to hit the coils again.

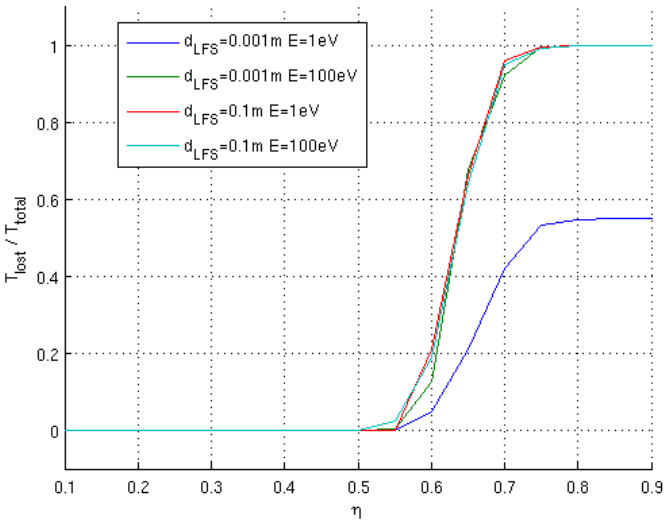

Figure 86: All particles with η≤0.5 are confined, so none is counted as a lost particle. All particles with η≥0.8 leave the torus or hit a TF coil. The particles with a pitch angle in between can be reflected at the TF coils. This depends on how close they get to the coil, hence on their start point's toroidal angle.

Figure 86 shows the relative amount of particles considered as lost from the total number of started particles. Up to $\eta=0.5$ the particles are mirrored at the x-points. At $0.5<\eta<0.8$ they approach the TF coils and get partially reflected at them. With $\eta>0.8$ the particles do not get reflected any more. This means the corresponding $|B|=(0.8^2+1)\times|B_0|$ line is inside the geometrical expansion of the coil.

P(η)

Figure 87 shows that P drops at a specific, energy independent, pitch angle. This can be understood as the shielding of the TF coils with a magnetic mirror. Particles with $\eta<0.8$ get reflected more likely before they hit the coil. So $P(\eta<0.8)$ is higher than $P(\eta\geq0.8)$

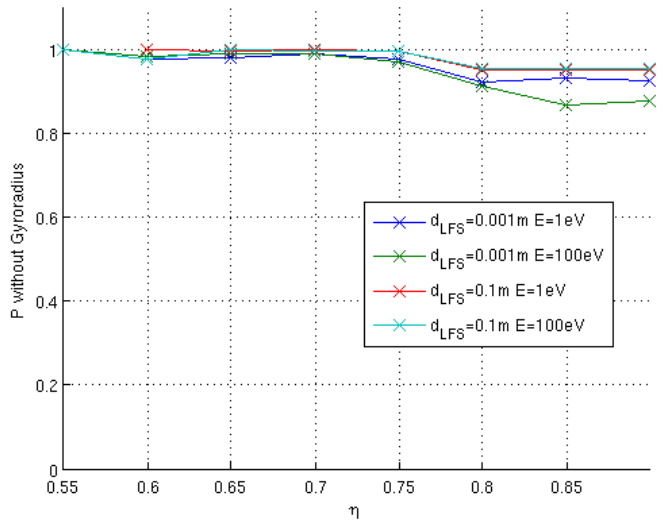

Figure 87: Since only particles with η>0.55 leave, P is only defined for those η.

M for the same parameters (s=12 cm, F=20, d=1 cm, square shape) is 0.87. $P(\eta<0.8)$ is higher than M thanks to the reflection because less trajectories hit the coils than fieldlines. $P(\eta\geq0.8)$ depends on the kinetic energy (the oscillation of P connected to the escape radius) but is still roughly the same as M.

2.4 Gyroradius

The particle's trajectory does not equal the gyrocentre's trajectory. The particle gyrates around the gyrocentre with the distance being called the gyroradius. Like described in II 3 “Lamor Radius“ equation 16 the gyroradius can be written as a function of E and η_0 instead of the velocity.

Gyroradius' Impact on P

It is too resource intensive to compute the exact path around the gyrocentre. So it is assumed that if the gyrocentre comes closer to the coil than its gyroradius at that point the particle hits it. This is a worst case approximation, since particles that are counted as hits could still evade the coil if their gyration brings them to the opposite side of the gyrocentre at the point where the algorithm says that they have hit it. So there are trajectories that are falsely counted as hits, but there are no trajectories that are falsely counted as no hits.

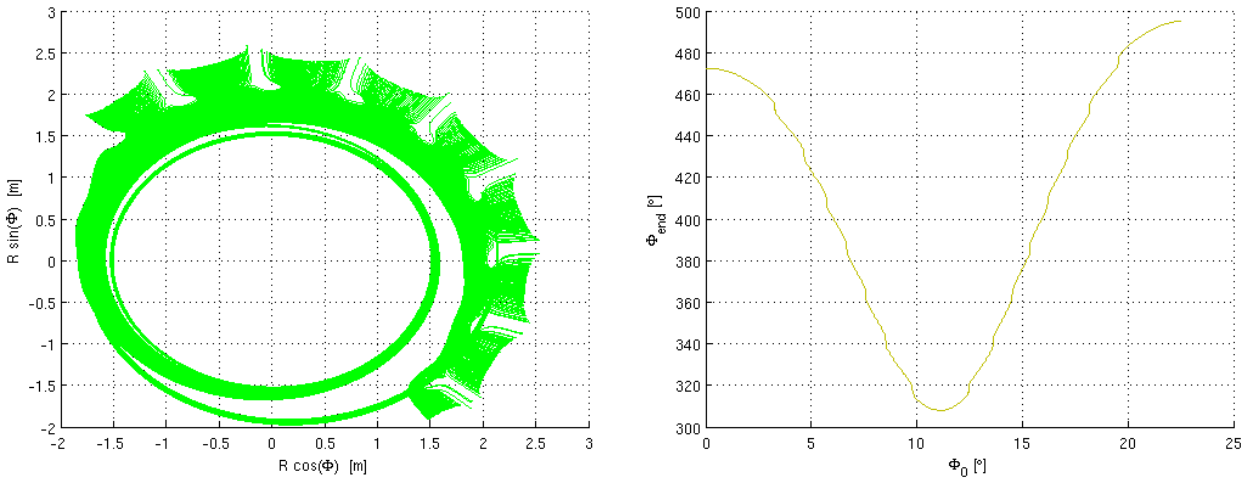

Figure 88: The left plot shows that trajectories started in a toroidal interval of $\pi/4$ length will have escape points in an interval with a length of π. The right plot shows the starting angle Φ_0 of the trajectories and their escape angle Φ_{end} . There, too, we can see that a start interval distributes along a larger set of escape angles.

Figure 88 shows that in contrast to the fieldline tracing the single particle tracing with drifts distributes a small toroidal start interval along a larger set of escape angles.

To estimate the impact of the gyroradius on P particles are started with 100 eV to show the maximal gyroradius. η is chosen to be 0.9 to ignore reflections at magnetic mirrors. Figure 89 illustrates the expansion of the gyroradius. The green lines are trajectories that do not hit the coil, red ones hit it. The first gyrocentre hitting the coil it is the middle blue line. The two blue lines next to it illustrate the expansion of the gyrocentre.

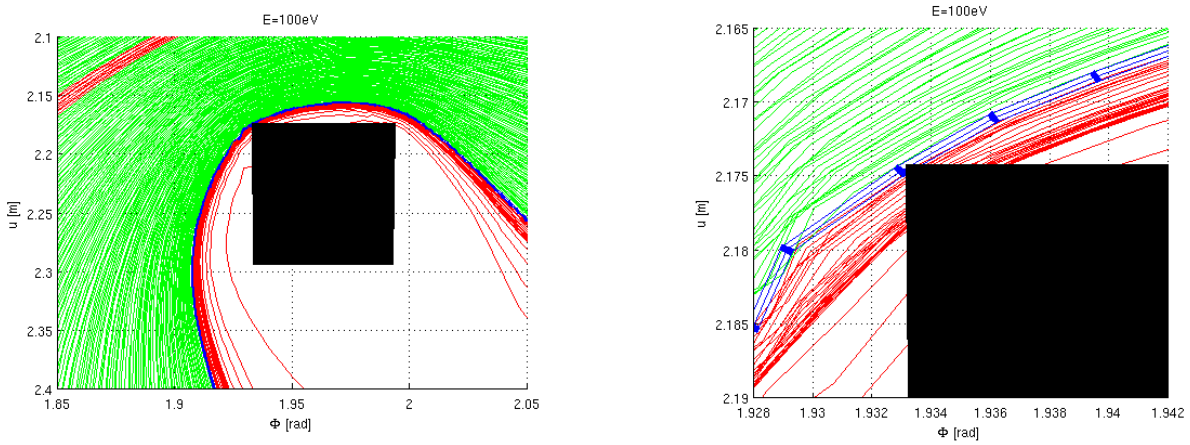

Figure 89: AUG s=12 cm η_0=0.9 E=100 eV The Green fieldlines evade, the red fieldlines hit the TF coil (black square). The three blue lines show the gyroradius. The middle line is the fieldline, the outer ones show the gyroradius. The expansion of the gyroradius is so small it is hard to see in the left plot. The right plot is a zoom on the coil's corner.

The size of the gyroradius is about two times the distance between two traced fieldlines. So when we take the gyroradius into account for hit determination two extra trajectories are extra hits per coil. There are nine coils enclosed by the examined trajectories. Hence P has to be decreased by about 0.04 (=2*9/450) as long as at least one trajectory hits the coil. For the maximal s at which no trajectory hits the coil we have to add less than 0.1 mm (maximal size of the gyroradius close to the hit-corner of the coil).

Since |B| drops rapidly outside the coils one concern was that the gyroradius could expand rapidly enough to hit the coil at R≈2.3 m. But a look at figure 89 should disperse this concern since the gyroradius does not expand significantly.

Since the gyroradius increases with decreasing η the η=0.9 particles do not have the maximal radius. Since particles with η<0.8 can get reflected if they get to close to the coils η=0.8 is the minimal choice. So the maximal gyroradius is higher by a factor of about 1.4.

$$r_g(\eta=0.8) = \sqrt{\frac{1-0.8^2}{1-0.9^2}} \cdot r_g(\eta=0.9) \approx 1.4 \cdot r_g(\eta=0.9) \qquad (46)$$

2.5 Summary

- P(d) oscillates for the same reason M(d) did. The trajectories show fluctuations in density. Their relative position to the TF coils is shifted when moving to another escape radius.

- P(E,η) shows fluctuations as well, since the kinetic energy (and the pitch angle) leads to drifts, which increase the escape radius. These fluctuations are within the same range as the P(d) oscillation.

- Particles with $\eta \leq 0.5$ are all reflected at the x-point. Particles with $0.5 < \eta \leq 0.8$ are reflected partially at the TF coils, depending on the whether they approach the coil or the gap between the coils. The reflected particles are reflected into the private region. From there they may escape since the toroidal angle of their next TF coil approach changes.

- The size of the gyroradius has only a minor impact on the allowed coil size ($\sim$0.1 mm).

- The trajectories started at a in a small toroidal angle, distribute along a larger angle when leaving the torus.

- High energy particles are confined even though started outside the confined plasma. The minimal kinetic energy at which they are confined increases with d. To minimize this effect the particles are started on the HFS.

3 MAST

Since the fieldline tracing already showed that the circle cross-sections are a good compromise between optimization and complexity those are used for the MAST particle tracing. The gyroradius is taken into account for hit determination with F=40. E is chosen to be 1 eV since the effect of E on P is within the range of variation coming from d. η_0 is chosen to be 0.9 to see the worst case (low magnetic shielding of the coils).

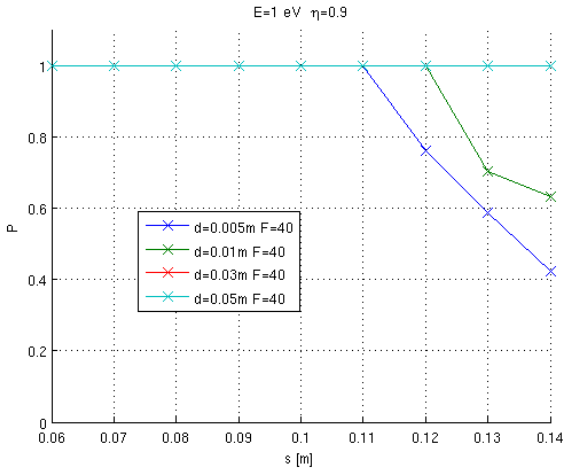

Figure 91: The optimal s is higher than at the fieldline tracing with circle shaped TF coils. This is because here more filaments are used.

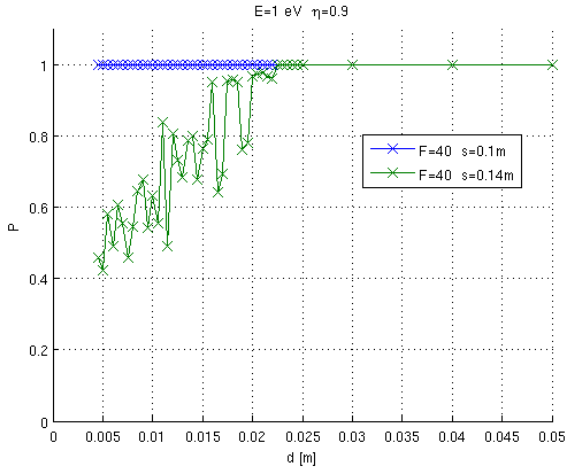

Figure 90: For s=10 cm no particle hits any coil down to a d of 4.5 mm. Particles with d≤4 mm are confined.

Figure 91 shows that the optimal size of the cross-section area is 11 cm for d=0.5 mm. Since the optimal s drops with decreasing d it is shown in figure 90 that a s of 10 cm will keep M equal to one for all d (with a resolution of 0.5 mm in d). Even though started on the outer midplane, particles with d=0.4 mm or lower are confined at the plasma (because of the drifts) and not counted as lost particles, so P is not defined for those values. So only particles with 4 mm<d<4.5mm could hit a coil with s=10 cm. Again we see that a higher escape radius (higher d) increases the possible size of the TF coils.

So it can be concluded that single particle tracing, including the $\nabla|B|$ drift and the curvature drift, does not forbid the possibility to guide the particles past the TF coils without impact on the coils.

VI Summary and Outlook

1 Summary

– The near-field effect of a solid coil compared to the one filament approximation shows that fieldlines are pushed away from the solid coils, thus reducing the number of particle impacts on the coil. Using the magnetic field from the one-filament coil is a worst case approximation for the hit probability.

– The poloidal field coils do not intercept any fieldline or single particle from the SOL neither at AUG nor at MAST. So the focus is on the toroidal field coils.

– There is a prohibited area around the coil which no fieldline or single particle (started in the SOL) enters. If the coil can be built with a cross-section smaller than this area no fieldline will be intercepted by the coil. This area around the AUG TF coils has a radius of about 7 cm, while the real coil needs a radius of about 25 cm. At MAST the radius of the prohibited area is of the same magnitude as at AUG but its TF coils carry much less electric current. Their cross-section area can fit, but its shape would need to be changed. Altering the shape should not affect the equilibrium significantly.

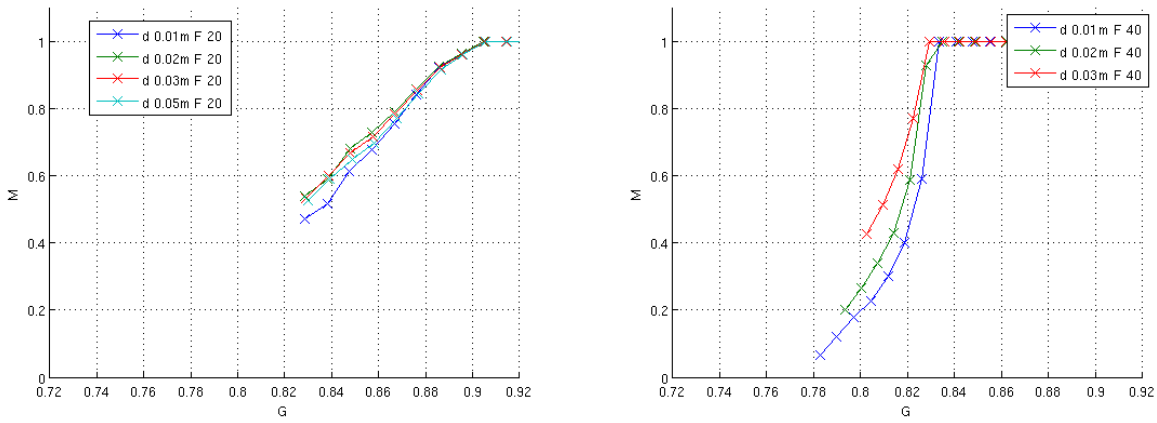

Figure 92 : M(G) G is the Geometric Transparency (the length covered by the TF coils divided by the circumference of the circle at the escape radius). The left plot shows AU, the right one shows MAST both with square cross-section shapes. Since G depends on the exit radius the different d lines are more close to each other than at the corresponding M(s) plots. We can see that M drops to zero when G is still larger than 0.5. So a simple M=G which would be assumed for an axisymmetric field and infinitesimally thin (in radial direction) coils is not close to the results of this study.

- The cross-section area a coil may have, can be maximized by optimizing its shape. It should be aligned to the most inner fieldline. The shapes that have been analysed in this study are from worst to best fit: square, circle and ellipse. The exact optimized shape changes with the poloidal angle.

- When increasing the fieldline start point's distance from the separatrix the intersection point with the TF coils shifts to a higher radius. A higher radius means larger gaps between the coils thus a decreased number of hits. So if the flux is brought to a higher radius (like the Super-X divertor) before it squeezes in between the TF coils, the impact on the coils can be reduced significantly. Respectively the size of the cross-sections area at which no particle hits the coil can be increased.

- The particle density shows aggregations when the flux is expanded. They originate from the magnetic field ripple from the TF coils. The location of the high density areas relative to the coils oscillates with the escape radius. So the fluctuations can be seen with the figure of merit depending on any parameter than influences the escape radius: M(d), P(d), P(E), P(η).

- When tracing single particle using Guiding Centre we observe that a smaller amount of particles hits the coils compared to the same test case with fieldlines. This is because particles with a low pitch angle cannot reach the coils. They get reflected by the coils near-field before they are intercepted by the surface. When looking at particles with high pitch angle the percentage of hits is about the same as when looking at fieldlines.

- The gyroradius close to the coils is small enough to have only a insignificant effect on the amount of hits. Instead the gyrocentre's trajectoriy may be checked for intersections with the coils.

2 Numerical Optimizations

From what I have learned during this study I suggest the following approach for future numerical implementations:

- Implement the hitcoil algorithm directly into the code that does the fieldline and particle tracing. This spares the need to save the fieldlines to the disk in a high accuracy. For visualisation purposes it comes in handy to save part of the fieldlines. But only the part that comes close to coils and or only every n^{th} step. With such an embedded code longer fieldlines can be traced so the analysis can be done for low d and for particles that are reflected into the private region. And more fieldlines (or trajectories) can be traced thus the accuracy can be increased.

- A new code exists that was written by P. Merkel which computes the vacuum magnetic field for solid coils. At present it supports quadrangular cross-sections. An expansion of this code for more generic shapes would make the parameter F deprecated sparing convergence checks.

- When creating new magnetic fields it should be able to improve performance and accuracy by calculating the field only in the region of the escape point. Then the grid resolution can be increased without consuming more resources. The fieldline's path far away from the TF coils does not change when altering the TF coils parameters. The parameter d must be translated into a start point inside this new grid.

- A code that searches the fieldlines that represent the borders between hit and no-hit areas can save the need to trace the fieldlines with equidistant toroidal start angles. Thus it should save computation time.

3 Ways to increase M and P

If such divertor would be considered for future devices M respectively P needs to be optimized to minimize the impact on plasma facing components, especially the TF coils.

Cross-Section Optimization

The already presented alterations of the TF coil's cross-section areas can significantly decrease the impact on the coils even with a simple choice like a circle shape. Maybe even narrowing the coil's cross-section area at the escape points is an option. Both methods have the advantage of not affecting the equilibrium. But the mechanical stability could become a issue.

Guiding Fieldlines to a maximal Radius

Increasing the radius of the escape point significantly increases the cross-section area that can be chosen at which P still equals one. The escape radius can be increased by using a Super-X divertor like particle guidance.

4 Final Conclusion

The tracing of fieldlines and single particles showed that even in existing tokamaks there is an area around the coils that is not targeted by particles started in the SOL. On the one hand by the path of the fieldlines which avoid an area around the coils. On the other by the high magnetic field around them which works as an magnetic mirror. The size is about the same for ASDEX Upgrade and MAST ($\sim$100 cm^2). At MAST this is about the real cross-section area. So the single particle tracing does not forbid the possibility of guiding the particles past the TF coils.

5 Proposed Studies

- Diffusion perpendicular to the fieldlines has to be taken into account. Particle as well as energy transport could have a significant impact on the distance the coils need to have to the fieldlines coming from the SOL.

- It is to expect that the maximal allowed size of the TF coil cross-section at MAST Upgrade is higher than at MAST. This is because MAST Upgrade will have a Super-X divertor. There the flux is guided to a maximal radius inside the TF coils. It will be interesting to see how the fieldline density behaves if the escape radius is kept constant (at the outer leg of the coil). If it is about constant in d then coil's shape could be optimized to have a maximal distance to the high density areas thus reducing the inevitable (from diffusion) residual impact.

- Additional Saddle-Coils that produce a magnetic field pointing radially outwards could be used to bundle the particle flux at the toroidal angles of the gaps between the coils. But this will alter the equilibrium itself.

VII References

[1] *Super-X divertors and high power density fusion devices*
P.M. Valanju, M.Kotschenreuther, S.M. Mahajan and J.Canik
Physics of Plasmas 16, 056110 (2009)

[2] *Geometrical properties of a snowflake divertor*
D.D. Ryutov
Physics of Plasmas 14, 064502 (2007)

[3] http://www.ccfe.ac.uk/MAST.aspx

[4] *Numerical algorithm for field line reconstruction from vector field distribution*
A. Belov, O. Filatov, V. Kukhtin, E.Lamzin, Yu. Severign, S. Sytchevsky
Plasma Devices and Operations, 2002, Vol. 10(4), pp. 263-268

[5] *Fast particle losses due to NTMs and magnetic field ripple*
E. Strumberger, S. Günter, E. Schwarz, C Tichmann and the ASDEX Upgrade Team
New Journal of Physics 10 (2008) 023017 (21pp)

[6] *Progress in the ITER Physics basis*
Special Issue, Nucl. Fusion 47, 6 (2007)

[7] *Application of Three-dimensional Codes to Tokamaks*
E. Strumberger, S. Günter, P. Merkel, E. Schwarz, C. Tichmann, H.P. Zehrfeld and the ASDEX Upgrade Team
29th EPS Conference on Plasma Phys. And Contr. Fusion Montreux, 17-21 June 2002
ECA Vol. 26B, P-2.090 (2002)

[8] *2D fluid modelling of the ASDEX upgrade scrape-off-layer up to the first wall*
F. Subba, X. Bonhin, D. Coster, R. Zanino
Computer Physics Communications 179 (2008) 194-198

VIII Appendix

1 Hitcoil Algorithm

1.1 Determining the closest Coil

The algorithm determines the coil closest to each point of the fieldline by using the symmetry of the tokamak.

$$nextcoil(i) = \left\lfloor \frac{3}{2} + \frac{N_{coils} \cdot \varphi(i)}{2 \cdot \pi} - \left\lfloor \frac{\varphi(i)}{2 \cdot \pi} + \frac{1}{2 \cdot N_{coils}} \right\rfloor \right\rfloor \tag{47}$$

$\varphi(i)$ Coordinate of i-th fieldline point
nextcoil Index of the closest Coil.

Analogously the function *sector*() is defined. It differs from *nextcoil*() by not assigning the closest coil but assigning the fieldline point to sectors which span from one coil to another. So the TF coils are the sector's borders.

Only the last coil the fieldline pass through while inside the torus is checked for hits since it is the one the fieldline comes closest to. The index of the last coil is determined using the observation that the last passed coil can only be one of the last fieldline point's sector's borders. The exact coil is determined by looking at the toroidal direction of the fieldline's points that are in the same sector. If the direction is not the same as of the start points it is the upper border, if it is the same direction the last passed coil is the lower border of the sector.

1.2 Determining the possibly intercepted part of fieldline

Only the points of the fieldline are considered that are within the last two sectors the fieldline passes. For all these points the distance to each point of the coil is computed. Only the centre of the coil's cross-section is used. Here it is important that the spacing of the coil's points is not too large. The index of the fieldline point and coil point, that have the minimal distance to each other, are return values of this routine, as well as the distance between them.

This the most resource intensive part. So it makes sense to apply some tweaks:

- Only the part of the coil that can be hit is considered (for MAST the lower leg of the TF coil).

- At first only every 10^{th} point of the fieldline is considered. Since Gourdon computes the fieldline with equidistant predefined steps (Δl) the distance of each 10^{th} point can be used to make a worst case approximation: $9*\Delta l$ is added to each computed distance. If a hit would be possible the distance of the neighbouring 18 fieldlines points is computed, too.

1.3 Elliptic shaped cross-sections

Since circle shaped cross-sections are just a special case of the elliptic ones no extra code was written for them (even though it could improve performance). The distance to the two foci of the ellipse is computed instead of the distance to the centre. If the minimal distance is smaller than two times the major axis plus the gyroradius (for particles) then the fieldline/trjectory is considered a hit.

The main numerical inaccuracy of this implementation is the dependence on the resolution of the fieldline's data and the resolution of the coil' data. Both must be much smaller than the coil's parameter s.

1.4 Square cross-sections

In order to simplify the problem the coordinates of the fieldline and the coil get transformed by using U on the cylindrical coordinates.

$$U=[\boldsymbol{u}\,\boldsymbol{v}\,\boldsymbol{w}]^{-1} \tag{48}$$

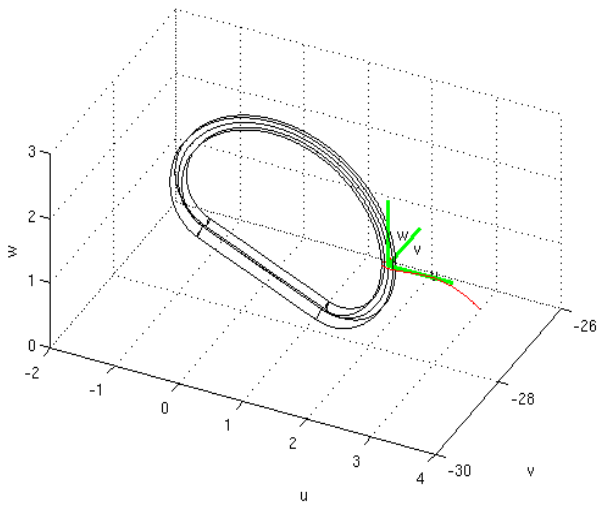

Figure 93: Coil and fieldlines in the coordinates transformed

These are the vectors in which the cross-section of the coil is defined (see III 1 “Creating the Coil's Numerical Data“). Since they are dependent on the poloidal angle the closest coil point is used (from VIII 1.2). The result can be seen in figure 93. In the projection to the poloidal cut, the fieldlines are nearly perpendicular to the coil at the escape point. So the transformation is used to make the problem two dimensional.

The coils are considered as square in cylindric coordinates with the Φ expansion at the side closer to the torus neutral point defining its edge length. This choice is due to the path of the fieldlines starting in the SOL that makes them hit the inner edges of the coils but not the outer ones.

Using a few if checks each fieldline point is assigned a value according to figure 95. If at least one fieldline point is in the middle sector it is a definitive hit.

If there is no value of 100 or any transition with less than 50 the fieldline cannot be a hit.

Figure 94

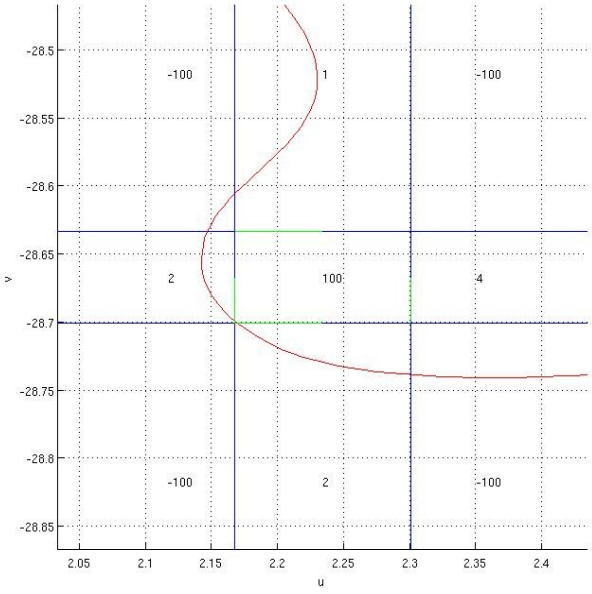

Figure 95

If there's at least one transition from one fieldline point to the next in which the assigned value changes by less than 50 and more than 0 then we have a case in which it could be a hit even though we don't know any fieldline point inside the coil. In this case another coordinate transformation is applied. It rotates the plane so that the fieldline (between the two points where the <50 transition happened) is parallel to the x-axis. If all of the four coil corner points are above or below the new y-coordinate of the fieldline the fieldline does not hit the coil, if not it does.

2 Construction of Elliptic Cross-Sections

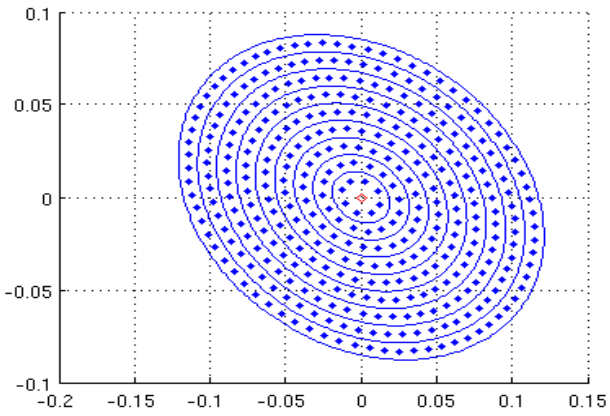

Figure 96: Elliptic cross-section of the TF coil. The blue rhombi are the current filaments and the blue line is the border of the coil. The red rhmobus in the middle is the original filament.

We have to demand that each filament represents an area of equal size. The angular dependency of the current density has to reflect the solid case. The current per filament is constant. The growth of the major (a) and minor radii (b) with each ring is constant. A short calculation with these requirements shows the number of filaments per ring where i is the number of the ring.

$$F_i = 8 \cdot i \tag{49}$$

A longer calculation gives us the angles at which we have to place the filaments. j is the index of a filaments in a given ring i.

$$\varphi_{ij} = \varphi_{rot} + \tan^{-1}\left(\frac{a}{b} \cdot \tan\left(\frac{2 \cdot \pi \cdot j}{F_i}\right)\right) \qquad j = 1, \ldots, 8 \cdot i \tag{50}$$

An additional shift in φ has to be considered since the tangent functions is not injective.

$$\tan^{-1} : \mathbb{R} \rightarrow \left]-\frac{\pi}{2}, \frac{\pi}{2}\right[\qquad \varphi_{ij,\mathrm{Shift}} = \frac{\pi}{2} \cdot \left\lfloor \frac{4 \cdot j}{F_i} - \frac{\pi}{4} \right\rfloor \tag{51}$$

A constant rotation φ_{rot} is added to adapt the coil's angle towards the fieldlines to minimize hitting. Also a constant offset φ_{i0} can be added that only shifts the filaments but does not change not geometry of the cross-section.

$$\varphi_{ij} = \varphi_{rot} + \tan^{-1}\left(\frac{a}{b} \cdot \tan\left(\frac{2 \cdot \pi \cdot j}{F_i} + \varphi_{i0}\right)\right) + \frac{\pi}{2} \cdot \left\lfloor \frac{4 \cdot j}{F_i} + \frac{2}{\pi} \cdot \varphi_{ij0} - \frac{\pi}{4} \right\rfloor$$

3 Configuration Parameters

3.1 Vacfield

Parameter	Description	AUG	MAST extended field (IV 5.4)	MAST
nf	number of grid points in toroidal direction between 2 TF coils	32	32	32
nr	number of grid points in radial direction	400	128	128
nz	number of grid points in Z	608	308	256
np	number of TF coils	16	12	12
r0	radial coordinate of the middle of the grid [m]	2.005	1.5	1.5
z0	z coordinate of the middle of the grid [m]	0	0	0
dr	radial expansion of the grid [m]	2	1	1
dz	z expansion of the grid [m]	3	2.9961	2.5
j_main	current per TF coil [MA]	1.054625	0.17	0.17

3.2 Gourdon

I had to alter the part of the Gourdon code that writes data to files to be able to save every step of the fieldlines/trajectories. Also the conditions when the tracing is aborted were changed, to only abort if the grid on which the magnetic field is defined is left or if the array of points gets too long.

Apart from organisation parameters (path- and file-names) this leaves hdpasz. This is the distance between the fieldline's/trajectory's points. If it is too low the path will be not exact enough, if too high the threshold for a fieldline is soon exceeded. Hdpasz was chosen to be 0.01 in this thesis.

4 Table of Abbreviations

AUG	ASDEX Upgrade
ASDEX	AxialSymmetric Divertor Experiment
CCFE	Culham Centre for Fusion Energy
FL	Fieldline
GC	Guiding Centre
HFS	High Field Side
IPP	Max-Planck-Institut für Plasmaphysik
LFS	Low Field Side
MAST	Mega Ampere Spherical Tokamak
PF	Poloidal Field
SOL	Scrape Off Layer
ST	Spherical Tokamak
TF	Toroidal Field